2104

VTT RESEARCH NOTES



Simo Hostikka, Matti Kokkala & Jukka Vaari

# Experimental Study of the Localized Room Fires

## NFSC2 Test Series

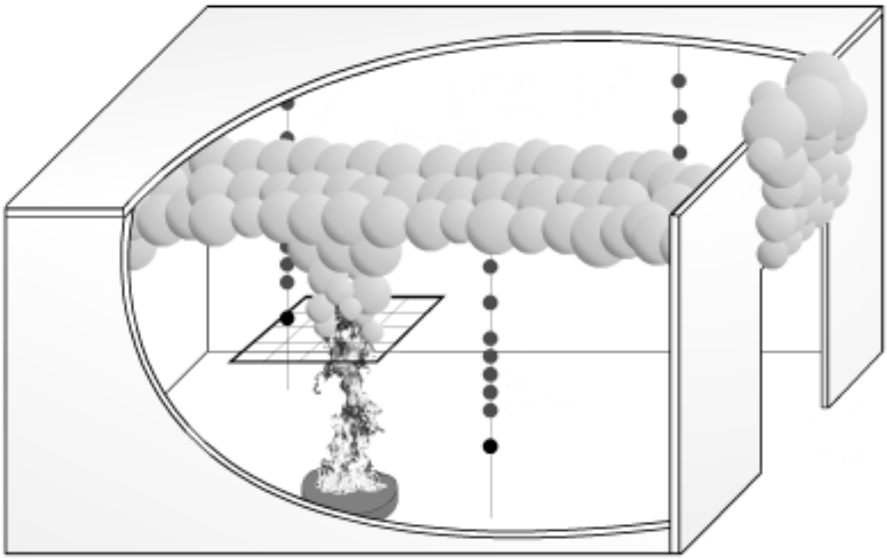

TECHNICAL RESEARCH CENTRE OF FINLAND

ESPOO 2001

VTT TIEDOTTEITA – MEDDELANDEN – RESEARCH NOTES 2104

# Experimental Study of the Localized Room Fires

## NFSC2 Test Series

Simo Hostikka, Matti Kokkala & Jukka Vaari

VTT Building Tehcnology

ECSC Steel Research Programme
Contract No. 7210-PR-060

TECHNICAL RESEARCH CENTRE OF FINLAND
ESPOO 2001

ISBN 951–38–5837–5 (soft back ed.)
ISSN 1235–0605 (soft back ed.)

ISBN 951–38–5838–3 (URL: http://www.inf.vtt.fi/pdf/)
ISSN 1455–0865 (URL: http://www.inf.vtt.fi/pdf/)



JULKAISIJA – UTGIVARE – PUBLISHER

Valtion teknillinen tutkimuskeskus (VTT), Vuorimiehentie 5, PL 2000, 02044 VTT
puh. vaihde (09) 4561, faksi (09) 456 4374

Statens tekniska forskningscentral (VTT), Bergsmansvägen 5, PB 2000, 02044 VTT
tel. växel (09) 4561, fax (09) 456 4374

Technical Research Centre of Finland (VTT), Vuorimiehentie 5, P.O.Box 2000, FIN–02044 VTT, Finland
phone internat. + 358 9 4561, fax + 358 9 456 4374

VTT Rakennus- ja yhdyskuntatekniikka, Rakennusfysiikka, talo- ja palotekniikka,
Kivimiehentie 4, PL 1803, 02044 VTT
puh. vaihde (09) 4561, faksi (09) 456 4815

VTT Bygg och transport, Byggnadsfysik, fastighets- och brandteknik,
Stenkarlsvägen 4, PB 1803, 02044 VTT
tel. växel (09) 4561, fax (09) 456 4815

VTT Building and Transport, Building Physics, Building Services and Fire Technology,
Kivimiehentie 4, P.O.Box 1803, FIN–02044 VTT, Finland
phone internat. + 358 9 4561, fax + 358 9 456 4815

Cover picture Simo Hostikka

Technical editing Leena Ukskoski

Otamedia Oy, Espoo 2001

Hostikka, Simo, Kokkala, Matti & Vaari, Jukka. Experimental Study of the Localized Room Fires. NFSC2 Test Series. Espoo 2001. Technical Research Centre of Finland, VTT Tiedotteita – Meddelanden – Research Notes 2104. 49 p. + app. 46 p.

**Keywords** fire tests, room fires, experimentation, fire safety, fire prevention, concrete structures, walls, ceilings, burning rate, gas temperature, heat flow

# Abstract

Two series of full scale fire tests have been carried out with an objective to produce well-documented data for the zone model and CFD code verification. The first test series consisted of 21 tests in $10 \times 7 \times 5$ m$^3$ test enclosure with $2.4 \times 3.0$ m$^2$ to ambient. The walls and ceiling were made of light weight concrete. Systematic variations of the fire size and locations were made to determine their effect on the fire environment. Burning rates, gas temperatures, wall temperatures, heat fluxes, flow velocities and species concentrations were measured during the tests. The second series consisted of eight tests in a $27 \times 13 \times 19$ m$^3$ test hall. Burning rates, gas temperatures and steel tube temperatures were measured to provide information about the smoke filling rate and heating of the steel structures. The boundary conditions were varied by changing the fire size and using mechanical exhaust of the smoke gas and open doors to ambient.

# Preface

This publication contains a detailed documentation of two series of large-scale fire tests carried out at VTT Building Technology during the years 1998 and 1999. The work was part of the project “Natural fire safety concept: Full scale tests, implementation in the Eurocodes and development of a userfriendly design tool” within the ECSC Steel Research Programme under contract Contract No. 7210-PR-060.

The work at VTT Building Technology was funded by ECSC (the European Steel and Coal Community), by Rautaruukki Oyj (Finland) and VTT (the Technical Research Centre of Finland).

Permission for publication of the report was obatined from the partners ProfilARBED (Luxembourg, Coorduinator of the European Project), Building Research Establishment (UK), Centre Technique Industriel de la Construction Metallique (France), Deutscher Stahlbau Verband e.V. (Germany), and TNO Bouw /The Netherlands). The authors would like to thank the European colleagues for fruitful discussions and guidance when planning the series of tests to be carried out.

Simo Hostikka

Matti Kokkala

Jukka Vaari

# Contents

# List of symbols

| | |
|---|---|
| $c_p$ | specific heat at constant pressure |
| $H$ | room height |
| $h$ | heat transfer coefficient |
| $\dot{Q}$ | rate of heat release |
| $\dot{m}$ | burning rate |
| $\Delta H_c$ | specific heat of combustion |
| $T$ | temperature |
| $t$ | time |
| $z$ | height |
| $u, v$ | fluid velocity |
| $V$ | volume |

**Greek symbols**

| | |
|---|---|
| $\varepsilon$ | emissivity |
| $\lambda$ | thermal conductivity |
| $\rho$ | density |
| $\chi$ | combustion efficiency |
| $\sigma$ | Stefan-Boltzman constant |
| $\phi$ | configuration factor |

**Subscripts**

| | |
|---|---|
| up | upper layer |
| low | lower layer |
| amb | ambient |
| R | radiation |
| TC | thermocouple |
| s | surface |
| F | flame |

# 1. Introduction

Although a large number of large-scale fire tests has been carried out in the fire laboratories around the world, the applicability of the results to model verification is limited. The tests are usually made for a special purpose and the measurements are supporting only that purpose, often for demonstration only. Additional measurements have been left out due to extra cost. Hardly any large-scale fire growth tests exist with systematic variations of one parameter at a time. Only in a few cases have repeated tests been made and, consequently, the repeatability of the tests is usually not known.

For performance based fire safety design the developing fire is of great importance, because the life losses most often occur in the early phase of the fire. In large spaces a localised fire may also need to be considered in structural design. Knowledge of the thermal exposure by a localised fire is therefore of great importance when developing general design methodologies.

The objective of the tests has been to produce a set of data for the verification of the zone models and CFD codes used in fire simulation. Test data is also produced about the temperature development of structures under the same conditions. Different methods of temperature and heat flux measurements have been applied to provide data for the modelling of the heat transfer during fire. These methods contain the gas temperature measurements using thermocouples and plate thermometers, structure temperature measurements in walls and measurements using heat flux gages. The experimental setup and the results of the first series of experiments, conducted in a $10 \times 7 \times 5$ m$^3$ enclosure, are described in Sections 2 and 3. Sections 4 and 5 then describe the setup and results of the second series of experiments, conducted in the $27 \times 13 \times 19$ m$^3$ test hall. The methods of data reduction and error analysis are described in the context of the first series of experiments. Comprehensive reviews of the results are given in appendices C–P, where plottings of most measurements are presented. Test data will be made publicly available for the validation computer codes in the future.[1]

[1] Contact Simo.Hostikka@vtt.fi for details

# 2. Description of the room experiments

## 2.1 Geometry

The experiments were conducted in a rectangular room having one door to the large fire testing hall at VTT. The whole room was located inside the hall, as illustrated in Figure 1. The hall has the following dimensions: length 27 m, width 14 m and height 19 m. The test room was approximately in the center of the hall. Smoke flowing out of the door was collected to the upper part of the hall as the mechanical ventilation of the hall was not used during the experiments.

An overview of the setup is illustrated in Figure 2 showing a fire plume inside a room and some of the measurement devices. The inner length of the experiment room was 10 m, width was 7.0 m and height 5.0 m. The walls and ceiling of the room were made of lightweight concrete ($\rho$ = 475 kg/m$^3$, $\lambda \approx$ 0.12 W/Km, $c_p \approx$ 900 J/kg.K) and the floor was normal concrete. The thickness of the walls was 0.30 m and the ceiling 0.25 m. In the beginning of the test series the moisture content of the walls and ceiling material was quite high, but an actual moisture measurement was not made. Approximately 10 % of the floor area was covered by steel plates blocking the air channels inlet under the floor.

The width and height of the door were 2.4 m and 3.0 m, respectively. However, the door width was changed to 1.2 m during some tests to find out the effect of the opening size.

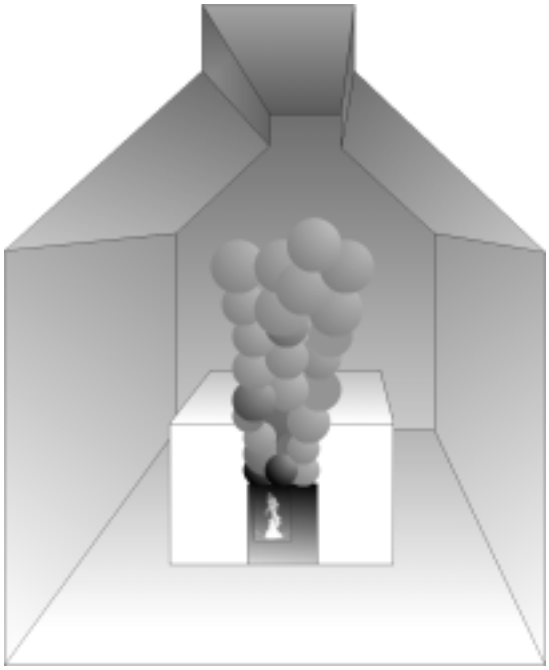

*Figure 1. An overview of the test hall.*

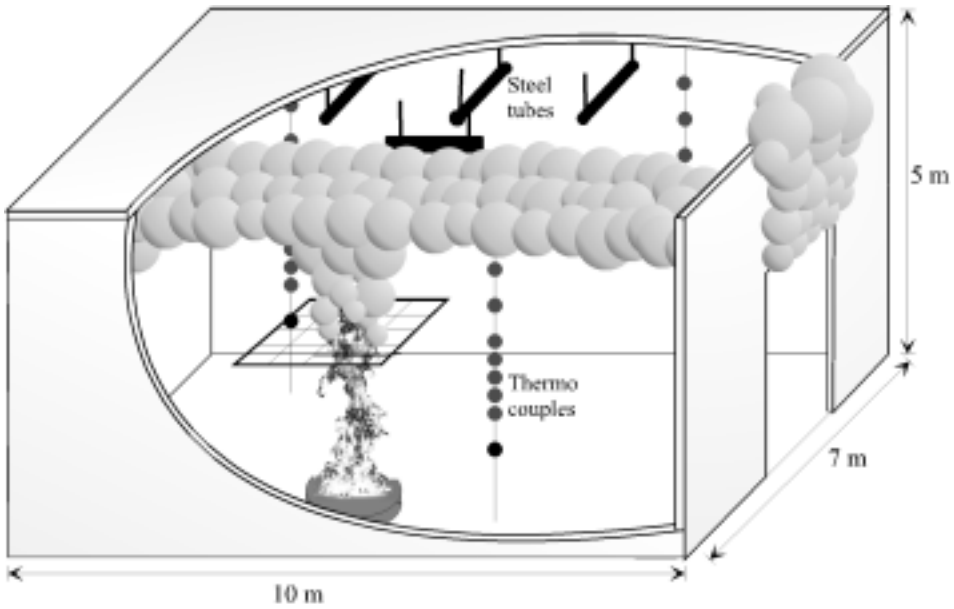


*Figure 2. An overview of the experimental setup.*

## 2.2 Fire Source

The burning fuel was heptane, except in two tests where a wood crib was burned for interlaboratory comparisons. These tests involving wood fuel are here called "calibration tests". Heptane was burned in circular steel pools placed on load cells for the mass loss measurement. Pool size was varied from 0.40 $m^2$ to 2.0 $m^2$ and four different locations were used for the pool. The locations are shown in Figure 3. Complete list of the variations is given in the following section. Water was used under the heptane to stabilise the fire. The amount of water was chosen such that the free height from the water surface to the pool edge was 0.13 m.

The rate of heat release was not measured during the tests. However, an estimate for the heat release rate can be calculated from the measured burning rates with equation

$$\dot{Q} = \chi \cdot \dot{m} \cdot \Delta H_c \qquad (1)$$

where $\chi$ is the efficiency of the combustion inside the room, $\dot{m}$ is the measure mass loss rate and $\Delta H_c$ is the heat of combustion of heptane. The suggested values for $\chi$ and $\Delta H_c$ are 0.8±0.1 and -44.6 MJ/kg, respectively.

The wooden fire load was made of cribs shown in Figure 4. Each crib had the following dimensions: 652 mm (length) x 70 mm (width) x 47.2 mm (height). Wooden fire loads

were ignited with heptane, 1.0 litre in first wood crib test (Test 10) and 0.7 litre in second (Test 14). In Test 10 the pool used for ignition heptane was quite large, 0.60 × 0.60 m$^2$, but smaller, 0.25 × 0.25 m$^2$ pool was used for Test 14. The water content of the wood was 9.7 % of the mass in the beginning of the experiments. Due to the different ignition mechanisms only the later of the two tests (Test 14) can be used as a calibration test.

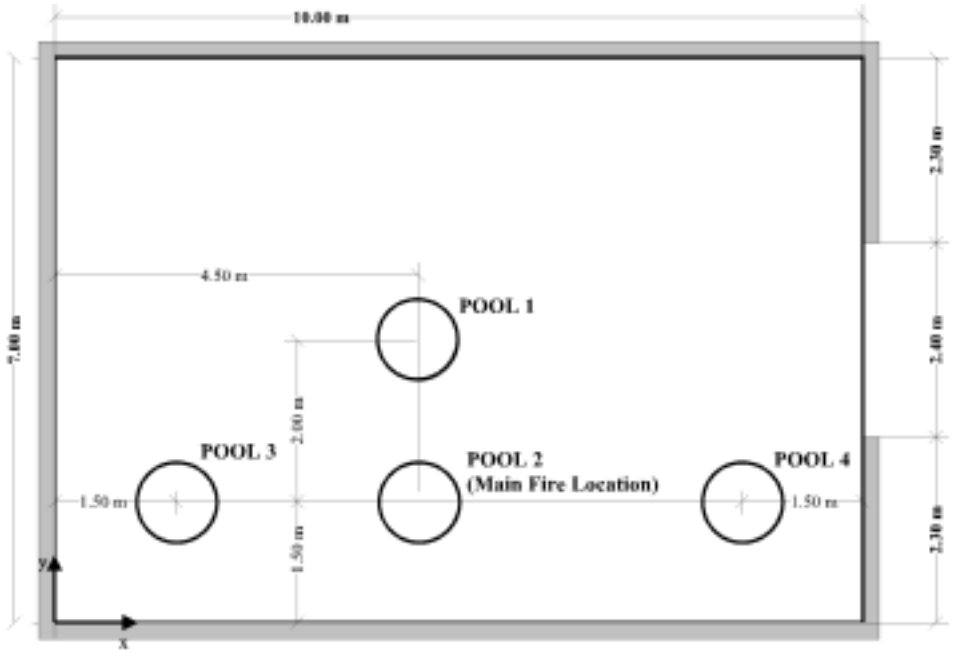


*Figure 3. Heptane pool locations in test room. The wooden fire load was placed in the main fire location (location 2).*

## 2.3 Test programme

Test series consisted of 10 different fires and 21 experiments. Some of the fires could therefore be repeated more than once. The following parameters were varied during the test series:

1. Pool size was varied to capture the effect of the heat release rate. Four different pool sizes were used: 0.40 m$^2$, 0.61 m$^2$, 1.07 m$^2$ and 2.0 m$^2$.

2. Four different pool locations were used. However, most experiments were done near the side wall, location 2 of Figure 3. The fire scenario was chosen to be asymmetric on purpose to avoid unwanted asymmetry that is possible due to the imperfect boundary conditions outside the room.

3. Door size was reduced from 2.4 m to 1.2 m in three experiments.

The key features of the fires are shown in Table 1. Some smaller variations were made in the instrumentation during the test series, but they will be explained later. The whole test series is summarised in Table 2. The first column shows the fire type, referring thus to Table 1, and second column shows the test number and date. Third column shows the pool location, fourth column shows the pool area and diameter and fifth column shows the duration of the experiment. The nominal amount of fuel and the approximated heat release rate are shown in the last two columns.

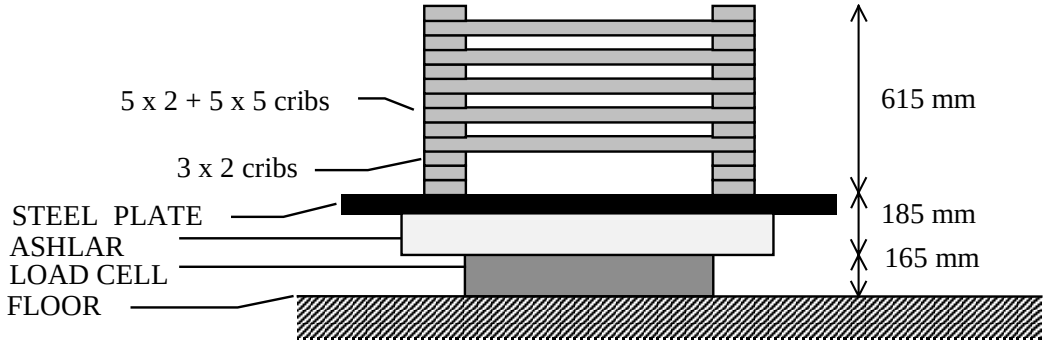


*Figure 4. Wooden fire load.*

*Table 1. Fire types in the NFSC 2 Room Test series in VTT. Fire type 10 is the interlaboratory calibration test.*

| Fire Type | Pool location | Pool area | Pool Diameter | Fuel surface height from the floor | Door width |
|---|---|---|---|---|---|
| 1 | #2 side wall | 0.40 $m^2$ | 0.71 m | 0.2 m | 2.4 m |
| 2 | #2 side wall | 0.61 $m^2$ | 0.88 m | 0.21 m | 2.4 m |
| 3 | #3 rear corner | 0.61 $m^2$ | 0.88 m | 0.21 m | 2.4 m |
| 4 | #1 center | 0.61 $m^2$ | 0.88 m | 0.21 m | 2.4 m |
| 5 | #4 front corner | 0.61 $m^2$ | 0.88 m | 0.21 m | 2.4 m |
| 6 | #2 side wall | 1.07 $m^2$ | 1.17 m | 0.44 m | 2.4 m |
| 7 | #1 center | 1.07 $m^2$ | 1.17 m | 0.44 m | 2.4 m |
| 7B | #1 center | 1.07 $m^2$ | 1.17 m | 0.44 m | 1.2 m |
| 8 | #2 side wall | 1.07 $m^2$ | 1.17 m | 0.44 m | 1.2 m |
| 9 | #2 side wall | 2.00 $m^2$ | 1.60 m | 0.25 m | 2.4 m |
| 10 | #2 side wall | Wood cribs | | | 2.4 m |

## 2.4 Instrumentation

About 150 channels of measurements and a video recording of the door side were made during the experiments. The measurement time step was one second during all the tests.

The following list presents the measured variables. Exact locations of the instruments are given in Appendix A.

1. Mass of the fuel was measured by placing the fuel on load cells. The mass loss rate was then calculated by numerical derivation of the mass curve. In the results, the data are shown as burning rates having positive values, instead of negative mass loss rates.

2. Gas temperatures were measured in three vertical rakes T1, T2 and T3. Each of these rakes consisted of 10 bare thermocouples (TCs) at different heights. In the beginning of the test series 0.1 mm TCs were used but starting from Test 12 0.5 mm TCs had to be used because the wires partially melted during Test 11. The locations of the gas temperature measurements are shown in Figures 5 and 6. The numbering of the TCs inside each rake goes from 1 to 10 starting from the lowest one.

3. Ceiling jet temperatures were measured using 0.5 mm thermocouples. 46 TCs (numbered C1–C46) were placed 0.10 m below the ceiling in the horizontal locations shown in Figure 7.

4. The horizontal temperature distribution inside the fire plume was measured with 25 thermocouples placed into a 5 x 5 grid above the pool location #2. The spacing of the TCs in the grid was 0.40 m. The numbering of the TCs is shown in Figure 13. The vertical position is shown in Figure 14. The height of the grid Zgrid was varied to keep the grid just above the flame tip, when the fire was in the location 2. When the fire source was in one of three other locations, the grid was placed 0.60 m below the ceiling. The values of Zgrid in each experiment are given in Appendix A. The thickness of the TCs was 0.5 mm.

5. Two 0.5 mm thermocouples (F1 and F2) were placed to the flame zone of the fire in location #2. F1 and F2 were located in the plume center line 1.00 m and 1.95 m below the grid, as shown in Figure 14. The actual purpose of these measurements was not to give a reliable measurement of the flame temperature, but to perform as indicators of the ignition time during the data processing.

6. Door jet gas temperatures were measured with 12 thermocouples (0.5 mm) in locations shown in Figure 8. All these TCs were in the same vertical plane with the outer surface of the wall.

7. Heat fluxes to thin steel objects were measured using ten plate thermometers placed P1…P10 in the locations shown in Figure 9. P1, P2, P3 and P10 were placed on the wall of the room. P4, P5, P7 and P8 in turn were placed just below the ceiling and P6 and P9 on the floor.

8. Heat fluxes to massive bodies were measured with one Gardon-type (R1) and four Schmidt-Boelter type heat flux gauges. The locations of the gauges R1–R5 are shown in Figure 10.

9. Six non-loaded steel tubes with round cross section were set-up to various positions in the room. Temperatures of the tubes were measured by attaching two thermocouples on each tube (S1–S12). The locations of the steel tubes are shown in Figures 11 and 12 and the dimensions are given in the following table.

| Steel tube properties | |
|---|---|
| Length | 800 mm |
| Diameter | 139.7 mm |
| Wall thickness | 5 mm |
| Weight | 14.3 kg |
| Material | Fe 52 D |

Unfortunately, the measurements were made using new data acquisition equipment being apparently incapable of measuring temperatures with thermocouples being attached to an electrically conductive material like steel. For that reason the steel temperatures are considered unreliable, and are **not reported**.

10. Heating of the lightweight concrete walls were measured using three measurement blocks. Each block had three thermocouples drilled near the block surface at different depths. The locations of the measurement blocks W1, W2 and W3 are shown in Figure 11.

11. Gas flow velocities were measured with bi-directional probes. Two probes (V1 and V2) were placed into the ceiling jet, 0.10 m below the ceiling in places shown in Figure 11. Six probes (V3 to V8) were placed to the door jet, as show in Figure 8.

*Table 2. NFSC 2 Room Test series in VTT. $\Delta m_{fuel}$ is the change of the load cell reading during the fire.*

| Fire Type | Test No. & Date | Pool location | Pool size | Duration (min) | Nominal amount of fuel | Nominal RHR (kW) | $\Delta m_{fuel}$ (kg) |
|---|---|---|---|---|---|---|---|
| 1 | Test 0 12.10.98 | #2 | 0.40 $m^2$ D = 0.71 m | 4:00 | 4 l (20 mm) | 950 | 2.92 |
| 1 | Test 1 13.10.98 | #2 | 0.40 $m^2$ D = 0.71 m | 4:00 | 4 l (20 mm) | 950 | 3.03 |
| 1 | Test 2 14.10.98 | #2 | 0.40 $m^2$ D = 0.71 m | 8.27 | 10 l (50 mm) | 1 440 | 7.22 |
| 2 | Test 3 15.10.98 | #2 | 0.61 $m^2$ D = 0.88 m | 7:45 | 15 l (20 mm) | 1 440 | 11.09 |
| 2 | Test 4 15.10.98 | #2 | 0.61 $m^2$ D = 0.88 m | 7:55 | 15 l (20 mm) | 1 440 | 11.48 |
| 2 | Test 5 16.10.98 | #2 | 0.61 $m^2$ D = 0.88 m | 8:14 | 15 l (20 mm) | 1 440 | 11.39 |
| 3 | Test 6 16.10.98 | #3 | 0.61 $m^2$ D = 0.88 m | 7:55 | 15 l (20 mm) | 1 440 | 11.04 |
| 4 | Test 7 19.10.98 | #1 | 0.61 $m^2$ D = 0.88 m | 8:00 | 15 l (20 mm) | 1 440 | 10.92 |
| 4 | Test 8 19.10.98 | #1 | 0.61 $m^2$ D = 0.88 m | 7:45 | 15 l (20 mm) | 1 440 | 10.97 |
| 5 | Test 9 20.10.98 | #4 | 0.61 $m^2$ D = 0.88 m | 7:18 | 15 l (20 mm) | 1 440 | 11.10 |
| 10 | Test 10 20.10.98 | #2 | Wood cribs | 21:30 (extinguished) | 50 kg | 700 | 38.21 |
| 6 | Test 11 21.10.98 | #2 | 1.07 $m^2$ D=1.17 m | 5:15 | 20 l | 2500 | 15.28 |
| 6 | Test 12 21.10.98 | #2 | 1.07 $m^2$ D=1.17 m | 5:07 | 20 l | 2500 | 14.60 |
| 6 | Test 13 22.10.98 | #2 | 1.07 $m^2$ D=1.17 m | 5:21 | 20 l | 2500 | 15.02 |
| 10 | Test 14 22.10.98 | #2 | Wood cribs | ≈ 40 min | 50 kg | 700 | 51.09 |
| 7 | Test 15 23.10.98 | #1 | 1.07 $m^2$ D=1.17 m | 5:15 | 20 l | 2500 | 14.79 |
| 7B | Test 16 23.10.98 | #1 | 1.07 $m^2$ D=1.17 m | 5:20 | 20 l | 2500 | 14.33 |
| 8 | Test 17 26.10.98 | #2 | 1.07 $m^2$ D=1.17 m | 5:20 | 20 l | 2500 | 14.37 |
| 8 | Test 18 26.10.98 | #2 | 1.07 $m^2$ D=1.17 m | 5:29 | 20 l | 2500 | 14.72 |
| 9 | Test 19 27.10.98 | #2 | 2.0 $m^2$ D=1.60 m | 5:30 | 40 l | 4800 | 21.81 |
| 9 | Test 20 27.10.98 | #2 | 2.0 $m^2$ D=1.60 m | 9:30 | 80 l | 4800 | 59.27 |

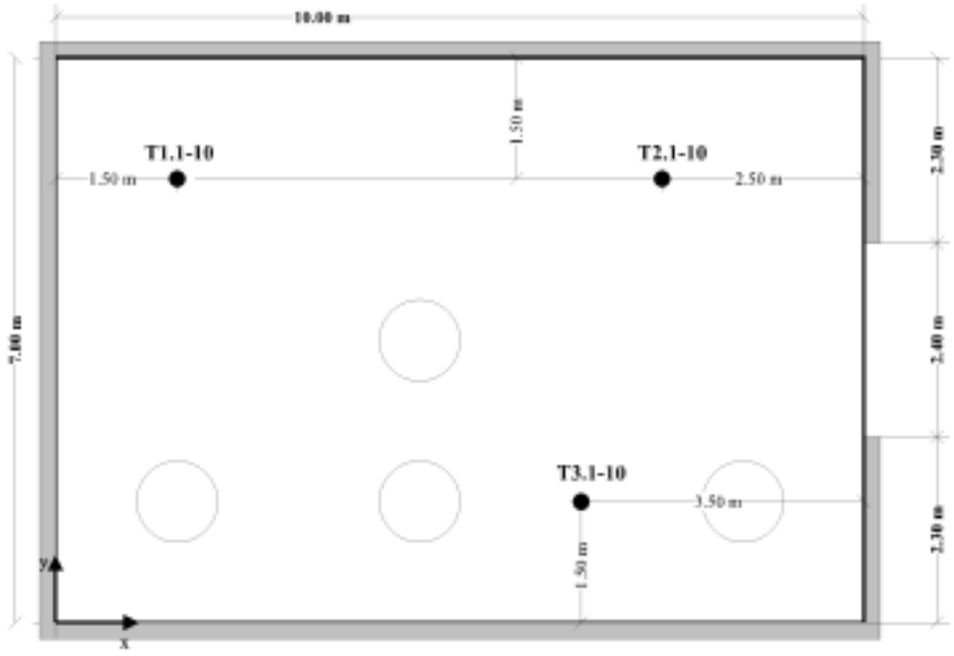


*Figure 5. Horizontal locations of the thermocouple rakes for gas temperature measurement.*

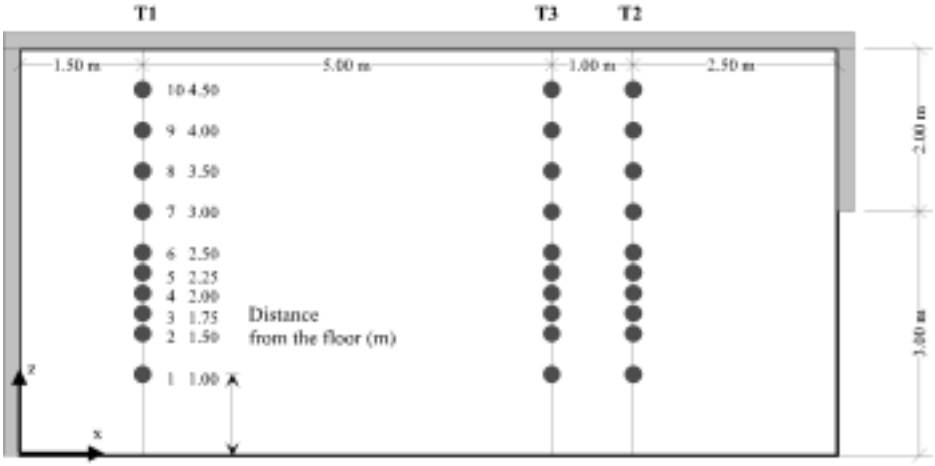


*Figure 6. Vertical locations of the thermocouples for gas temperature measurement.*

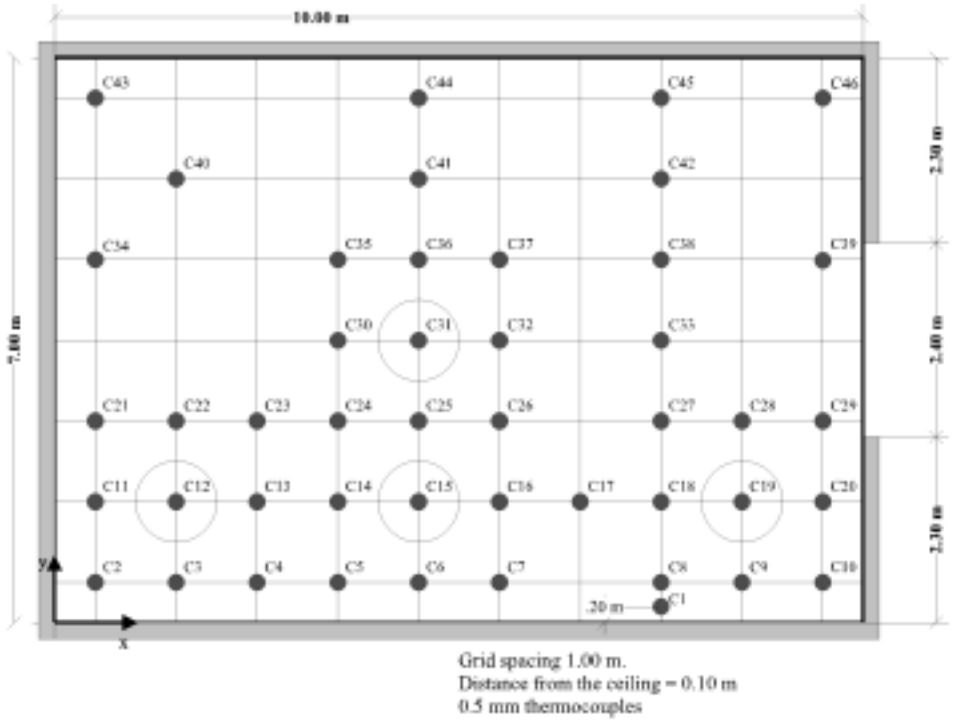


*Figure 7. Thermocouple locations for the ceiling jet temperature measurement.*

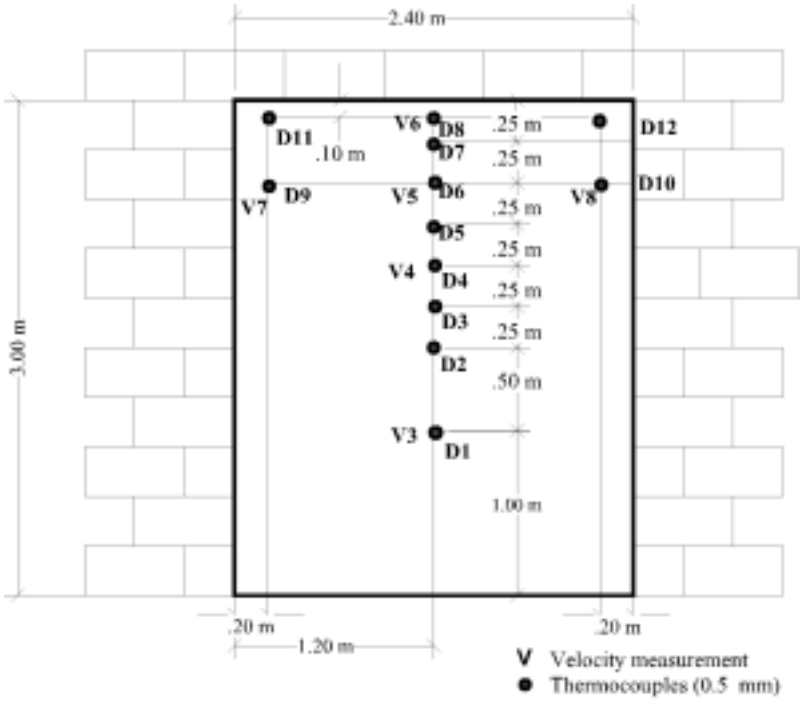


*Figure 8. Locations of the door gas temperature (D) and velocity (V) measurements.*

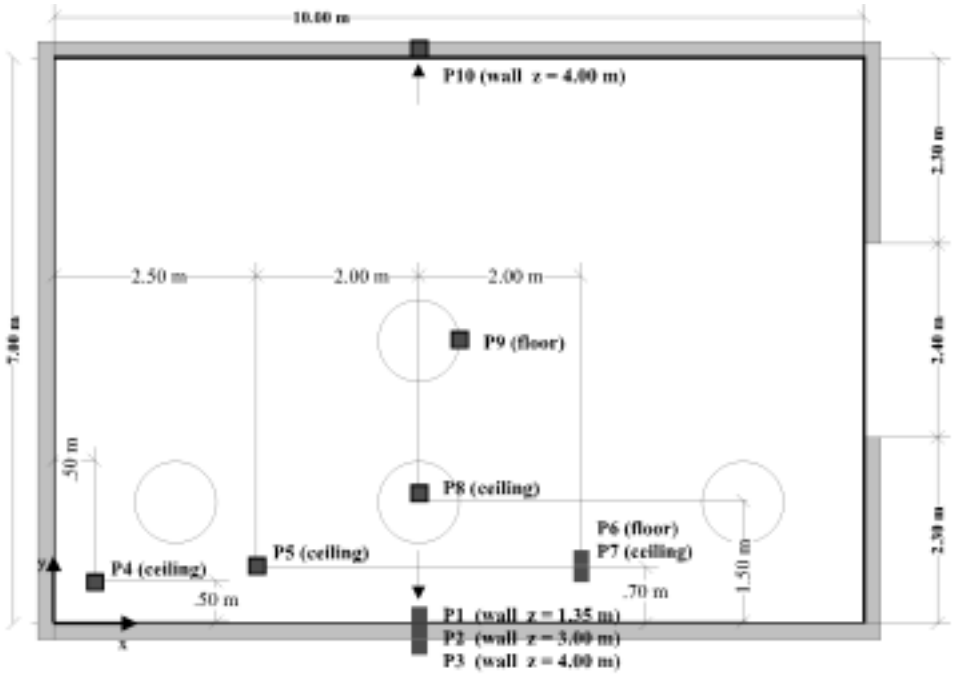


*Figure 9. Locations of the plate thermometers.*

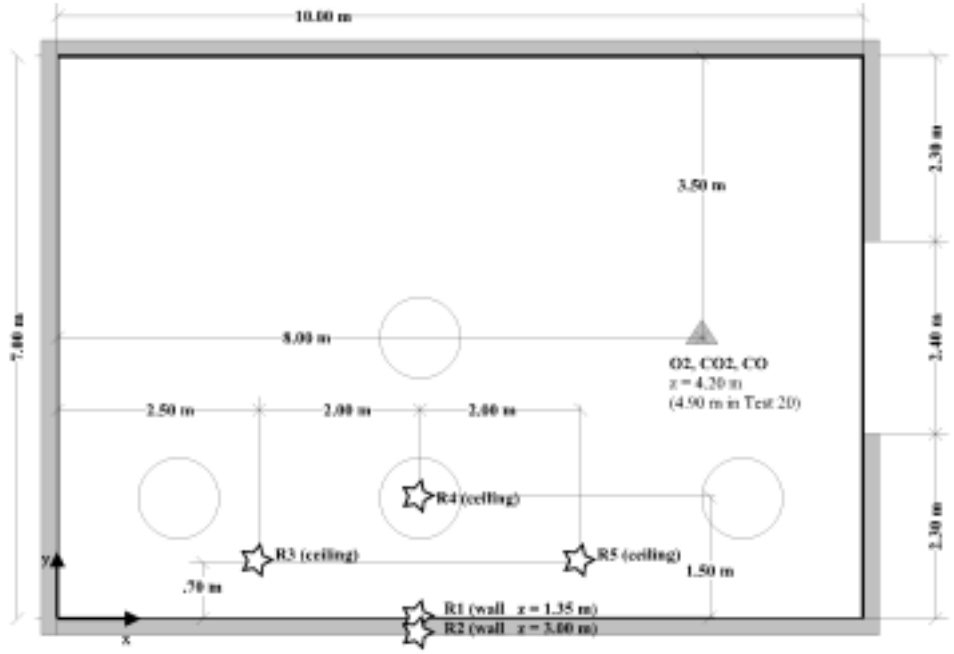


*Figure 10. Locations of the heat flux gages and the gas sample line.*

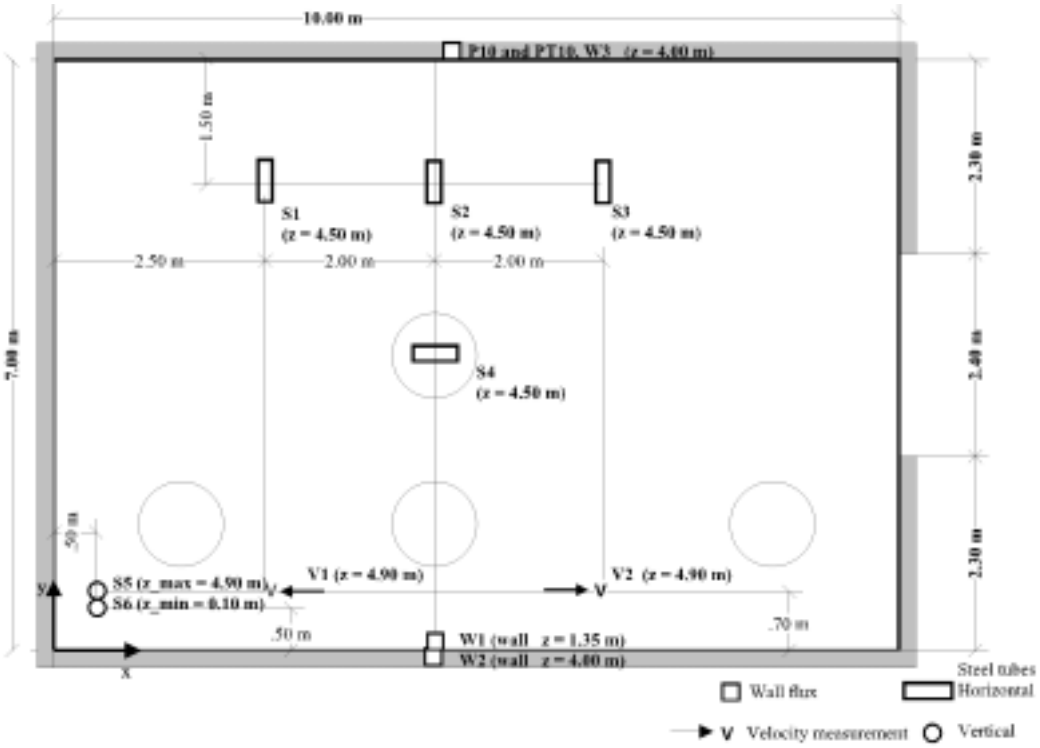


*Figure 11. Locations of the steel tubes (S1-S6), wall heat flux measurement blocks (W1-W3) and the ceiling jet velocity measurement probes (V1 and V2). The arrows show the direction of the positive velocity.*

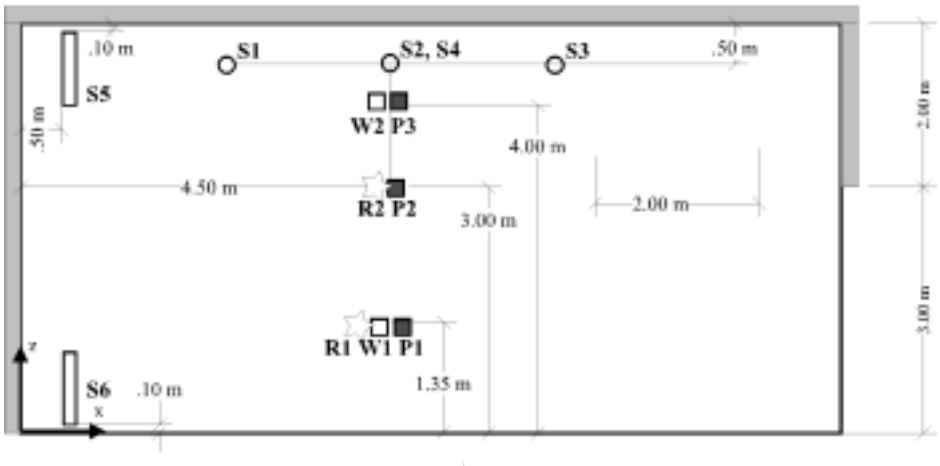


*Figure 12. Vertical view of the steel tube and wall instrumentation locations.*

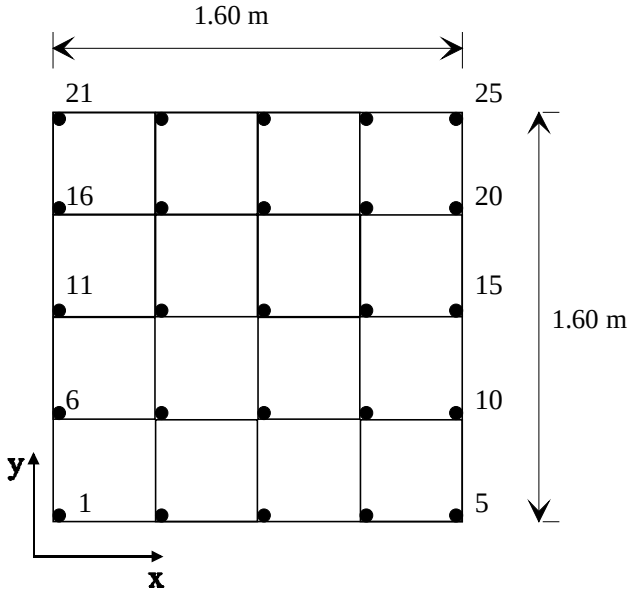


*Figure 13. Size and numbering of the plume temperature measurement grid.*

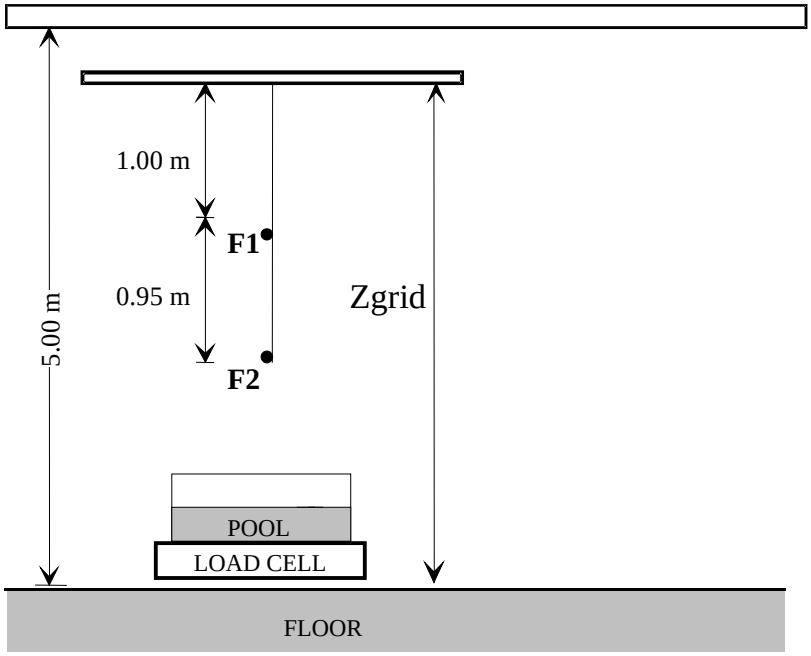


*Figure 14. Positions of the plume and flame temperature measurements.*

# 3. Results of the room experiments

## 3.1 Calculation of the interface height and layer temperatures

An obvious variable for the comparison of the test and calculation results is the upper layer temperature in association with the height of the layer interface. Several methods for their experimental determination have been reported during the years. A traditional method of Cooper *et al*. (1982) is the so-called *N-percent rule*. In this method the interface height $z_i$ at time $t$ is defined to be the elevation at which the temperature first satisfies the following equation

$$\frac{T(z_{i1},t)-T_{amb}}{T(z_{top},t)-T_{amb}}=\frac{N}{100} \tag{2}$$

In the literature the values suggested for $N$ range from 10 to 20. The average temperatures in the upper and lower layers ($T_{up1}$ and $T_{low1}$) are then calculated as mean values of the measurements in the upper and lower sides of $z_{i1}$, respectively.

Mathematically more consistent method for the comparison of experimental and zone model data is to calculate the volumetric temperature and density integrals of the room space and find the three unknowns, $z_{i2}$, $T_{up2}$ and $T_{low2}$, that produce the same values for the integrals

$$(H-z_{i2})T_{up2}+z_{i2}T_{low2}=\int_0^H T(z,t)dz=I_1 \tag{3}$$

$$(H-z_{i2})\frac{1}{T_{up2}}+z_{i2}\frac{1}{T_{low2}}=\int_0^H\frac{1}{T(z,t)}dz=I_2\,. \tag{4}$$

Equation (3) results from the definition of the zone model concept, and Equation (4) from the conservation of mass in the zone model approximation. Assuming that $T_{low2}$ can be taken from the lowest measurement points, the interface height can be solved from the above equations

$$z_{i2}=\frac{T_{low2}\left(I_1\cdot I_2-H^2\right)}{I_1+I_2T_{low2}^2-2T_{low2}H}\,. \tag{5}$$

$T_{up2}$ is then calculated as a mean value of $T(z,t),\ z\geq z_i$. An example of the resulting temperature profile is shown in Figure 15.

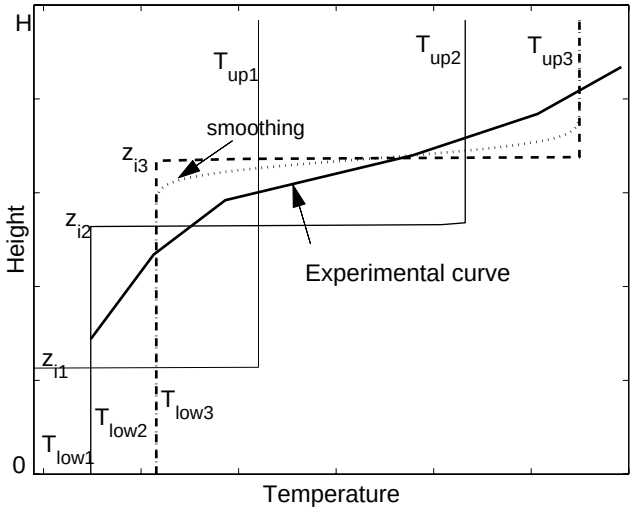


*Figure 15. Examples of the experimental and calculated temperature profiles.*

Yet another method is presented by He *et al*. (1998) where the three unknowns $z_i$, $T_{up}$ and $T_{low}$ are calculated by minimizing the quadratic error of assumed zone shape temperature profile and the measured profile, shown in Figure 15. A square root of the quadratic error was used in a form

$$E(z_i, T_{up}, T_{low}, t) = \left\{ \int_0^{z_i} \left[T(z,t) - T_{low}\right]^2 dz + \int_{z_i}^{H} \left[T(z,t) - T_{up}\right]^2 dz \right\}^{1/2} \tag{6}$$

and the resulting interface height and layer temperatures were chosen such that

$$E(z_{i3}, T_{up3}, T_{low3}, t) = \min_{\Omega^-}\{E\}, \ (z_i, T_{up}, T_{low}) \in \Omega^- \tag{7}$$

where $\Omega^-$ is a local neighborhood of the values $z_{i3}$, $T_{up3}$ and $T_{low3}$ at time $t$-$\Delta t$, where $\Delta t$ is the measurement time step. Here, for numerical stability of the minimization process a little bit smoothed version of the step function can be used by defining arbitrarily the temperature profile as

$$T_3(z) = T_{low3} + \frac{T_{up3} - T_{low3}}{2}\left\{1 + erf\left[10 \cdot (z - z_{i3})\right]\right\} \tag{8}$$

shown with dotted line in Figure 15. However, the calculation of the minimum with this function can be relatively slow.

In this work the integral method, ie. Equation (5), was used. The reliability of the interface height results was checked by applying the other two methods as well. It was

observed that all the methods gave very similar results, which is natural as the fire scenario was a very typical two layer situation.

## 3.2 Radiation errors in thermocouples

Bare thermocouples were used to measure the gas temperatures during the experiment. Two kinds of radiation errors were expected to take place: First, the flame temperatures were assumed to be underpredicted as the thermocouple head radiates heat to the relatively cold surrounding of the flame. However, as the role of the flame temperature measurements was not so important in this test series, a quantitative analysis of these errors is not made. Secondly, the lower layer gas temperatures are typically overpredicted by bare thermocouple measurements because of the radiation from the flame. Rough estimates of this error were actually measured by two methods: *i*) By using thermocouples of two different sizes (0.1 and 0.5 mm) and *ii*) by placing thin folios between the lowest thermocouples and the flame. An example of the observed radiation errors is shown in Figure 16, showing almost 50°C error in temperature. As the smoke from the heptane fires is quite non-transparent, it was assumed that the upper layer thermocouples see only the surrounding smoke, not the flame, and the errors inside the hot layer are can be assumed small.

Several methods have been reported for the estimation of radiation errors. Following the procedure of Blevins & Pitts (1999) the bare thermocouple is assumed to be in a flowing gas of temperature $T$ surrounded by hot surfaces in temperature $T_s$. Let us define the radiation error as difference of the thermocouple reading $T_{TC}$ and true gas temperature $\Delta T_R = T_{TC} - T$. Based on the energy balance of the thermocouple and its surroundings the radiation error can be calculated from the following equation

$$\Delta T_R = \frac{\sigma\varepsilon}{h}\left(T_s^4 - T_{TC}^4\right). \tag{9}$$

where $\sigma$ is Stefan-Boltzman constant 56.7 nW/m$^2$K$^4$, $\varepsilon$ is emissivity of the thermocouple surface. $h$ is the convection coefficient, which can be can be calculated from the properties of the thermocouple and the surrounding gas using the following equation

$$h = \frac{\lambda}{d}\left(2 + 0.6\sqrt{\mathrm{Re}}\sqrt[3]{\mathrm{Pr}}\right). \tag{10}$$

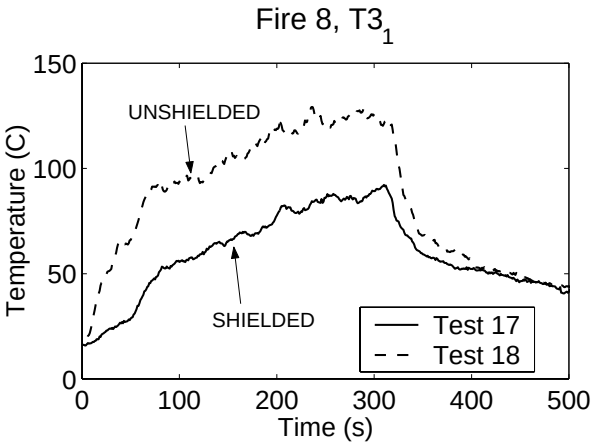


*Figure 16. An example of the radiation error caused by the flame radiation to the lowest temperature measurement in rake T3.*

where $d$ is the diameter of thermocouple head, $\lambda$ is thermal conductivity of air (0.0257 W/Km) and Pr is the air Prandtl number (Pr = 0.7). Re is the Reynolds number Re=$\rho ud/\mu$, where $u$ is flow velocity and $\mu$ is the dynamic viscosity of air. Both $\lambda$ and $\mu$ were assumed to be temperature dependent by correlations found in most fluid dynamic text books, but usually an adequate accuracy is achieved by using constant values.

In the experiment the source of the radiation is the flame above the pool. The size of the radiating surface can therefore be normalized using the measured burning rate $\dot{m}$. The temperature of the radiating surface is the average flame temperature $T_F$. Here it is assumed to be 1200 K. The equation for the radiation error now becomes

$$\Delta T_R(t,\dot{m}(t)) = \frac{\sigma\varepsilon}{h}\left(\phi_{FTC}\frac{\dot{m}(t)}{\max(\dot{m}(t))}T_F^4 - T_{TC}^4\right) \tag{11}$$

where $\phi_{FTC}$ is the effective configuration factor from flame to thermocouples during the strongest phase of the fire.

The current model has basically two unknown parameters: $u$ and $\phi_{FTC}$. These parameters were calibrated by fitting the estimated radiation errors to the measured errors. As the parameters were found, the current error model was used to correct the measured temperatures at *three lowest thermocouples* of each of the rakes T1, T2 and T3. Some errors are therefore left to the higher TCs in the very beginning of each test.

## 3.3 Time averaging

For the comparison with most computational models the experimental results must be smoothed. This smoothing is made by time averaging over a sliding window of width $t_w$. The length of the window is chosen to give as smooth data as possible, but retaining the fluctuations related to the natural time scales of the smoke layers. The following approximation was used

$$t_w = \frac{1}{2}\frac{V_{up}}{\dot{V}_{out}} \tag{12}$$

where $V_{up}$ is the upper layer volume and $\dot{V}_{out}$ is the volumetric flow out of the room. For most test of the current test series width $t_w$ = 20 s was used.

## 3.4 Baseline noise distribution

To estimate the source and magnitude of the fluctuations in the measured quantities it is necessary to distinguish the noise generated by the measurement instrumentation. This information was gained by measuring the baseline signal before the actual experiments. Figure 17 shows the distribution of noise for various quantities in Tests 3 and 4. As can be seen, the scattering from the mean value is typically less than 0.5 °C for temperature measurements, less than 0.1 kW/m$^2$ for heat fluxes and less than 0.1 m/s for velocities.

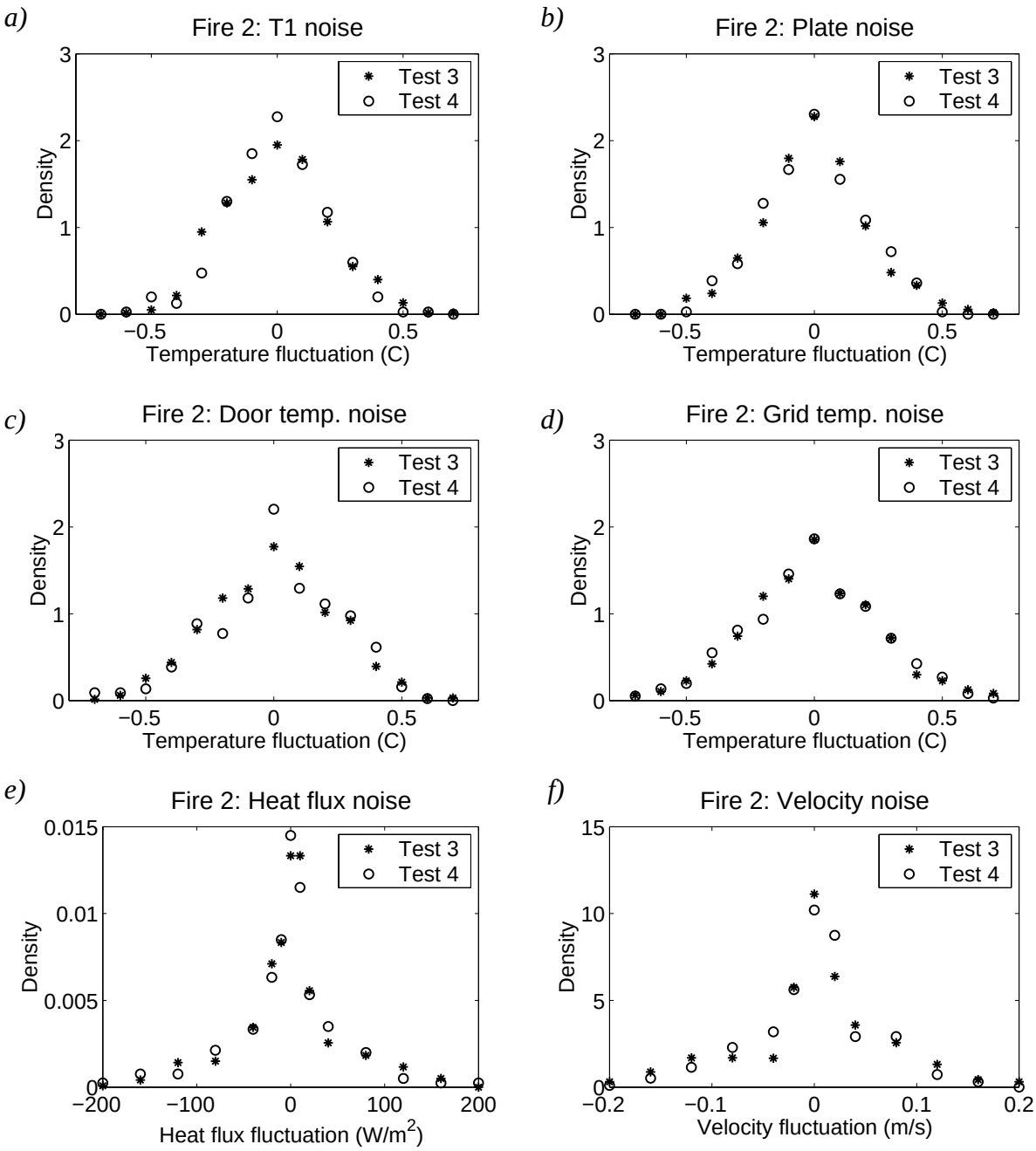


*Figure 17. Noise distributions before the ignition in Fire 2: a) Gas temperature measurements in rake T1. b) Plate thermometers. c) Door jet gas temperature. d) Grid gas temperatures. e) Heat flux gauges. f) Velocity measurements.*

## 3.5 Fluctuations during the fires

Many of the measured quantities contained very strong fluctuations during the fire. Although some noise was generated by the measurement system itself, as shown in the previous section, the most important source of fluctuations was turbulence. Different

scales of fire generated turbulence affected on practically all measurements but the conventional measurement techniques are not capable of capturing these scales in a manner that is needed for CFD model validation. However, to give a picture of the strength of the observed fluctuations, a series of figures, analogous to previous section, is given showing the effect of the pool size on the fluctuation distributions.

Here it must be noticed that all the measurement devices have relatively large inertia meaning that they are slow, when compared to the turbulent time scales. Time constants of the thermocouples measuring gas temperature, for example, are about 0.5 seconds (0.1 mm TC) or 3 seconds (0.5 mm TC). Faster fluctuations are therefore filtered off by the measurement device. Another limiting factor is the time step of one second.

Figure 18 shows the fluctuation distributions for various variables in Fires 1, 2, 6 and 9. Figure a) shows the fluctuations for gas temperatures in rake T1, averaged over thermocouples 3–10. The lowest two thermocouples had much narrower distributions. It can be seen, that the distributions become narrower, as the 0.1 mm thermocouples were replaced by 0.5 mm thermocouples between Fires 2 and 6. In all other variables the distributions become wider as the fire becomes stronger.

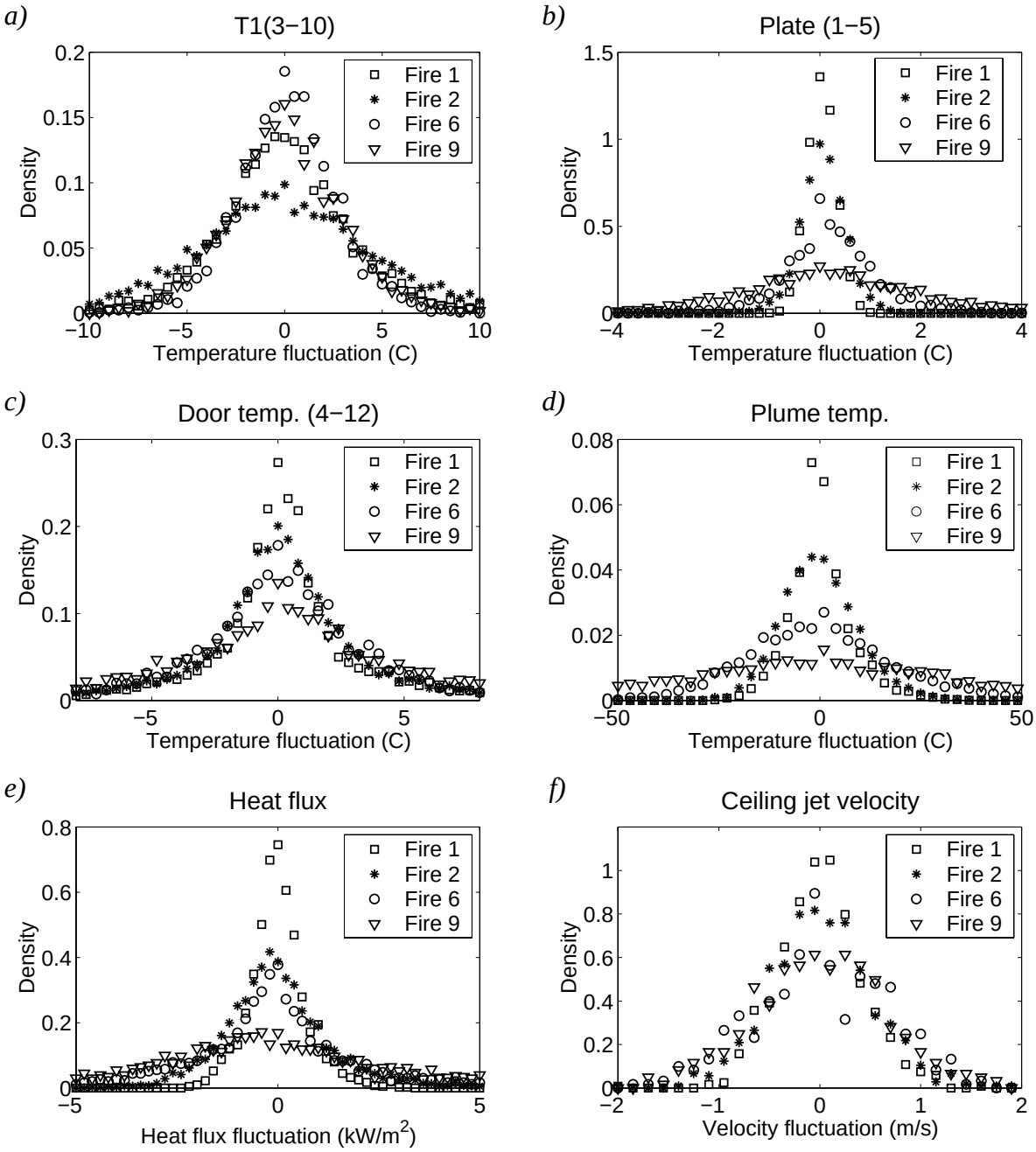


*Figure 18. Effect of the pool size on the noise distributions: a) Gas temperature measurements in rake T1 (TCs 3–10). b) Plate thermometers 1–5. c) Door jet gas temperatures 4–12. d) Plume gas temperatures (9 TCs in the center of the grid). e) Heat flux gauges. f) Ceiling jet velocity measurements.*

## 3.6 Experimental uncertainty and error limits

The order of the experimental uncertainty is shown as errorbars in the figures presenting the results of the test series. The experimental uncertainties of the time averaged

quantities were estimated from the scattering of the results from repeated tests like Tests 0, 1 and 2 (Fire 1), Tests 7 and 8 (Fire 4) and Tests 11, 12 and 13 (Fire 6). The same level of uncertainty was then applied to those tests, where no repeated tests were made. This of course does not take into account the systematic uncertainty that is related to some measurements like velocities. The overall uncertainties of the point measurements, like gas temperatures, flow velocities and heat fluxes, were estimated based on the *magnitude of the fluctuations*, by showing the 90 % confidence interval around the time averaged value. For most cases the error limits are about 10 % of the measured value.

## 3.7 Effect of the pool size

The effect of the pool size on various variables is shown in Figure 19. The results are given for fires 1, 2, 6 and 9, having pool sizes 0.40, 0.61, 1.07 and 2.0 $m^2$, respectively. The error bars have two different meanings: For burning rates, layet temperatures and interface heights they indicate the scattering between the individual tests, but for all the other quantities they indicate the 90 % limits for the fluctuations.

Figure 19a shows the burning rate per fuel area. As can be seen, the burning rate is stronger with the larger pools, which is probably due to the increased radiation from the hot gas layer to the fuel surface. Figure 19c shows that the interface height is practically independent of the pool size, although the mean and local temperatures, Figures 19b, c and d, clearly get higher when the pool size is increased. The large errorbars of the velocity measurements in Figures 19f–j are caused by the strong fluctuations of the data, and assumed uncertainty caused by the long pressure lines of the bi-directional probes. Large uncertainties were also related to the heat flux measurements of Fire 9, shown in Figures 19k–n. The temperatures of the gas and structures became so high during the tests of Fire 9, that the water cooling of the heat flux gauges was assumed to be insufficient. Figure 19q shows the temperature difference between the ceiling jet and the mean temperature of the upper layer at time 200 s, on the line going above the fire source parallel to the x-axis. The temperature difference is scaled by the factor $\dot{Q}^{2/3}$, where $\dot{Q}$ is the rate of heat release. As can be seen from the figure, the power 2/3, which is found adequate for the unconfined ceiling jets (see e.g. Drysdale 1999), is not sufficient to describe the dependence on the RHR in confined case.

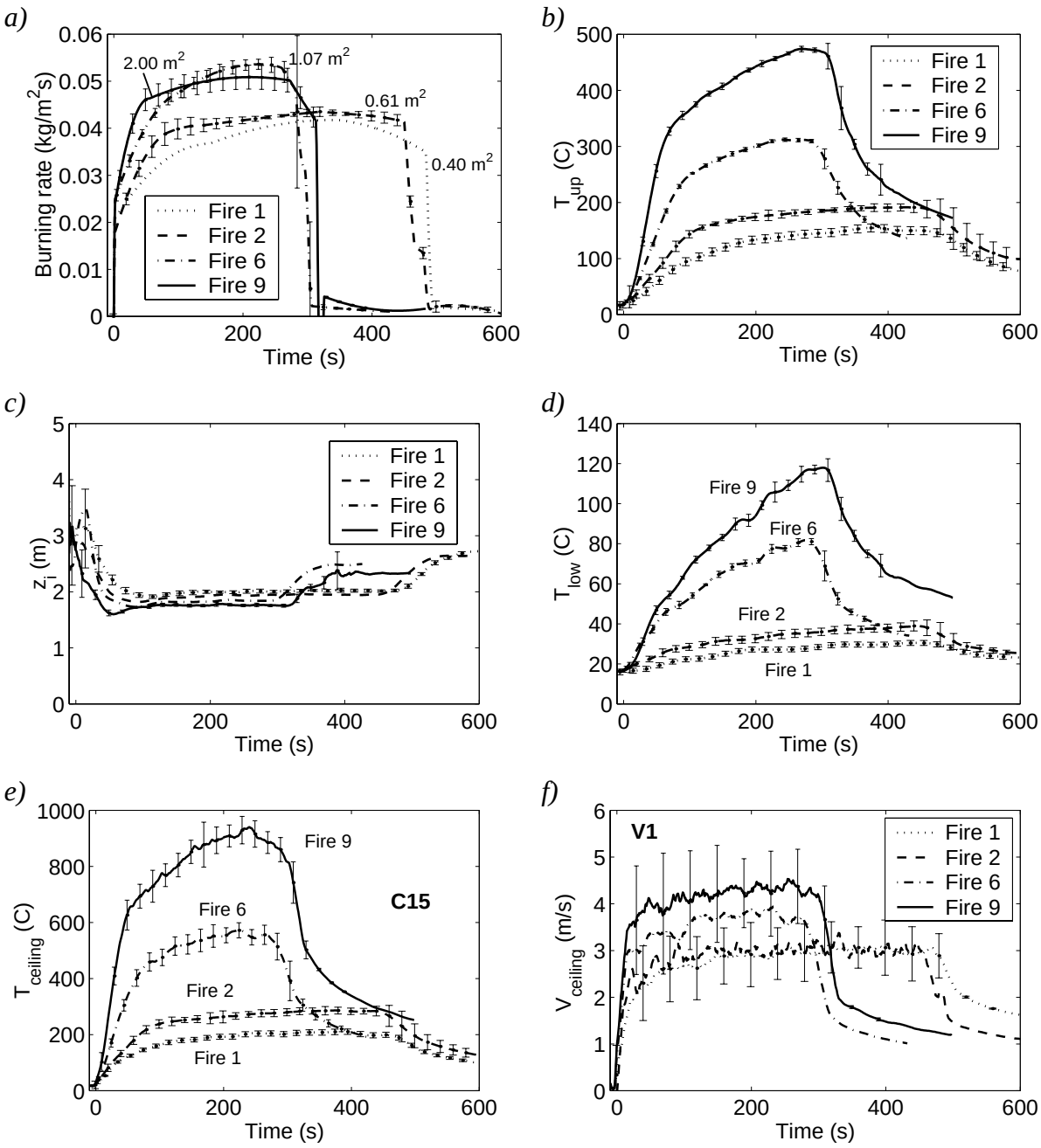
a)
Burning rate (kg/m2s)
Time (s)
2.00 m2
1.07 m2
0.61 m2
0.40 m2
Fire 1
Fire 2
Fire 6
Fire 9
b)
T up (C)
Time (s)
c)
z i (m)
Time (s)
d)
T low (C)
Time (s)
Fire 9
Fire 6
Fire 2
Fire 1
e)
T ceiling (C)
Time (s)
C15
f)
V ceiling (m/s)
Time (s)
V1

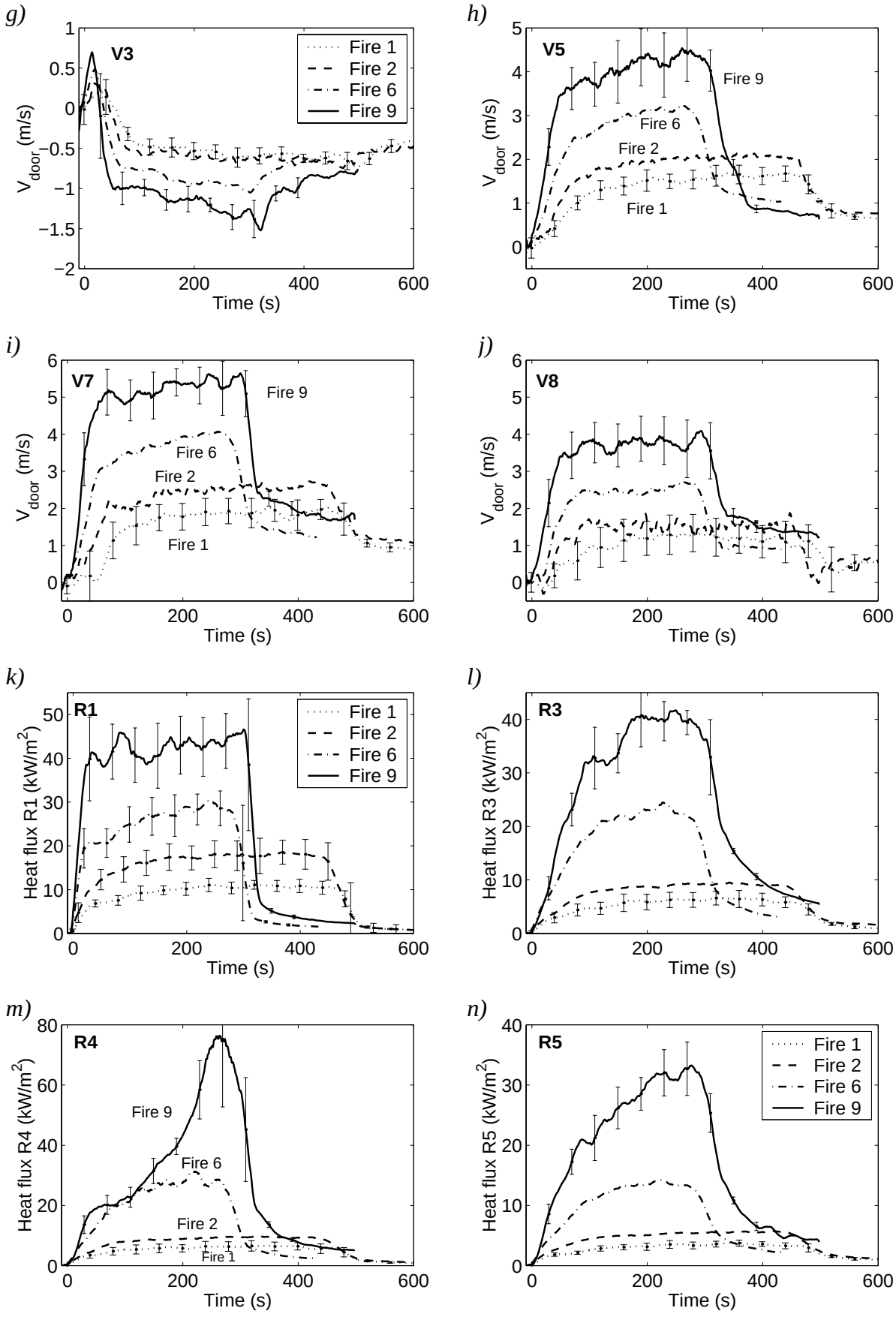
g)
V3
Fire 1
Fire 2
Fire 6
Fire 9
V_door (m/s)
Time (s)
h)
V5
Fire 9
Fire 6
Fire 2
Fire 1
V_door (m/s)
Time (s)
i)
V7
Fire 9
Fire 6
Fire 2
Fire 1
V_door (m/s)
Time (s)
j)
V8
V_door (m/s)
Time (s)
k)
R1
Fire 1
Fire 2
Fire 6
Fire 9
Heat flux R1 (kW/m2)
Time (s)
l)
R3
Heat flux R3 (kW/m2)
Time (s)
m)
R4
Fire 9
Fire 6
Fire 2
Fire 1
Heat flux R4 (kW/m2)
Time (s)
n)
R5
Fire 1
Fire 2
Fire 6
Fire 9
Heat flux R5 (kW/m2)
Time (s)

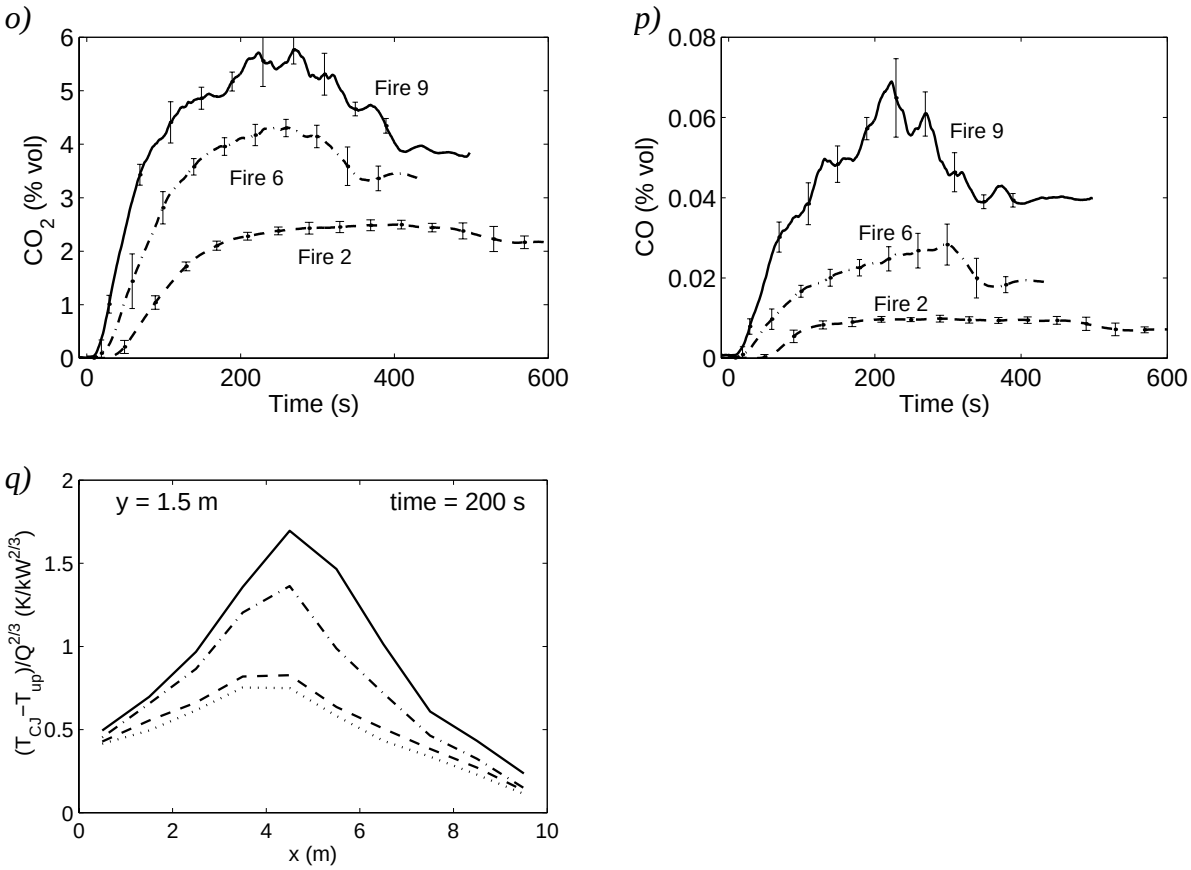


*Figure 19. Effect of the pool size on:*

*a) Burning rate.*
*b) Upper layer temperature.*
*c) Interface height.*
*d) Lower layer temperature.*
*e) Ceiling jet temperature C15 directly above the fire.*
*f) Ceiling jet velocity V1.*
*g)–j) Door flow velocities V3, V5, V7 and V8.*
*k)–n) Heat fluxes R1, R3, R4 and R5.*
*o) $CO_2$ concentration.*
*p) CO concentration.*
*q) Scaled temperature rise in the ceiling jet in x-direction at time = 200 s.*

*For figures a-d the error bars indicate the scattering between the time averages of the individual tests, but for other figures they indicate the 90 % limits for the fluctuations.*

## 3.8 Effect of the pool location

The effect of the pool location is studied in Figure 20 by making a comparison of results from Fires 2, 3, 4 and 5 with pool locations #2, #3, #1 and #4, respectively. Most variables seem to be practically independent of the location of the fire source. Some effect can be seen in the door velocities. The effect on the heat fluxes is naturally strong, because the measurement locations were unchanged.

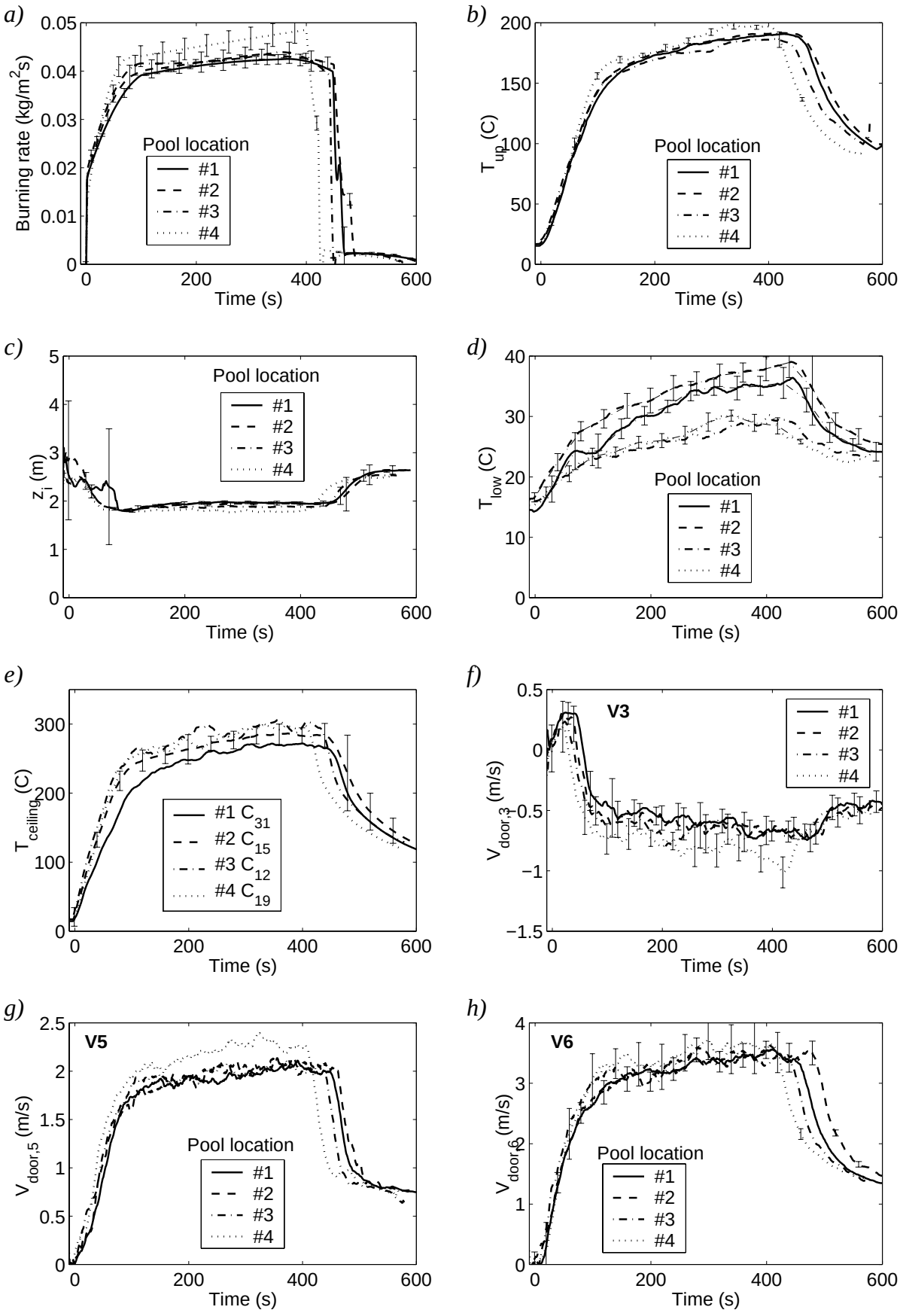
a)
Burning rate (kg/m$^2$s)
Time (s)
Pool location
#1
#2
#3
#4
b)
$T_{up}$ (C)
Time (s)
Pool location
#1
#2
#3
#4
c)
$z_i$ (m)
Time (s)
Pool location
#1
#2
#3
#4
d)
$T_{low}$ (C)
Time (s)
Pool location
#1
#2
#3
#4
e)
$T_{ceiling}$ (C)
Time (s)
#1 $C_{31}$
#2 $C_{15}$
#3 $C_{12}$
#4 $C_{19}$
f)
V3
$V_{door,3}$ (m/s)
Time (s)
#1
#2
#3
#4
g)
V5
$V_{door,5}$ (m/s)
Time (s)
Pool location
#1
#2
#3
#4
h)
V6
$V_{door,6}$ (m/s)
Time (s)
Pool location
#1
#2
#3
#4

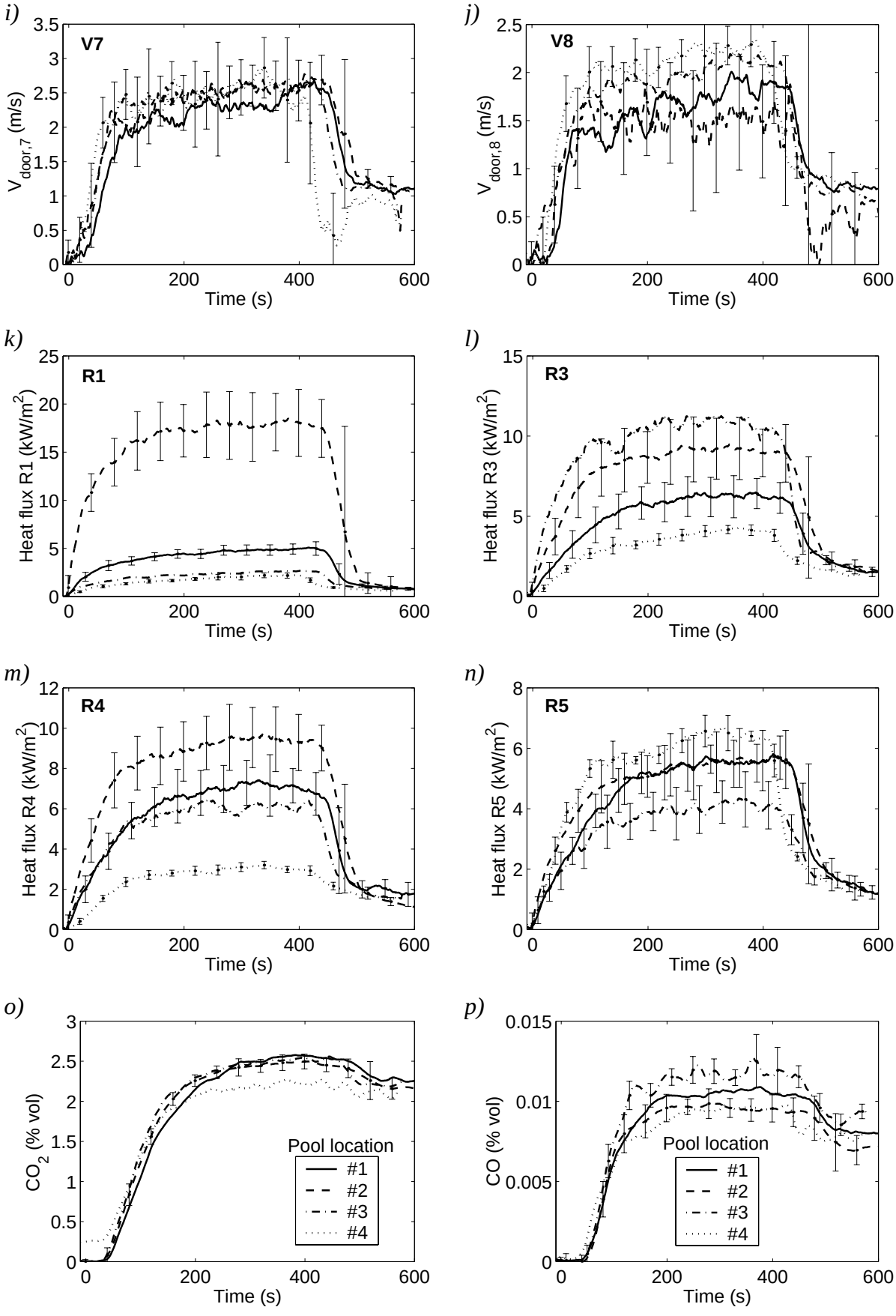
i)
V7
$V_{door,7}$ (m/s)
Time (s)
j)
V8
$V_{door,8}$ (m/s)
Time (s)
k)
R1
Heat flux R1 (kW/m$^2$)
Time (s)
l)
R3
Heat flux R3 (kW/m$^2$)
Time (s)
m)
R4
Heat flux R4 (kW/m$^2$)
Time (s)
n)
R5
Heat flux R5 (kW/m$^2$)
Time (s)
o)
$CO_2$ (% vol)
Pool location
#1
#2
#3
#4
Time (s)
p)
CO (% vol)
Pool location
#1
#2
#3
#4
Time (s)

*q)*

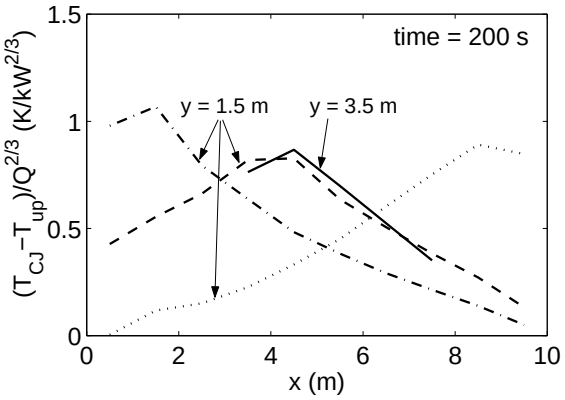


*Figure 20. Effect of the pool size on:*

*a) Burning rate.*
*b) Upper layer temperature.*
*c) Interface height.*
*d) Lower layer temperature.*
*e) Ceiling jet temperature C15 directly above the fire.*
*f)–j) Door flow velocities V3, V5, V6, V7 and V8.*
*k)–n) Heat fluxes R1, R3, R4 and R5. o) $CO_2$ concentration.*
*p) CO concentration.*
*q) Scaled temperature rise in the ceiling jet in x-direction at time = 200 s.*

*Meaning of the error bounds is explained in the caption of Figure 19.*

## 3.9 Effect of the door width

The effect of the door width is studied in Figure 21 by making a comparison of results from fires 6 and 8, where the door widths $w_d$ were 2.4 and 1.2 m, respectively. As a result of the narrowing of the door, the temperature inside the smoke layer seemed to increase, and the interface height became lower. Other effects, like heat fluxes, were naturally consequences of these effects.

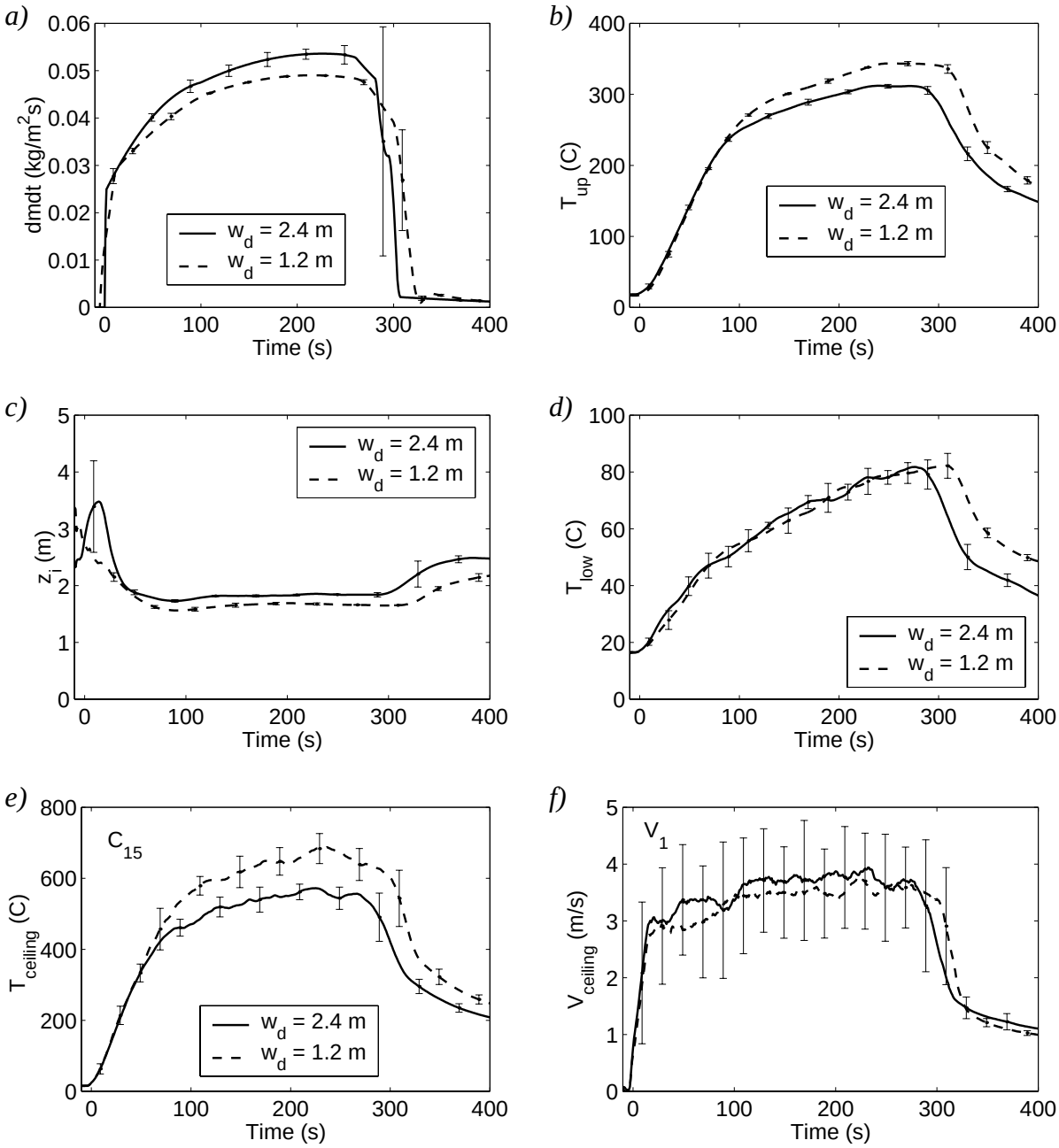

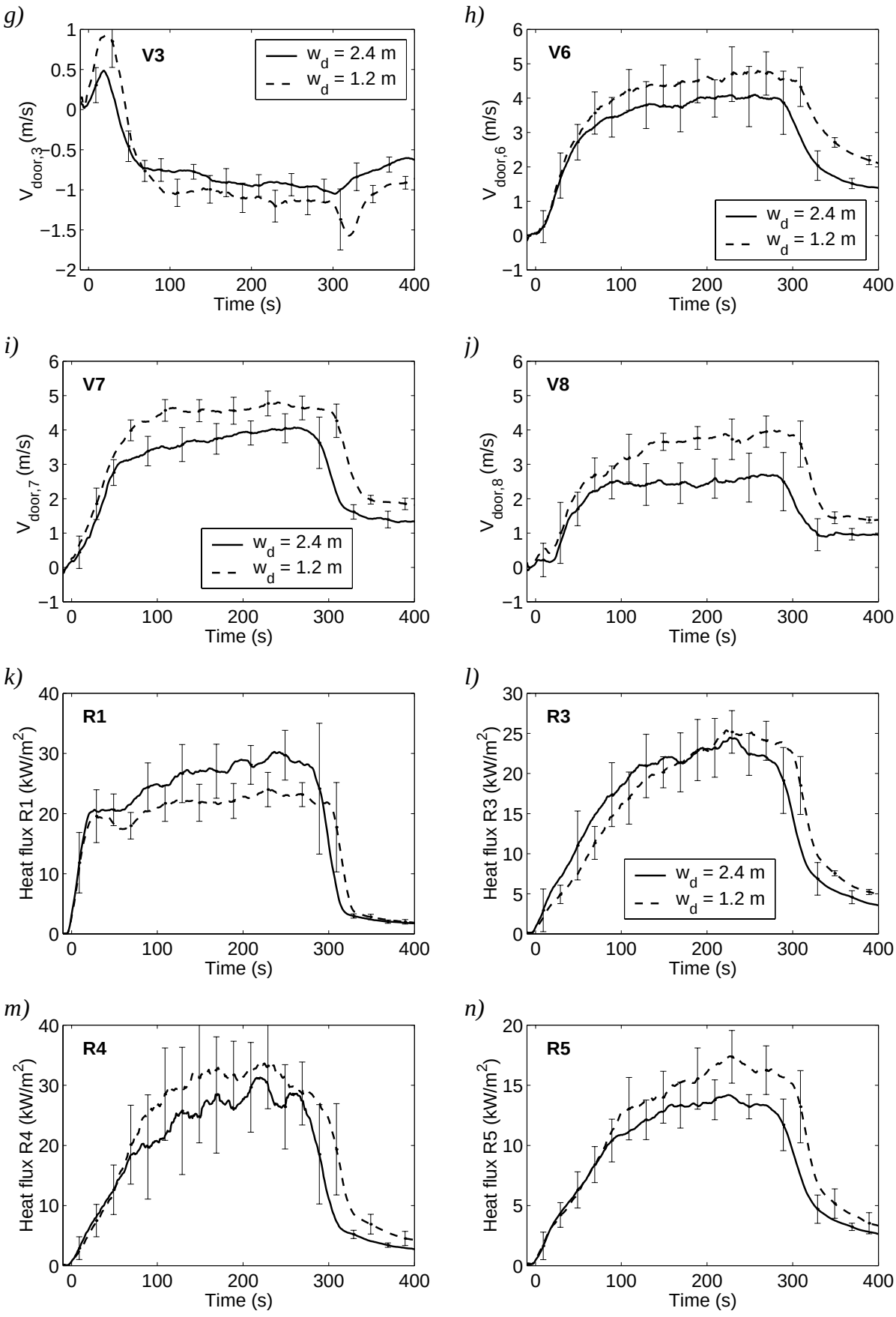
g)
V3
$w_d$ = 2.4 m
$w_d$ = 1.2 m
$V_{door,3}$ (m/s)
Time (s)
h)
V6
$V_{door,6}$ (m/s)
i)
V7
$V_{door,7}$ (m/s)
j)
V8
$V_{door,8}$ (m/s)
k)
R1
Heat flux R1 (kW/m$^2$)
l)
R3
Heat flux R3 (kW/m$^2$)
m)
R4
Heat flux R4 (kW/m$^2$)
n)
R5
Heat flux R5 (kW/m$^2$)

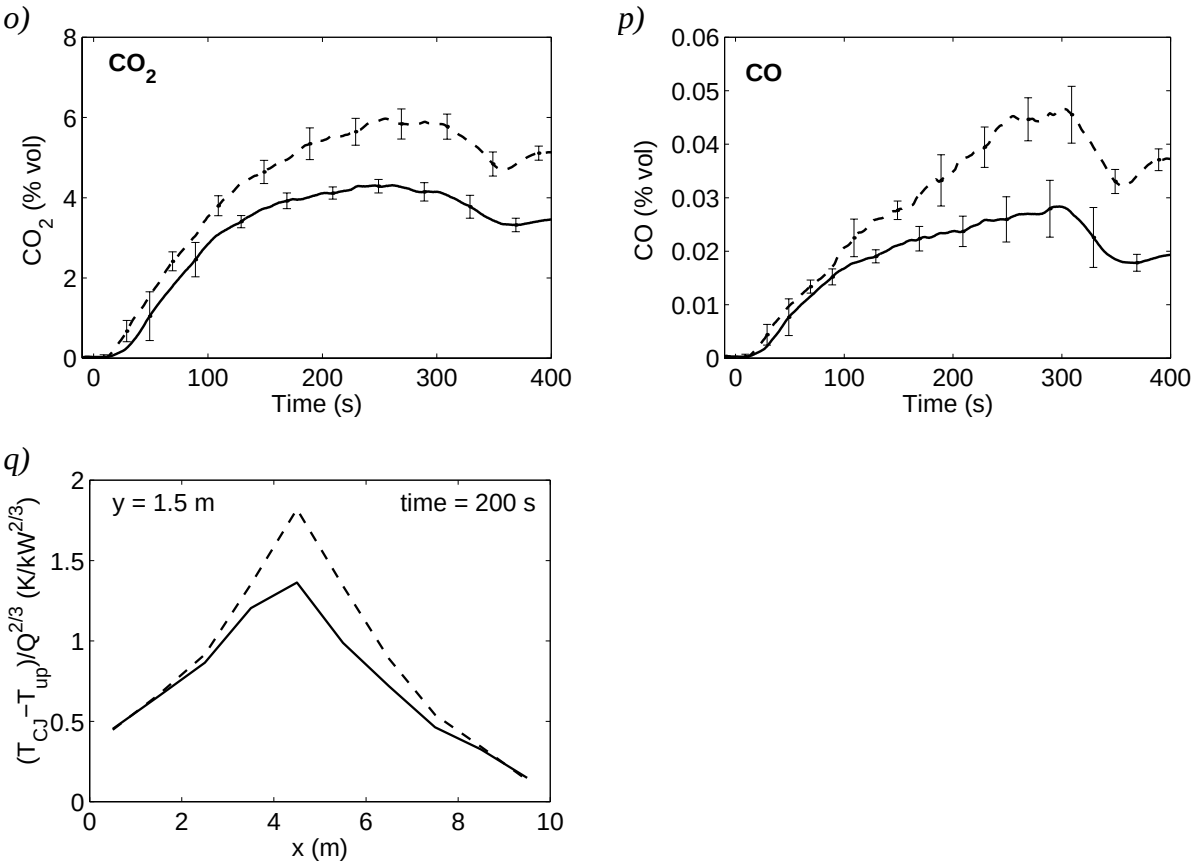


*Figure 21. Effect of the pool size on:*
*a) Burning rate.*
*b) Upper layer temperature.*
*c) Interface height.*
*d) Lower layer temperature.*
*e) Ceiling jet temperature C15 directly above the fire.*
*f) Ceiling jet velocity V1.*
*g)–j) Door flow velocities V3, V5, V6, V7 and V8.*
*k)–n) Heat fluxes R1, R3, R4 and R5. o) $CO_2$ concentration.*
*p) CO concentration.*
*q) Scaled temperature rise in the ceiling jet in x-direction at time = 200 s.*

*Meaning of the error bounds is explained in the caption of Figure 19.*

# 4. Description of the hall experiments

The experiments were conducted in the large fire testing hall at VTT. The hall has the following dimensions: length 27 m, width 14 m and height 19 m. An overview of the hall is shown in Figure 22. The walls and ceiling of the hall are made of sheet metal insulated by mineral wool. The concrete floor was partially covered by steel plates.

In the both ends of the hall there are 4.0 m high doors to ambient. During the first five tests (Fire types 1 and 2) the doors were closed, but during the last three tests (type 3) they were 0.80 m open to allow the flow of the air needed to replace the 11 $m^3/s$ mechanical exhaust. Mechanical exhaust was taken from the exhaust duct placed in approximately middle of the hall, as shown in Figures 23 and 24.

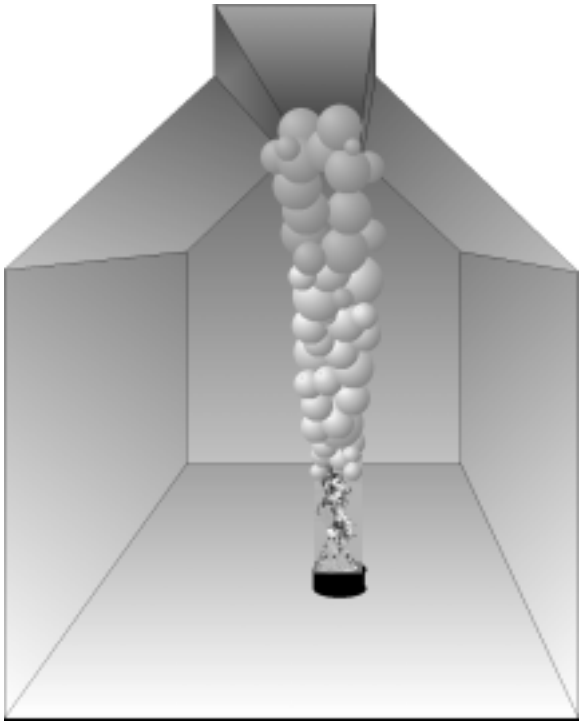

*Figure 22. An overview of the test hall.*

The fuel was heptane burned in circular steel pools placed on load cells for the mass loss measurement. Pool size was varied from 1.07 $m^2$ to 2.0 $m^2$. Water was used under the heptane to stabilise the fire. The height of the fuel surface was 1.0 m from the floor in all tests. The horizontal location of the pool is shown in Figure 23.

Test series consisted of three different fires and eight experiments. The test series is summarised in Table 3 showing the approximate duration of the fire, total mass of the burnt fuel, approximate rate of heat release and the ventilation conditions.

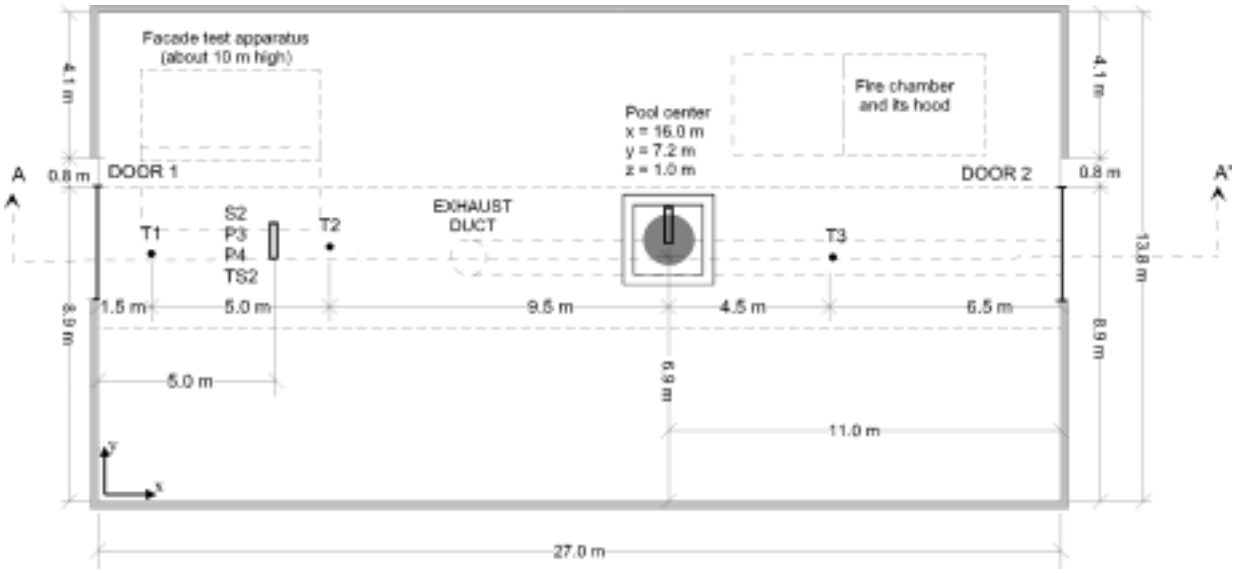


*Figure 23. Plan view of the experimental setup.*

*Table 3. NFSC 2 Hall Test series at VTT.*

| Test No. | Fire Type | Pool size | Duration (min:s) | Fuel mass (kg) | RHR approx. (kW) | Ventilation |
|---|---|---|---|---|---|---|
| Test 1 2.6.99 | 1 | 1.07 $m^2$ D=1.17 m | 7:03 | 18.2 | 2000 | No, doors closed |
| Test 2 3.6.99 | 1 | 1.07 $m^2$ D=1.17 m | 4:10 | 18.7 | 2000 | No, doors closed |
| Test 3 3.6.99 | 2 | 2.0 $m^2$ D=1.60 m | 6:34 | ≈ 30 | 3700 | No, doors closed |
| Test 4 3.6.99 | 2 | 2.0 $m^2$ D=1.60 m | 6:26 | 29.2 | 3700 | No, doors closed |
| Test 5 3.6.99 | 2 | 2.0 $m^2$ D=1.60 m | 6:24 | 29.1 | 3700 | No, doors closed |
| Test 6 7.6.99 | 3 | 2.0 $m^2$ D=1.60 m | 5:47 | 29.3 | 4000 | Exhaust 11 $m^3/s$ Doors 2 × 0.8×4.0 $m^2$ |
| Test 7 7.6.99 | 3 | 2.0 $m^2$ D=1.60 m | 5:42 | 29.1 | 4000 | Exhaust 11 $m^3/s$ Doors 2 × 0.8×4.0 $m^2$ |
| Test 8 7.6.99 | 3 | 2.0 $m^2$ D=1.60 m | 8:37 | 43.5 | 4000 | Exhaust 11 $m^3/s$ Doors 2 × 0.8×4.0 $m^2$ |

About 70 channels of measurements and a video recording of the flame area were made during the experiments. The measurement time step of the gas temperatures and velocities was one second. For steel and plate thermometer temperatures the time step was two seconds, although the data is delivered in the same time steps as the gas temperatures. The measured variables are listed below. The exact locations of the measurements are given in Appendix B.

1. Mass of the fuel was measured by placing the fuel on load cells. The mass loss rate was then calculated by numerical derivation of the mass curve.

2. Gas temperatures were measured in three vertical rakes T1, T2 and T3. Each of these rakes had 10 K-type, 0.1 mm thermocouples. The locations of the gas temperature measurements are shown in Figures 23 and 24.
3. Fire plume temperatures were measured with 0.5 mm K-type thermocouples placed at two 3 × 3 grids. Grids were located at heights 7.0 m (Grid1) and 13.0 (Grid2), as shown in Figure 25. The horizontal locations were directly above the pool. The spacing of Grid 1 was 1.0 m and Grid 2 1.5 m, as shown in Figure 26.
4. Two non-loaded steel tubes were set-up inside the room. Heat fluxes to the steel tubes with square cross section were measured by attaching two thermocouples on each tube (S1.1, S1.2, S2.1 and S2.2). Tubes were made of 4 mm thick steel and their dimensions were 1000 mm × 100 mm × 100 mm. Steel tube instrumentation is shown in Figure 27 and the locations of the steel tubes are shown in Figures 23 and 25. Steel tube 1 is the one located directly above the pool and Steel tube 2 is located under the ceiling 11 meters off the plume center line.
5. Gas flow velocities in the doors were measured with bi-directional probes. Three probes were placed to each door at heights 0.5 m, 2.0 m and 3.5 m, as shown in Figure 28. Positive flow direction was selected from outside to inside the hall. Door 1 was located at $x$ = 0 m and Door 2 at $x$ = 27 m. The door height was 4.0 m.

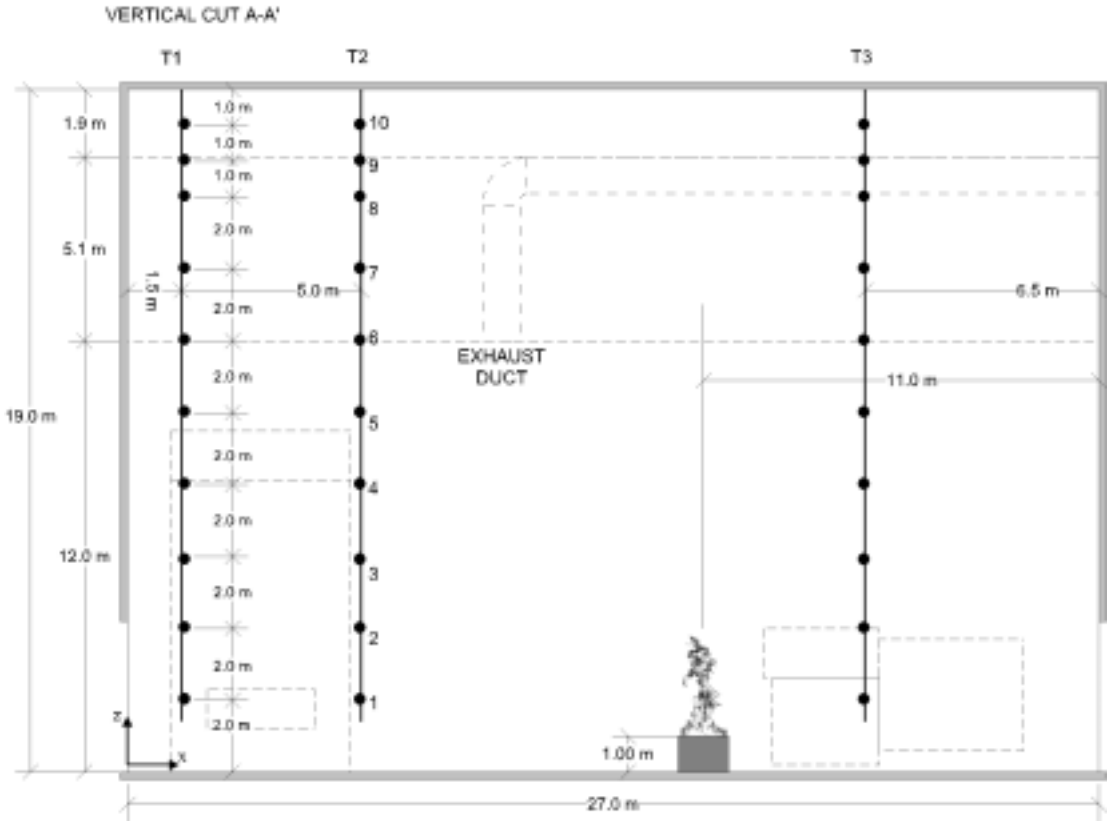


*Figure 24. Locations of the thermocouple rakes used for the gas temperature measurement.*

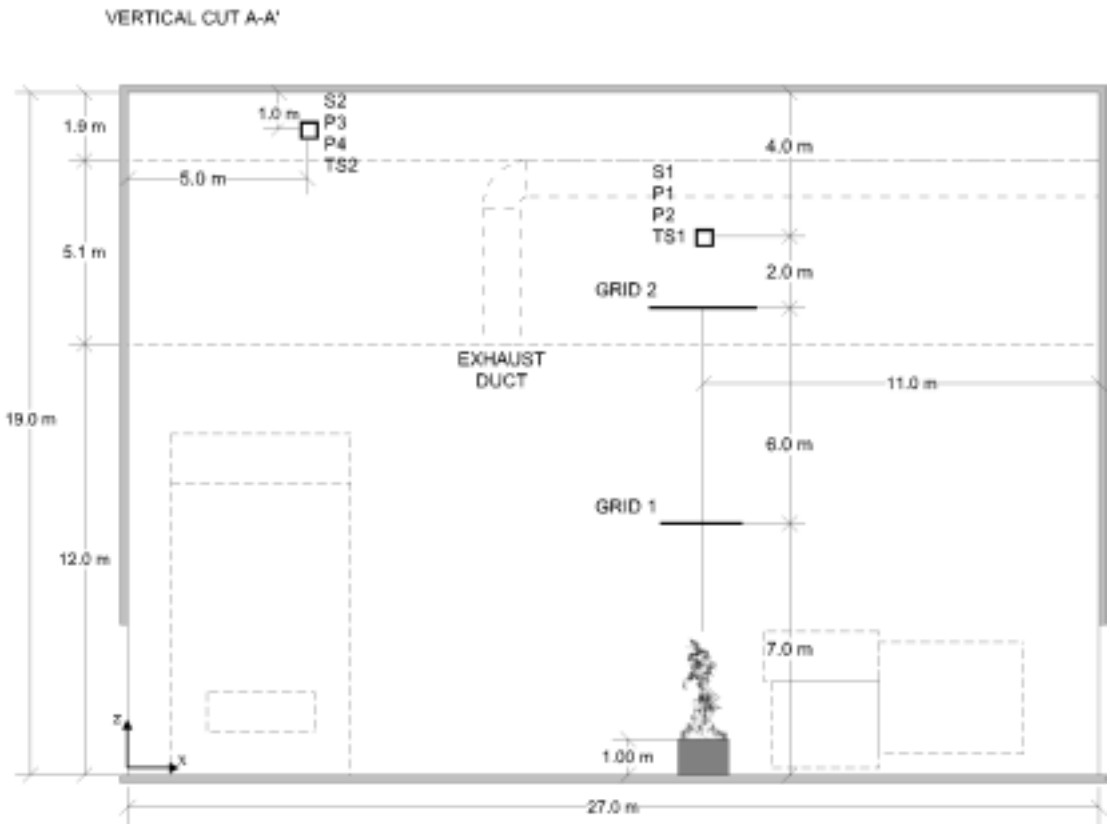


*Figure 25. The locations of the grids and steel tubes.*

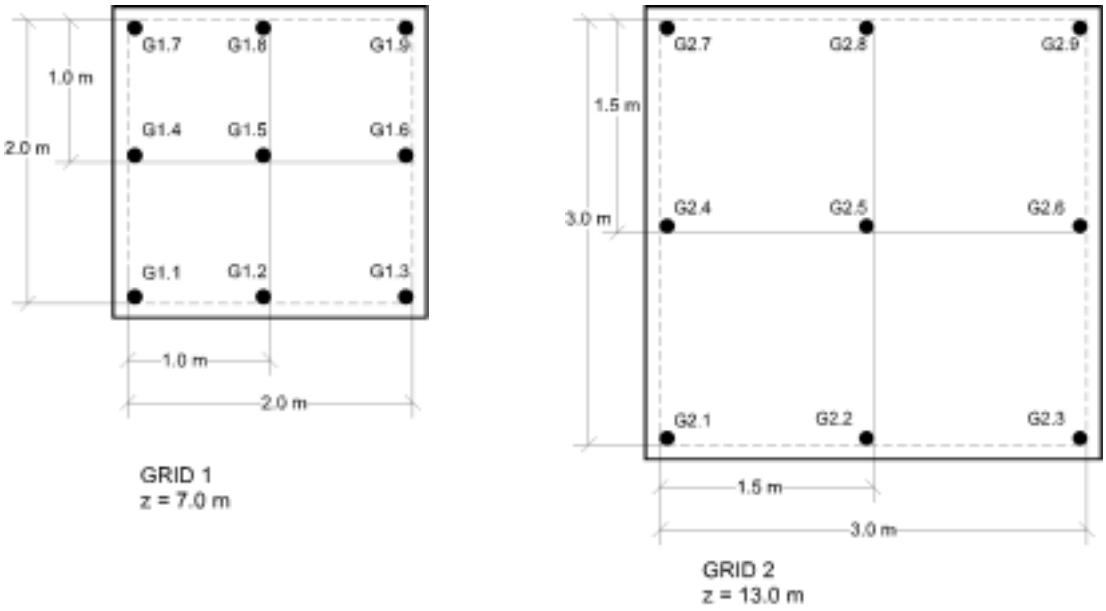


*Figure 26. Grid geometry.*

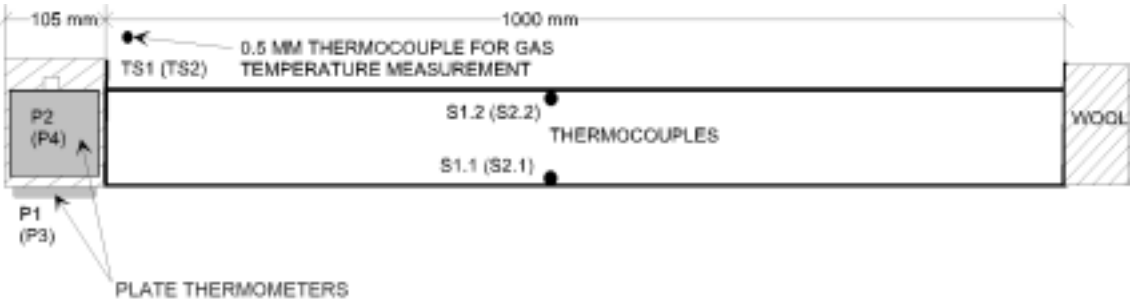


*Figure 27. Steel tube instrumentation. First labels apply for steel tube 1 just above the fire source and labels in parentheses apply for the steel tube 2.*

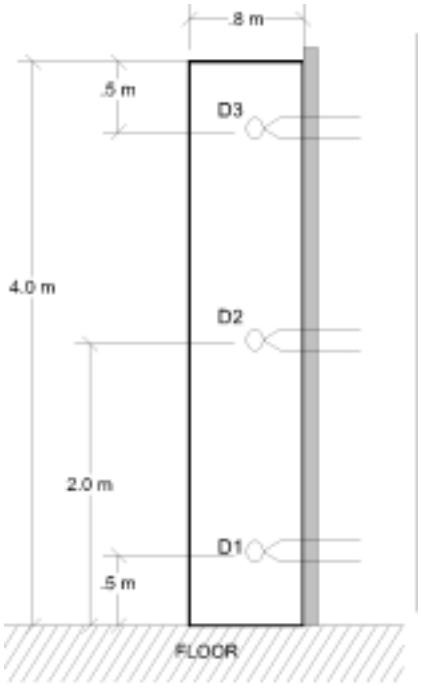


*Figure 28. Velocity measurement locations in Door 1 (x = 0.0 m). Door 2 had similar instrumentation. Positive direction of the velocity was defined to be out of the door.*

# 5. Results of the hall experiments

A summary of the experimental results is shown in Figures 29*a–l*. Each figure contains the results of one measured variable with all three fire types. Each line is an average of the results obtained in the individual tests of that type. Solid lines correspond to fire type 1 (average of Tests 1 and 2), dashed lines to fire type 2 (average of Tests 3 to 5) and dotted lines to fire type 3 (average of Tests 6 and 7). Test 8 was excluded from the averaging because the amount of fuel was different. The corresponding curves for all the individual tests are given in the Appendices N–P.

The methods of data reduction used for the interface height and layer temperature calculation are reported in context of the room tests. No radiation corrections were to the gas temperature measurements because the thermocouples were relatively thin (0.1 mm), and because the distance between them and the fire was several meters.

From the results we can see the strong effect of the pool size on temperatures. The ventilation in turn has hardly any effect on the temperature data, although the burning rate of the ventilated tests was clearly higher than in the non-ventilated tests.

More detailed analysis of the spatial temperature distributions is possible from the complete test data. However, the plume temperature measurements made by $3 \times 3$ grids are too coarse for determination of the horizontal temperature distributions.

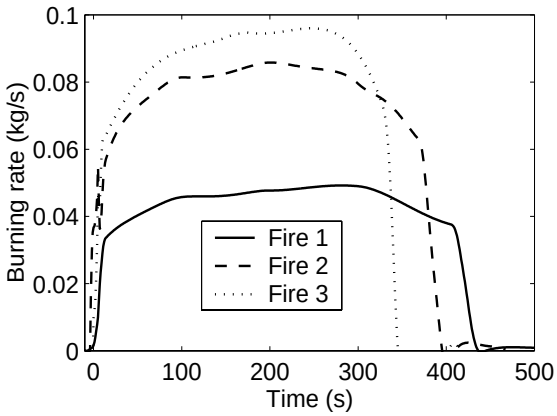


*Figure 29a. Mass loss rates in Fire 1.*

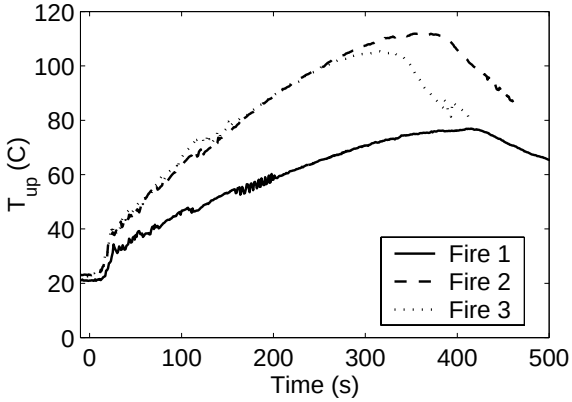


*Figure 29b. Upper layer temperatures.*

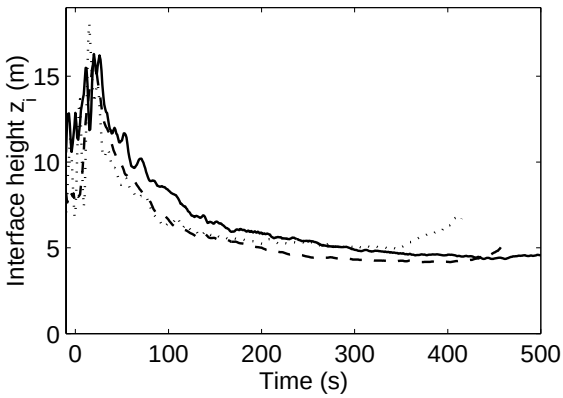


*Figure 29c. Interface heights.*

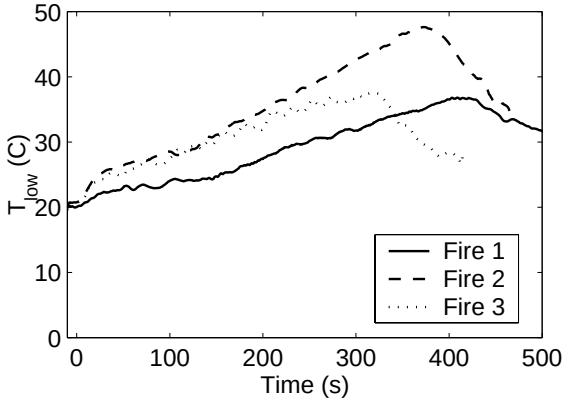


*Figure 29d. Lower layer temperatures.*

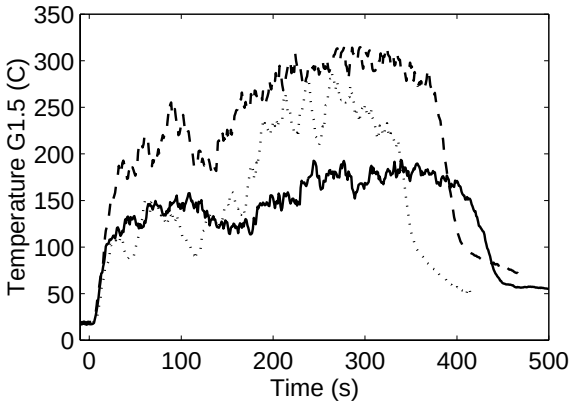


*Figure 29e. Gas temperatures in the center of Grid 1.*

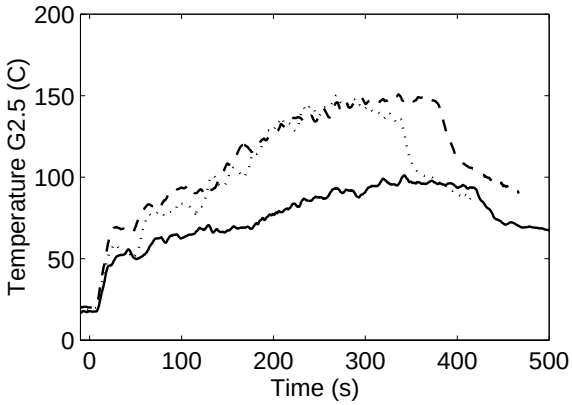


*Figure 29f. Gas temperatures in the center of Grid 2.*

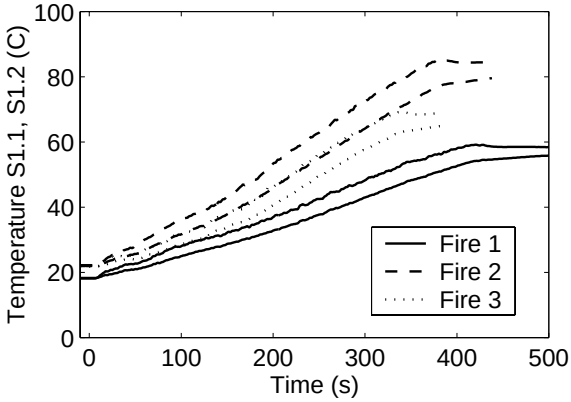


*Figure 29g. Steel tube 1 temperatures.*

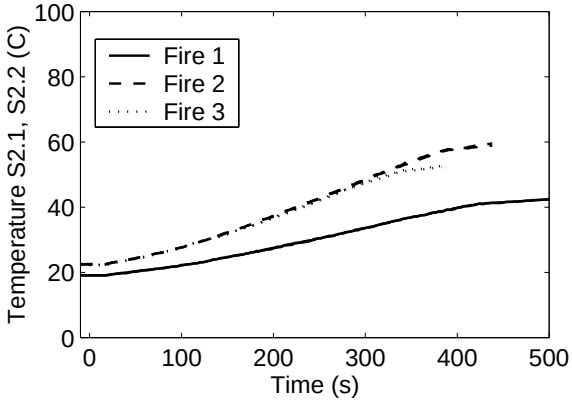


*Figure 29h. Steel tube 2 temperatures.*

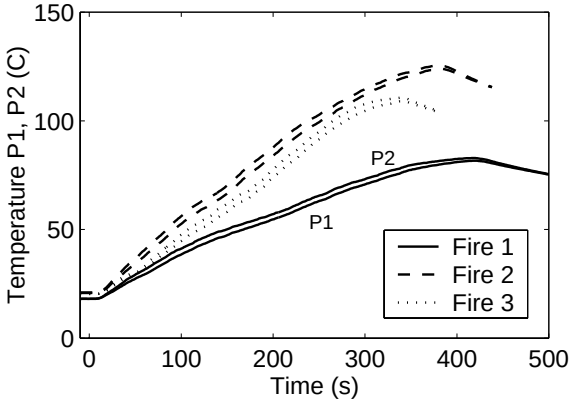


*Figure 29i. Plate temperatures P1 and P2.*

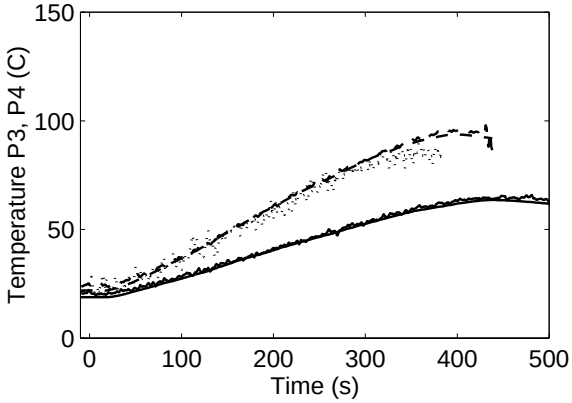


*Figure 29j. Plate temperatures P2 and P3.*

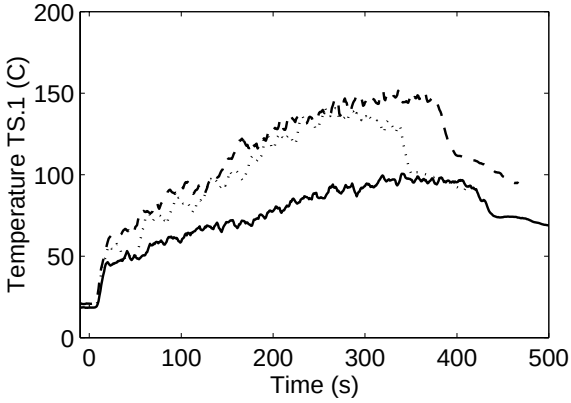


*Figure 29k. Gas temperatures TS.1.*

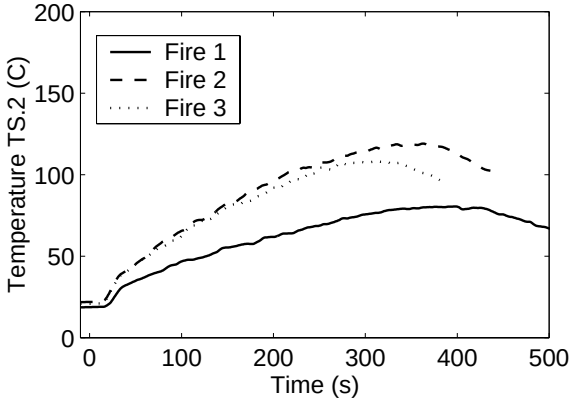


*Figure 29l. Gas temperatures TS.2.*

# 6. Summary

The experimental setup and the results of the two series of full-scale fire tests have been presented. The results show that the repeatability of the localised heptane fires is good. This makes the results valuable during the verification process of computer codes for fire simulation. The fires range from small 0.40 $m^2$ heptane pools to wood cribs and 2.0 $m^2$ pools. The first series of experiments can be used to study the effects of the fire size, fire location and door size on the burning rates and conditions inside the enclosure. The second series in turn shows the effect of the pool size and door opening on the conditions inside a large hall-type enclosure. A full set of data will be made available to enable detailed comparisons between computer code results and measurements.

# References

Blevins, L.G. & Pitts, W.M. 1999. Modeling of bare and aspirated thermocouples in compartment fires. Fire Safety Journal 33, pp. 239–259.

Cooper, L.Y., Harkleroad, M., Quintiere, J. & Rinkinen, W. 1982. An Experimental Study of Upper Hot Layer Stratification in Full-Scale Multiroom Fire Scenarios. Journal of Heat Transfer, Vol. 104, November, pp. 741–749.

Drysdale, D. 1999. An introduction to fire dynamics. 2nd edition. John Wiley & Sons, Chichester.

He, Y., Fernando, A. & Luo, M. 1998. Determination of interface height from measured parameter profile in enclosure fire experiment. Fire Safety Journal 21, pp. 19–38.

# Appendix A: Locations of the measurements in the room fire experiments

All coordinates are given in meters (m).

Vertical distribution of gas temperature (0.1/0.5 mm thermocouples)

| ID | x | y | z | ID | x | y | z | ID | x | y | z |
|---|---|---|---|---|---|---|---|---|---|---|---|
| T1.1 | 1.5 | 5.5 | 1.0 | T2.1 | 7.5 | 5.5 | 1.0 | T3.1 | 6.5 | 1.5 | 1.0 |
| T1.2 | 1.5 | 5.5 | 1.5 | T2.2 | 7.5 | 5.5 | 1.5 | T3.2 | 6.5 | 1.5 | 1.5 |
| T1.3 | 1.5 | 5.5 | 2.0 | T2.3 | 7.5 | 5.5 | 2.0 | T3.3 | 6.5 | 1.5 | 2.0 |
| T1.4 | 1.5 | 5.5 | 2.25 | T2.4 | 7.5 | 5.5 | 2.25 | T3.4 | 6.5 | 1.5 | 2.25 |
| T1.5 | 1.5 | 5.5 | 2.5 | T2.5 | 7.5 | 5.5 | 2.5 | T3.5 | 6.5 | 1.5 | 2.5 |
| T1.6 | 1.5 | 5.5 | 2.75 | T2.6 | 7.5 | 5.5 | 2.75 | T3.6 | 6.5 | 1.5 | 2.75 |
| T1.7 | 1.5 | 5.5 | 3.0 | T2.7 | 7.5 | 5.5 | 3.0 | T3.7 | 6.5 | 1.5 | 3.0 |
| T1.8 | 1.5 | 5.5 | 3.5 | T2.8 | 7.5 | 5.5 | 3.5 | T3.8 | 6.5 | 1.5 | 3.5 |
| T1.9 | 1.5 | 5.5 | 4.0 | T2.9 | 7.5 | 5.5 | 4.0 | T3.9 | 6.5 | 1.5 | 4.0 |
| T1.10 | 1.5 | 5.5 | 4.5 | T2.10 | 7.5 | 5.5 | 4.5 | T3.10 | 6.5 | 1.5 | 4.5 |

Ceiling jet temperature (0.5 mm thermocouples)

| ID | x | y | z | ID | x | y | z | ID | x | y | z |
|---|---|---|---|---|---|---|---|---|---|---|---|
| C1 | 7.5 | 0.2 | 4.9 | C17 | 6.5 | 1.5 | 4.9 | C33 | 7.5 | 3.5 | 4.9 |
| C2 | 0.5 | 0.5 | 4.9 | C18 | 7.5 | 1.5 | 4.9 | C34 | 0.5 | 4.5 | 4.9 |
| C3 | 1.5 | 0.5 | 4.9 | C19 | 8.5 | 1.5 | 4.9 | C35 | 3.5 | 4.5 | 4.9 |
| C4 | 2.5 | 0.5 | 4.9 | C20 | 9.5 | 1.5 | 4.9 | C36 | 4.5 | 4.5 | 4.9 |
| C5 | 3.5 | 0.5 | 4.9 | C21 | 0.5 | 2.5 | 4.9 | C37 | 5.5 | 4.5 | 4.9 |
| C6 | 4.5 | 0.5 | 4.9 | C22 | 1.5 | 2.5 | 4.9 | C38 | 7.5 | 4.5 | 4.9 |
| C7 | 5.5 | 0.5 | 4.9 | C23 | 2.5 | 2.5 | 4.9 | C39 | 9.5 | 4.5 | 4.9 |
| C8 | 7.5 | 0.5 | 4.9 | C24 | 3.5 | 2.5 | 4.9 | C40 | 1.5 | 5.5 | 4.9 |
| C9 | 8.5 | 0.5 | 4.9 | C25 | 4.5 | 2.5 | 4.9 | C41 | 4.5 | 5.5 | 4.9 |
| C10 | 9.5 | 0.5 | 4.9 | C26 | 5.5 | 2.5 | 4.9 | C42 | 7.5 | 5.5 | 4.9 |
| C11 | 0.5 | 1.5 | 4.9 | C27 | 7.5 | 2.5 | 4.9 | C43 | 0.5 | 6.5 | 4.9 |
| C12 | 1.5 | 1.5 | 4.9 | C28 | 8.5 | 2.5 | 4.9 | C44 | 4.5 | 6.5 | 4.9 |
| C13 | 2.5 | 1.5 | 4.9 | C29 | 9.5 | 2.5 | 4.9 | C45 | 7.5 | 6.5 | 4.9 |
| C14 | 3.5 | 1.5 | 4.9 | C30 | 3.5 | 3.5 | 4.9 | C46 | 9.5 | 6.5 | 4.9 |
| C15 | 4.5 | 1.5 | 4.9 | C31 | 4.5 | 3.5 | 4.9 | | | | |
| C16 | 5.5 | 1.5 | 4.9 | C32 | 5.5 | 3.5 | 4.9 | | | | |

Door flow temperature (0.5 mm thermocouples)

| ID | x | y | z | ID | x | y | z |
|---|---|---|---|---|---|---|---|
| D1 | 7.3 | 3.5 | 1.0 | D7 | 7.3 | 3.5 | 2.75 |
| D2 | 7.3 | 3.5 | 1.5 | D8 | 7.3 | 3.5 | 2.9 |
| D3 | 7.3 | 3.5 | 1.75 | D9 | 7.3 | 2.5 | 2.5 |
| D4 | 7.3 | 3.5 | 2.0 | D10 | 7.3 | 4.5 | 2.5 |
| D5 | 7.3 | 3.5 | 2.25 | D11 | 7.3 | 2.5 | 2.9 |
| D6 | 7.3 | 3.5 | 2.5 | D12 | 7.3 | 4.5 | 2.9 |

Fire plume temperature (0.5 mm thermocouples)

| ID | x | y | z | ID | x | y | z |
|---|---|---|---|---|---|---|---|
| G1 | 3.7 | 0.7 | zgrid | G14 | 4.9 | 1.5 | zgrid |
| G2 | 4.1 | 0.7 | zgrid | G15 | 5.3 | 1.5 | zgrid |
| G3 | 4.5 | 0.7 | zgrid | G16 | 3.7 | 1.9 | zgrid |
| G4 | 4.9 | 0.7 | zgrid | G17 | 4.1 | 1.9 | zgrid |
| G5 | 5.3 | 0.7 | zgrid | G18 | 4.5 | 1.9 | zgrid |
| G6 | 3.7 | 1.1 | zgrid | G19 | 4.9 | 1.9 | zgrid |
| G7 | 4.1 | 1.1 | zgrid | G20 | 5.3 | 1.9 | zgrid |
| G8 | 4.5 | 1.1 | zgrid | G21 | 3.7 | 2.3 | zgrid |
| G9 | 4.9 | 1.1 | zgrid | G22 | 4.1 | 2.3 | zgrid |
| G10 | 5.3 | 1.1 | zgrid | G23 | 4.5 | 2.3 | zgrid |
| G11 | 3.7 | 1.5 | zgrid | G24 | 4.9 | 2.3 | zgrid |
| G12 | 4.1 | 1.5 | zgrid | G25 | 5.3 | 2.3 | zgrid |
| G13 | 4.5 | 1.5 | zgrid | | | | |

Height of the thermocouple grid for the fire plume temperature measurement and the height of the fuel surface

| Test | zgrid | max($z_{fuel}$) | min($z_{fuel}$) |
|---|---|---|---|
| 0-2 | 3.26 | 0.2 | 0.19 |
| 3-5 | 3.81 | 0.21 | 0.19 |
| 6-9 | 4.73 | 0.21 | 0.19 |
| 10 | 3.4 | 0.87 | |
| 11-13 | 4.4 | 0.44 | 0.42 |
| 14 | 3.4 | 0.965 | 0.35 |
| 15-18 | 4.4 | 0.44 | 0.42 |
| 19-20 | 4.4 | 0.25 | 0.23 |

Flame temperature (0.5 mm thermocouple)

| ID | x | y | z |
|---|---|---|---|
| F26 | 4.5 | 1.5 | zgrid-1.0 |
| F27 | 4.5 | 1.5 | zgrid-1.95 |

Plate thermometers

| ID | x | y | z | direction | ID | x | y | z | direction |
|---|---|---|---|---|---|---|---|---|---|
| P1 | 4.5 | 0.0 | 1.35 | +y | P6 | 6.5 | 0.7 | 0.0 | +z |
| P2 | 4.5 | 0.0 | 3.0 | +y | P7 | 6.5 | 0.7 | 5.0 | -z |
| P3 | 4.5 | 0.0 | 4.0 | +y | P8 | 4.5 | 1.5 | 5.0 | -z |
| P4 | 0.5 | 0.5 | 5.0 | -z | P9 | 5.5 | 3.5 | 0.0 | +z |
| P5 | 2.5 | 0.7 | 5.0 | -z | P10 | 4.5 | 7.0 | 4.0 | -y |

Heat flux gauges

| ID | x | y | z | direction |
|---|---|---|---|---|
| R1 | 4.5 | 0.0 | 1.35 | +y |
| R2 | 4.5 | 0 | 3.0 | +y |
| R3 | 2.5 | 0.7 | 5.0 | -z |
| R4 | 4.5 | 1.5 | 5.0 | -z |
| R5 | 6.5 | 0.7 | 5.0 | -z |

Gas velocity (bi-directional probes)

| ID | x | y | z | direction | ID | x | y | z | direction |
|---|---|---|---|---|---|---|---|---|---|
| V1 | 2.5 | 0.7 | 4.9 | ±x | V5 | 7.3 | 3.5 | 2.5 | ±x |
| V2 | 6.5 | 0.7 | 4.9 | ±x | V6 | 7.3 | 3.5 | 2.9 | ±x |
| V3 | 7.3 | 3.5 | 1.0 | ±x | V7 | 7.3 | 2.5 | 2.5 | ±x |
| V4 | 7.3 | 3.5 | 2.0 | ±x | V8 | 7.3 | 4.5 | 2.5 | ±x |

Wall temperatures (0.5 mm thermocouples)

| ID | x | y | z | ID | x | y | z | ID | x | y | z |
|---|---|---|---|---|---|---|---|---|---|---|---|
| W1.1 | 4.5 | -0.003 | 1.35 | W2.1 | 4.5 | -0.0045 | 4.0 | W3.1 | 4.5 | 7.005 | 4.0 |
| W1.2 | 4.5 | -0.009 | 1.35 | W2.2 | 4.5 | -0.006 | 4.0 | W3.2 | 4.5 | 7.007 | 4.0 |
| W1.3 | 4.5 | -0.0095 | 1.35 | W2.3 | 4.5 | -0.010 | 4.0 | W3.3 | 4.5 | 7.0095 | 4.0 |

Species concentration sampling location

| ID | x | y | z |
|---|---|---|---|
| CO | 8 | 3.5 | 4.2 |
| CO2 | 8 | 3.5 | 4.2 |
| O2 | 8 | 3.5 | 4.2 |

For Test #20 z = 4.9

# Appendix B: Locations of the measurements in the hall fire experiments

All coordinates are given in meters (m).

Vertical distribution of gas temperature (0.1 mm thermocouples)

| ID | x | y | z | ID | x | y | z | ID | x | y | z |
|---|---|---|---|---|---|---|---|---|---|---|---|
| T1.1 | 1.5 | 6.9 | 2.0 | T2.1 | 6.5 | 6.9 | 2.0 | T3.1 | 20.5 | 6.9 | 2.0 |
| T1.2 | 1.5 | 6.9 | 4.0 | T2.2 | 6.5 | 6.9 | 4.0 | T3.2 | 20.5 | 6.9 | 4.0 |
| T1.3 | 1.5 | 6.9 | 6.0 | T2.3 | 6.5 | 6.9 | 6.0 | T3.3 | 20.5 | 6.9 | 6.0 |
| T1.4 | 1.5 | 6.9 | 8.0 | T2.4 | 6.5 | 6.9 | 8.0 | T3.4 | 20.5 | 6.9 | 8.0 |
| T1.5 | 1.5 | 6.9 | 10.0 | T2.5 | 6.5 | 6.9 | 10.0 | T3.5 | 20.5 | 6.9 | 10.0 |
| T1.6 | 1.5 | 6.9 | 12.0 | T2.6 | 6.5 | 6.9 | 12.0 | T3.6 | 20.5 | 6.9 | 12.0 |
| T1.7 | 1.5 | 6.9 | 14.0 | T2.7 | 6.5 | 6.9 | 14.0 | T3.7 | 20.5 | 6.9 | 14.0 |
| T1.8 | 1.5 | 6.9 | 16.0 | T2.8 | 6.5 | 6.9 | 16.0 | T3.8 | 20.5 | 6.9 | 16.0 |
| T1.9 | 1.5 | 6.9 | 17.0 | T2.9 | 6.5 | 6.9 | 17.0 | T3.9 | 20.5 | 6.9 | 17.0 |
| T1.10 | 1.5 | 6.9 | 18.0 | T2.10 | 6.5 | 6.9 | 18.0 | T3.10 | 20.5 | 6.9 | 18.0 |

Fire plume temperature (0.5 mm thermocouples)

Grid 1

| ID | x | y | z | ID | x | y | z | ID | x | y | z |
|---|---|---|---|---|---|---|---|---|---|---|---|
| G1.1 | 15.0 | 6.2 | 7.0 | G1.4 | 15.0 | 7.2 | 7.0 | G1.7 | 15.0 | 8.2 | 7.0 |
| G1.2 | 16.0 | 6.2 | 7.0 | G1.5 | 16.0 | 7.2 | 7.0 | G1.8 | 16.0 | 8.2 | 7.0 |
| G1.3 | 17.0 | 6.2 | 7.0 | G1.6 | 17.0 | 7.2 | 7.0 | G1.9 | 17.0 | 8.2 | 7.0 |

Grid 2

| ID | x | y | z | ID | x | y | z | ID | x | y | z |
|---|---|---|---|---|---|---|---|---|---|---|---|
| G2.1 | 14.5 | 5.7 | 13.0 | G2.4 | 14.5 | 7.2 | 13.0 | G2.7 | 14.5 | 8.7 | 13.0 |
| G2.2 | 16.0 | 5.7 | 13.0 | G2.5 | 16.0 | 7.2 | 13.0 | G2.8 | 16.0 | 8.7 | 13.0 |
| G2.3 | 17.5 | 5.7 | 13.0 | G2.6 | 17.5 | 7.2 | 13.0 | G2.9 | 17.5 | 8.7 | 13.0 |

Steel tube temperature measurements

| ID | x | y | z | ID | x | y | z |
|---|---|---|---|---|---|---|---|
| S1.1 | 16.0 | 7.5 | 15.0 | S2.1 | 5.0 | 7.5 | 15.0 |
| S1.2 | 16.0 | 7.5 | 15.1 | S2.2 | 5.0 | 7.5 | 15.1 |

Plate thermometers

| ID | x | y | z | direction |
|---|---|---|---|---|
| P1 | 16.0 | 7.0 | 15.0 | -z |
| P2 | 16.0 | 7.0 | 15.0 | +x |
| P3 | 5.0 | 7.0 | 15.0 | -z |
| P4 | 5.0 | 7.0 | 15.0 | +x |

Gas temperature in the vicinity of the steel tubes (0.5 mm thermocouples)

| ID | x | y | z |
|---|---|---|---|
| TS1 | 16.0 | 7.0 | 15.2 |
| TS2 | 5.0 | 7.0 | 15.2 |

Door flow velocity measurements (bi-directional probes). Positive direction was out of the door.

| | Door 1 | | | | | Door 2 | | | |
|---|---|---|---|---|---|---|---|---|---|
| ID | x | y | z | direction | ID | x | y | z | direction |
| D1 | 0 | 9.3 | 0.5 | ±x | D4 | 27 | 9.3 | 0.5 | ±x |
| D2 | 0 | 9.3 | 2.0 | ±x | D5 | 27 | 9.3 | 2.0 | ±x |
| D3 | 0 | 9.3 | 3.5 | ±x | D6 | 27 | 9.3 | 3.5 | ±x |

# Appendix C: Results of the room fire type 1

The following figures show the results of the individual tests for type 1 fire. The differences in the lengths of the curves are due to the differences in the amount of fuel. No radiation corrections have been done to the gas temperature measurements.

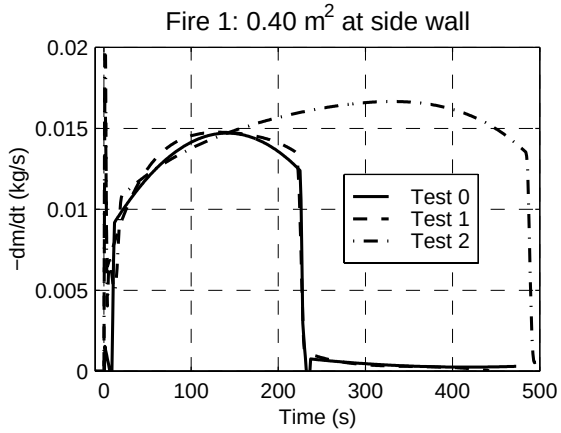


*Figure 30a. Mass loss rates.*

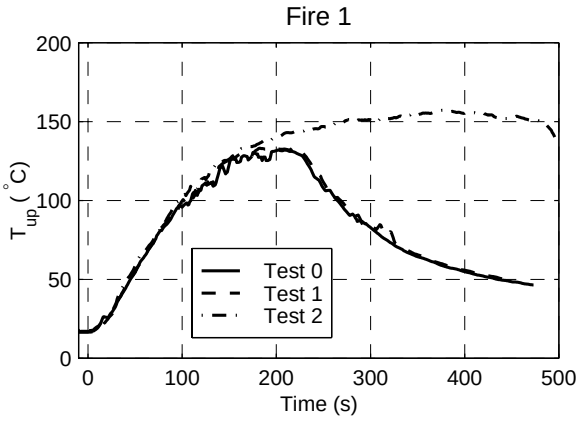


*Figure 30b. Upper layer temperature.*

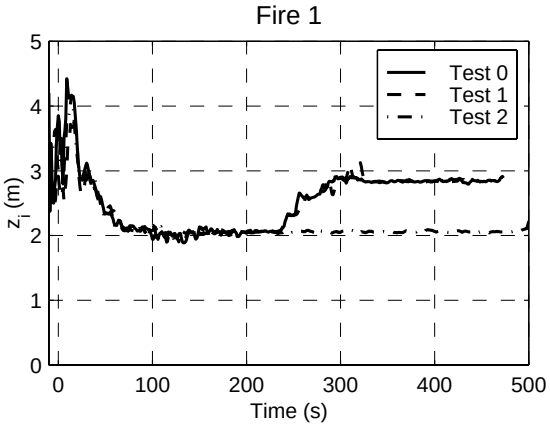


*Figure 30c. Interface heights.*

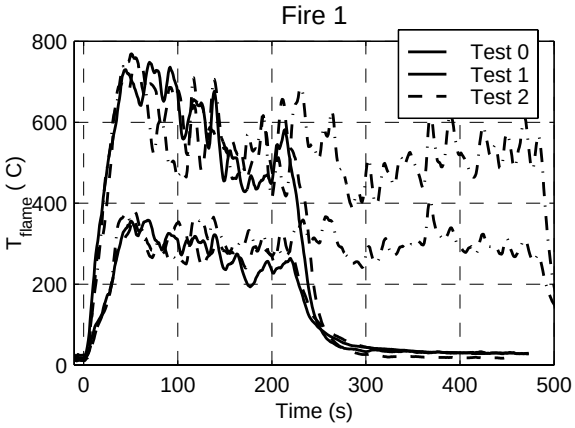


*Figure 30d. Flame temperature.*

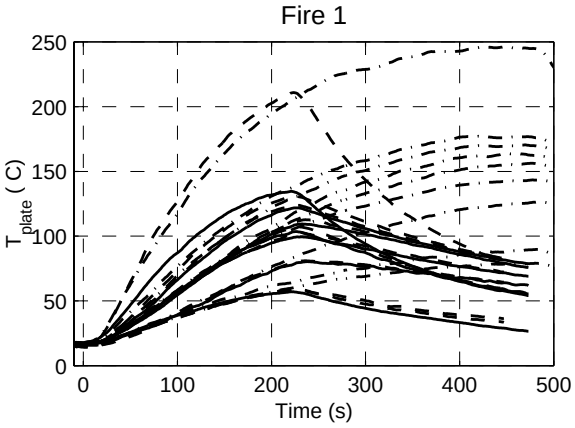


*Figure 30e. Plate temperatures.*

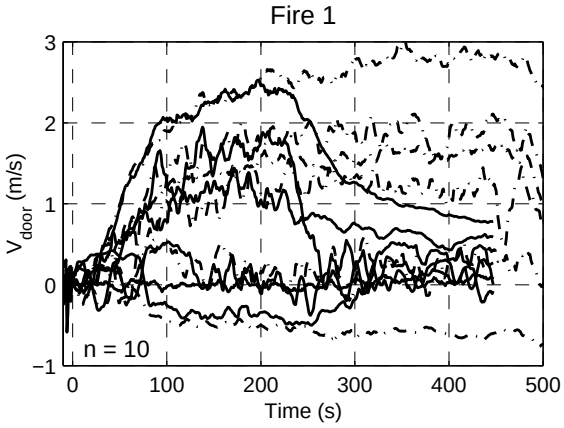


*Figure 30f. Door flow velocities.*

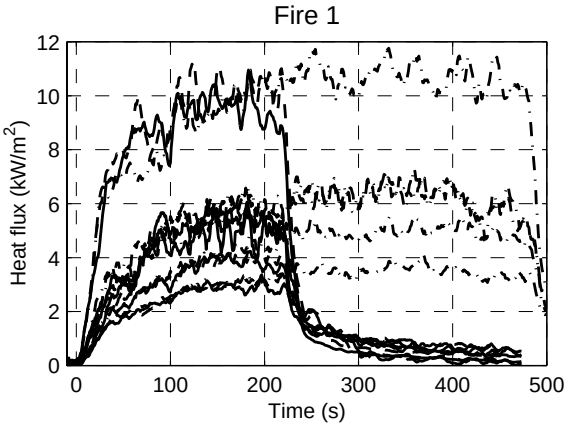


*Figure 30g. Heat fluxes.*

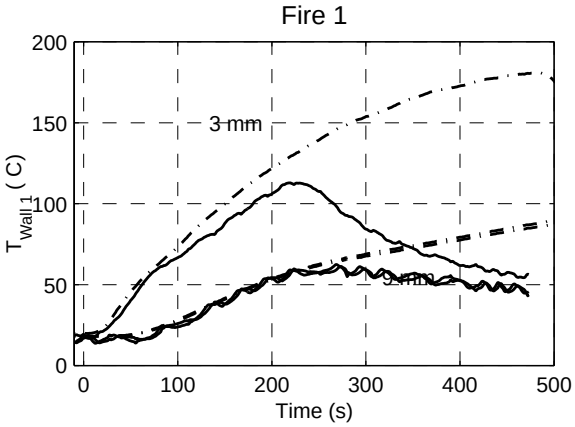


*Figure 30h. Wall temperatures W1. Distances (mm) are from the wall surface.*

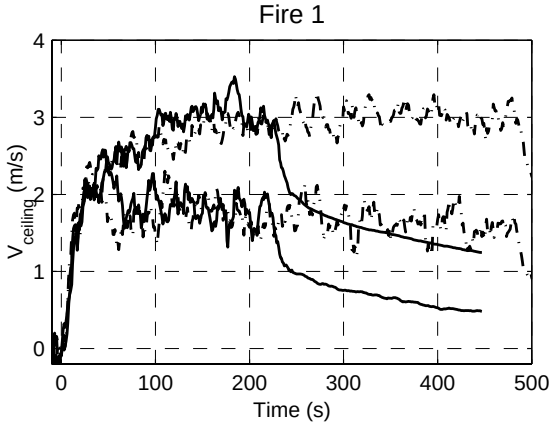


*Figure 30i. Ceiling jet velocities.*

# Appendix D: Results of the room fire type 2

The following figures show the results of the individual tests for type 2 fire.

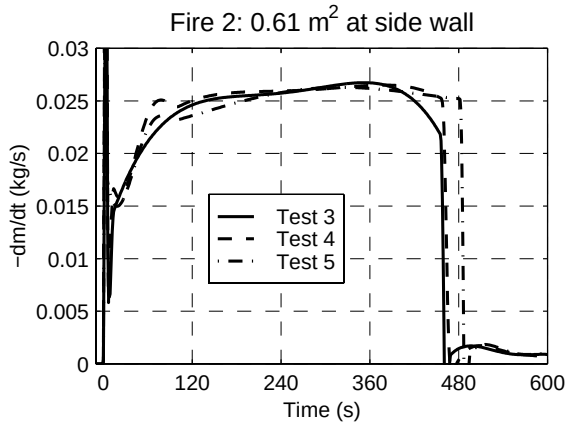


*Figure 31a. Mass loss rates.*

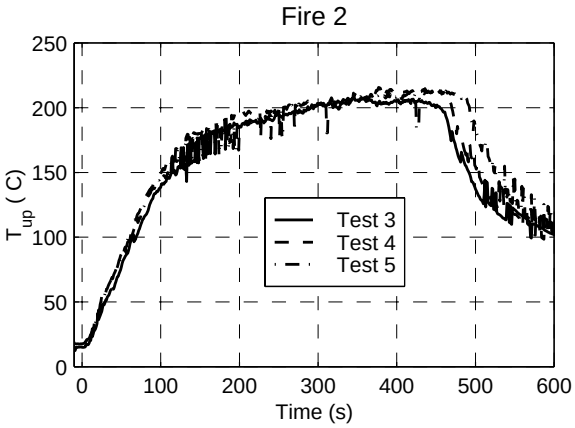


*Figure 31b. Upper layer temperatures.*

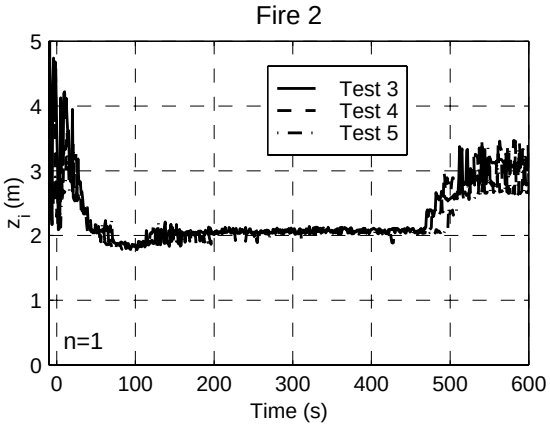


*Figure 31c. Interfaces heights.*

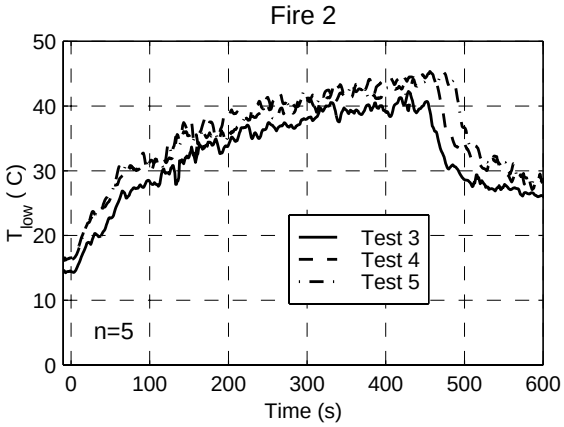


*Figure 31d. Lower layer temperatures.*

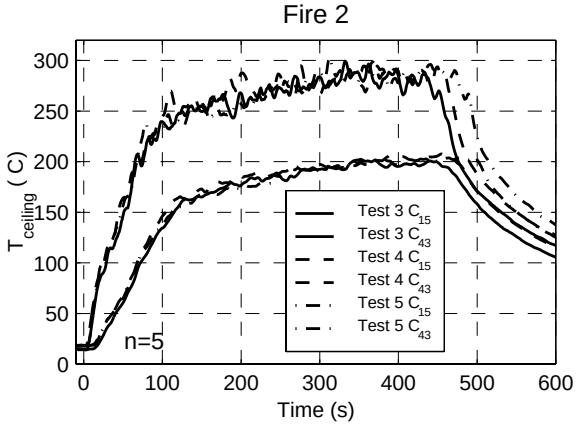


*Figure 31e. Ceiling jet temperatures.*

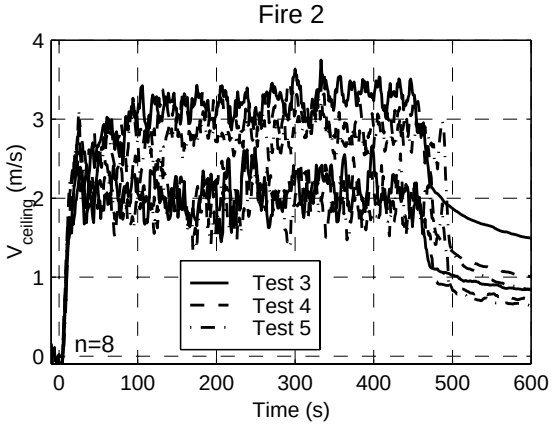


*Figure 31f. Ceiling jet velocities.*

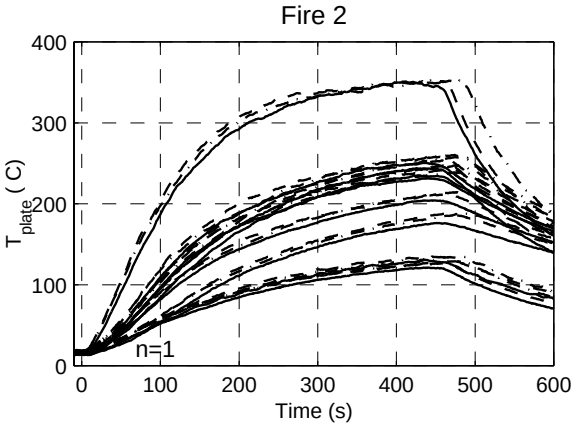


*Figure 31g. Plate temperatures.*

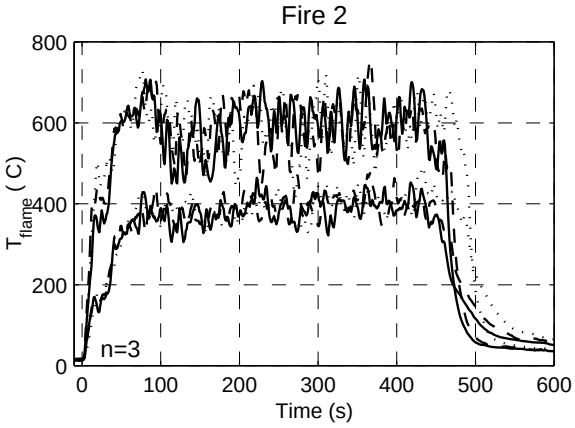


*Figure 31h. Flame temperatures.*

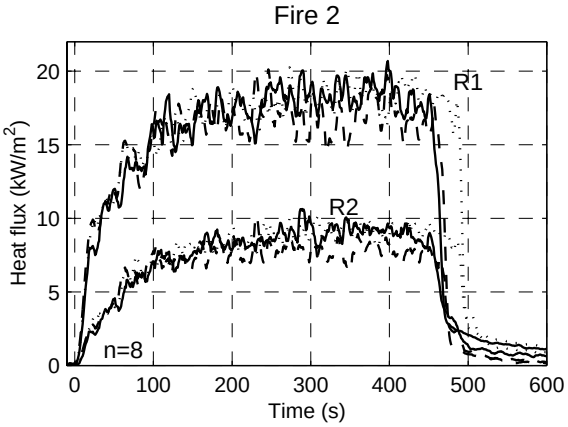


*Figure 31i. Heat fluxes.*

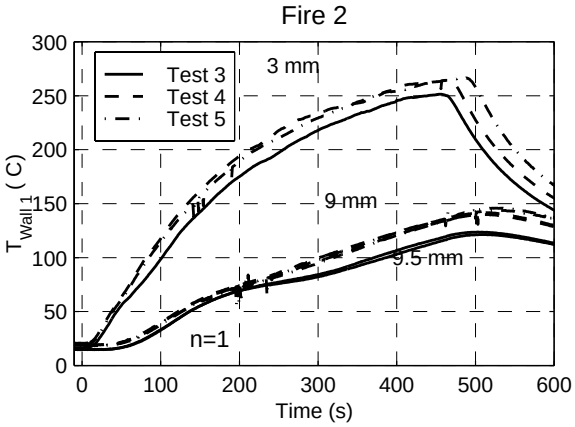


*Figure 31j. Wall temperatures W1. Distances (mm) are from the wall surface.*

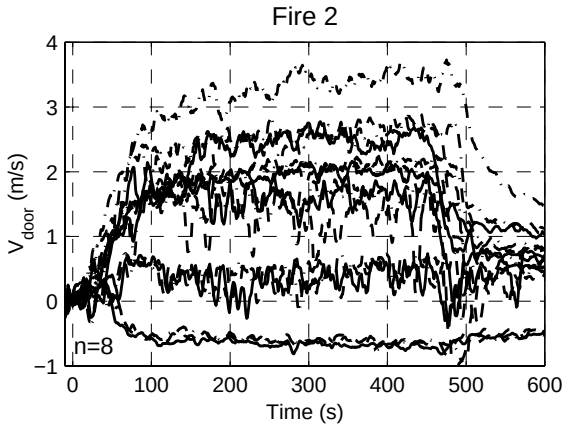


*Figure 31k. Door flow velocities.*

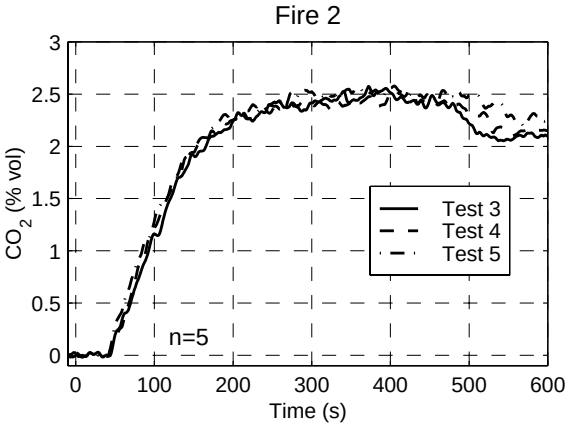


*Figure 31m. $CO_2$ concentrations.*

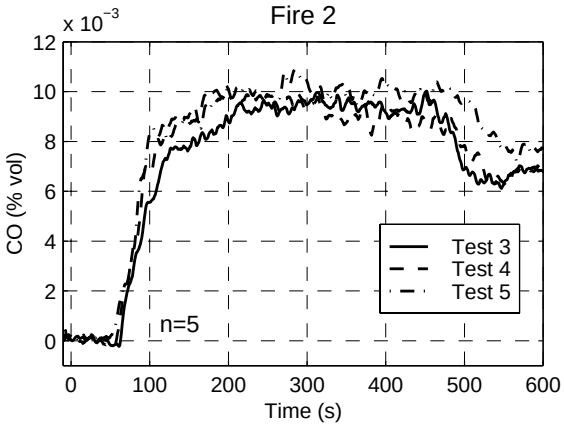


*Figure 31n. CO concentrations.*

# Appendix E: Results of the room fire type 3

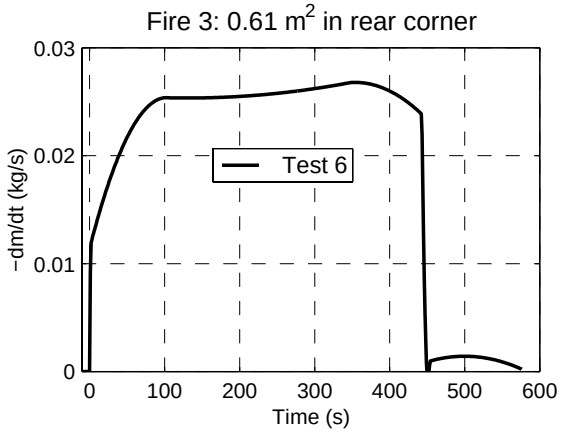


*Figure 32a. Mass loss rate.*

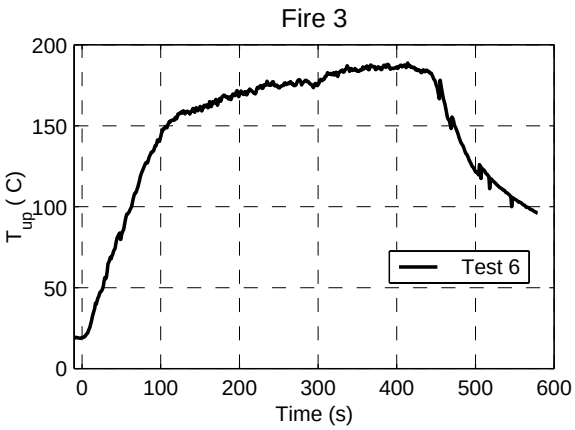


*Figure 32b. Upper layer temperature.*

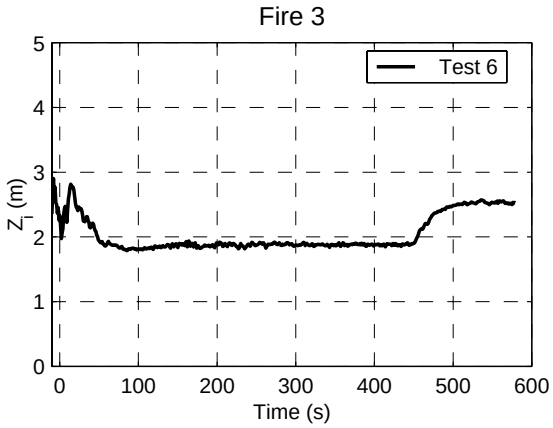


*Figure 32c. Interface height.*

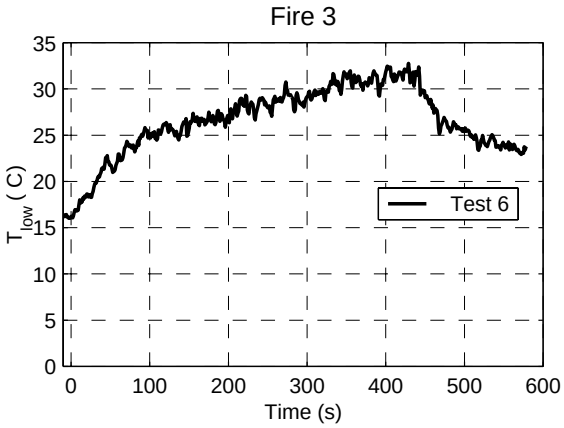


*Figure 32d. Lower layer temperature.*

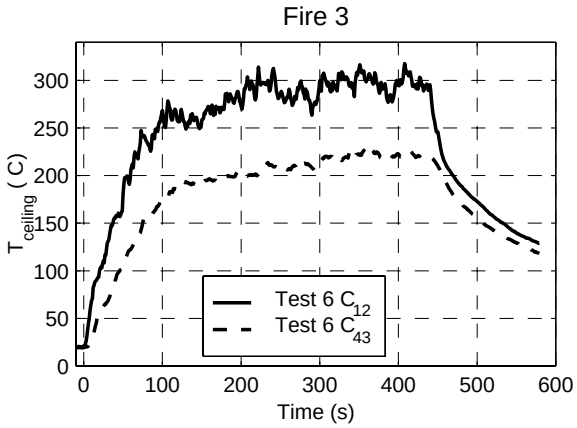


*Figure 32e. Ceiling jet temperatures.*

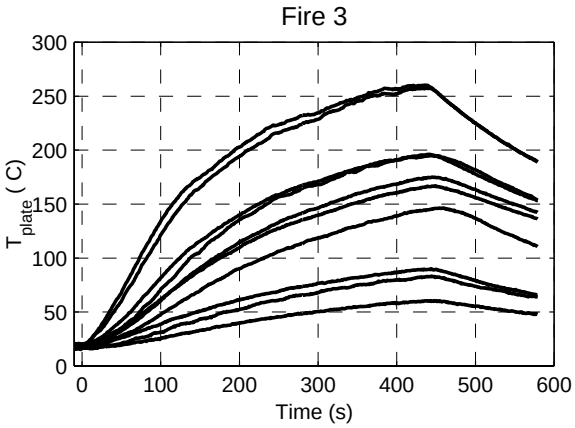


*Figure 32f. Plate temperatures.*

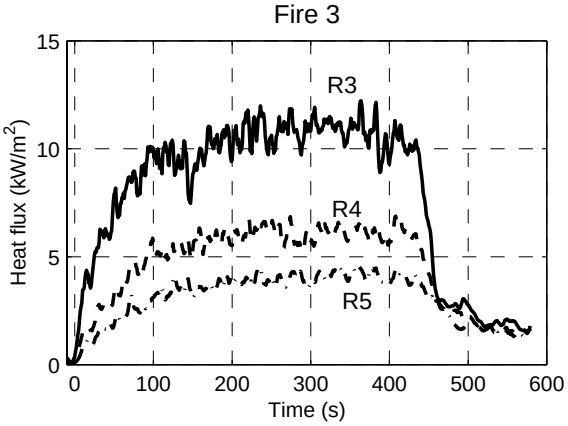


*Figure 32g. Heat fluxes.*

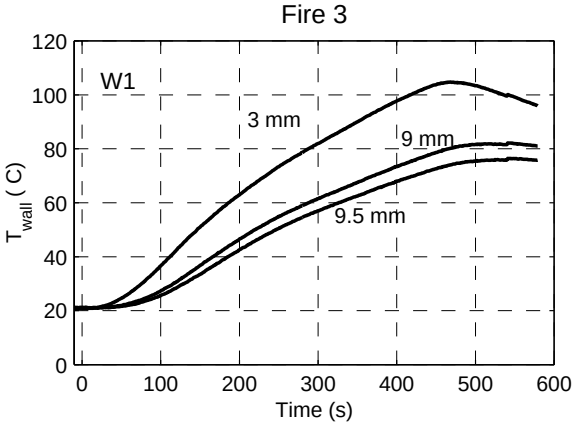


*Figure 32h. Wall temperatures W1. Distances (mm) are from the wall surface.*

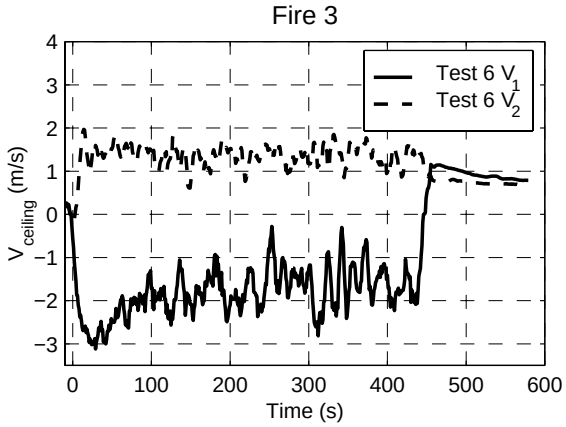


*Figure 32i. Ceiling jet velocities.*

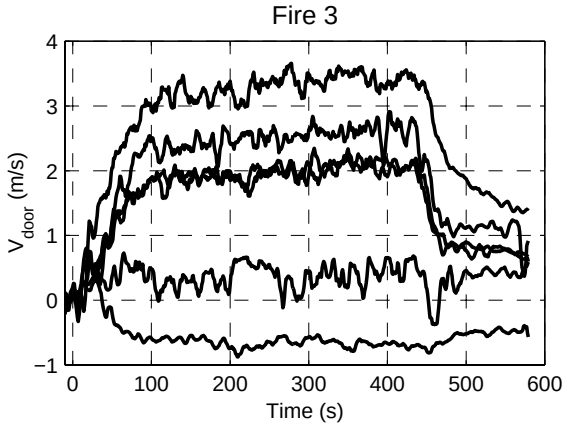


*Figure 32j. Door flow velocities.*

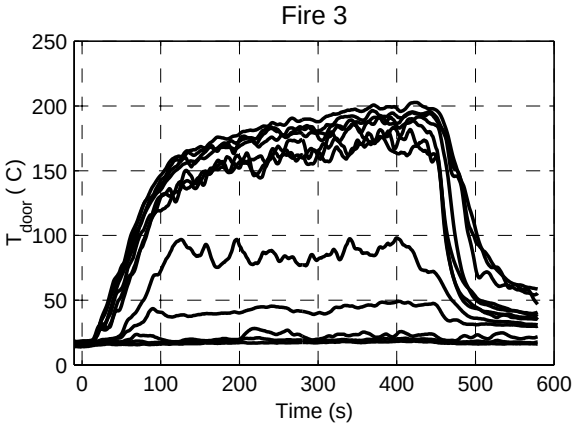


*Figure 32k. Door flow temperatures.*

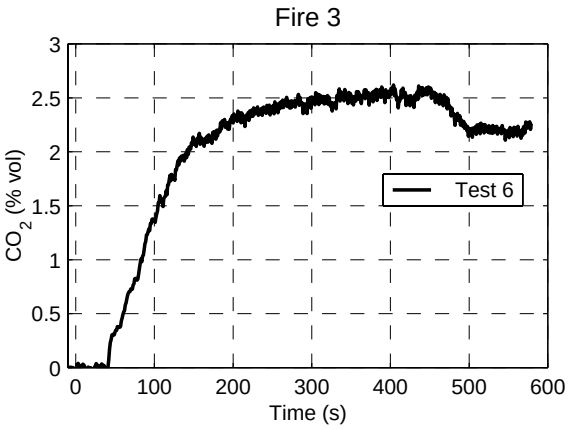


*Figure 32l. $CO_2$ concentration.*

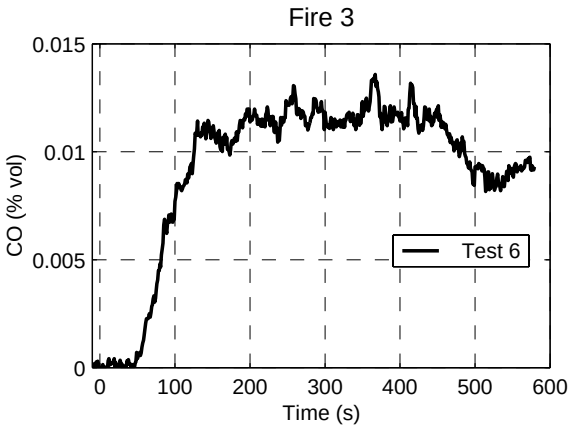


*Figure 32m. CO concentration.*

# Appendix F: Results of the room fire type 4

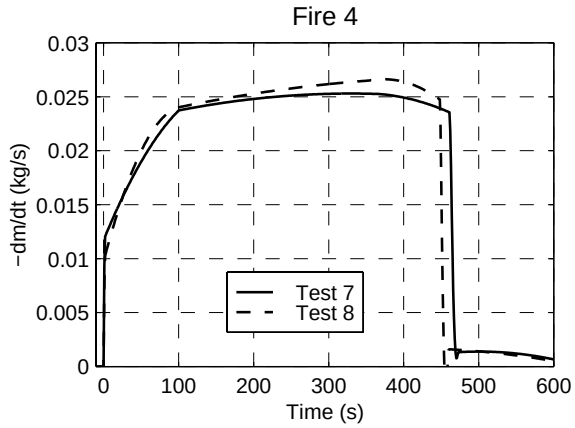


*Figure 33a. Mass loss rate.*

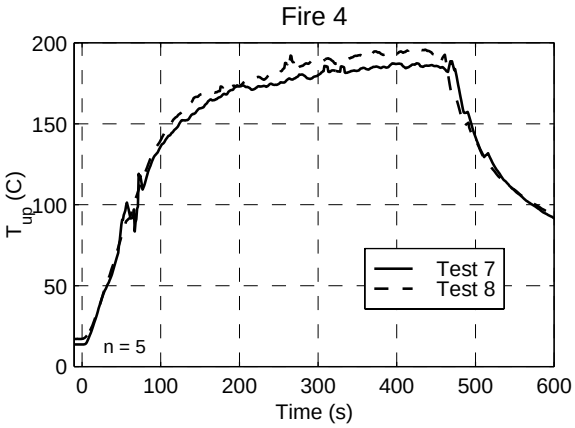


*Figure 33b. Upper layer temperature.*

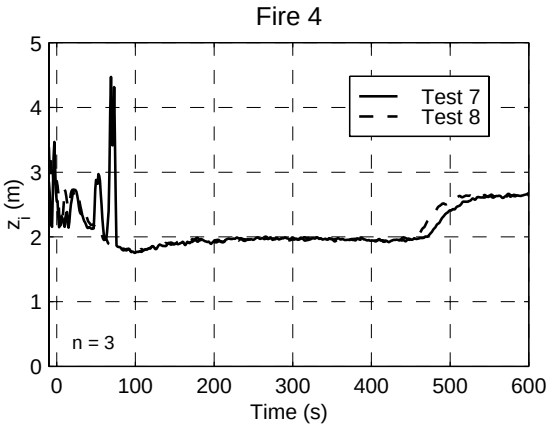


*Figure 33c. Interface height.*

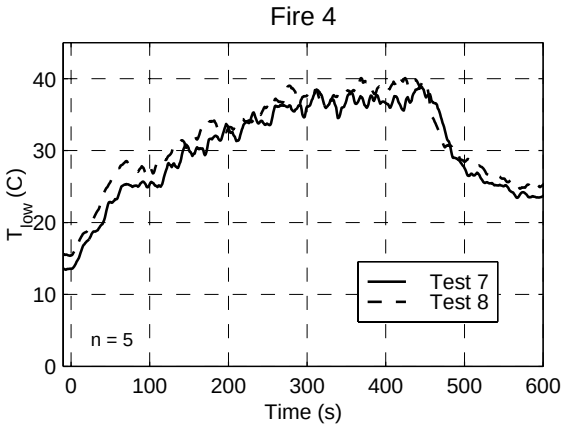


*Figure 33d. Lower layer temperature.*

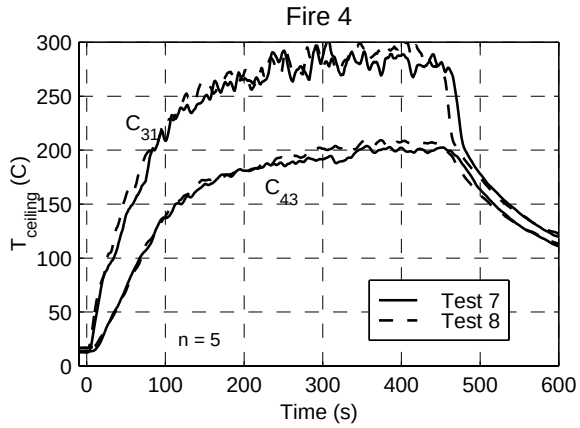


*Figure 33e. Ceiling jet temperatures.*

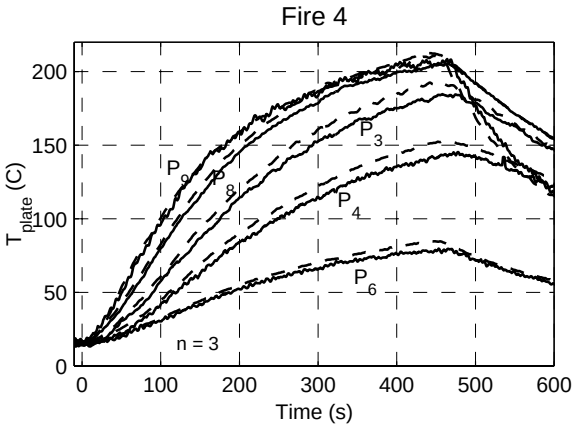


*Figure 33f. Plate temperatures.*

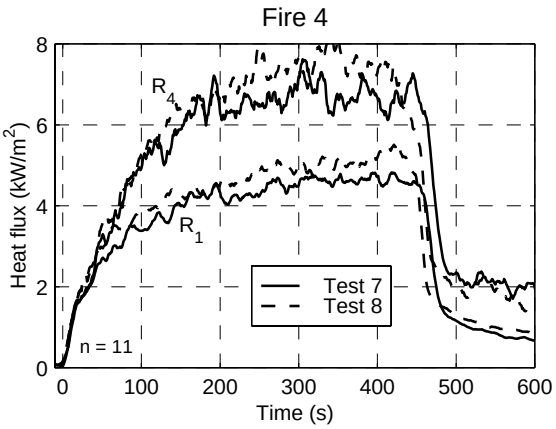


*Figure 33g. Heat fluxes.*

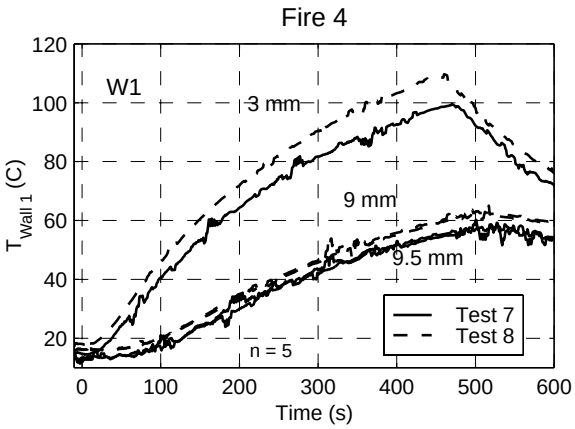


*Figure 33h. Wall temperatures W1. Distances (mm) are from the wall surface.*

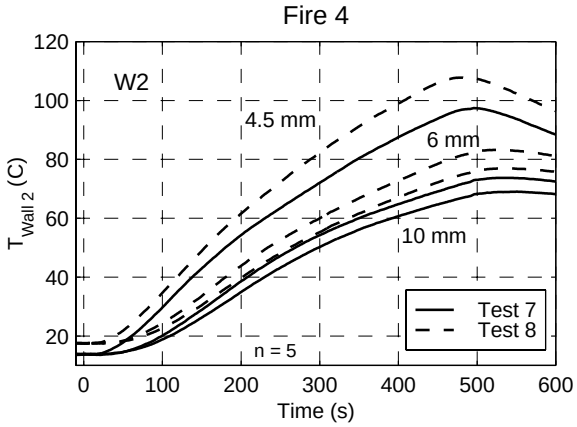


*Figure 33i. Wall temperatures W2. Distances (mm) are from the wall surface.*

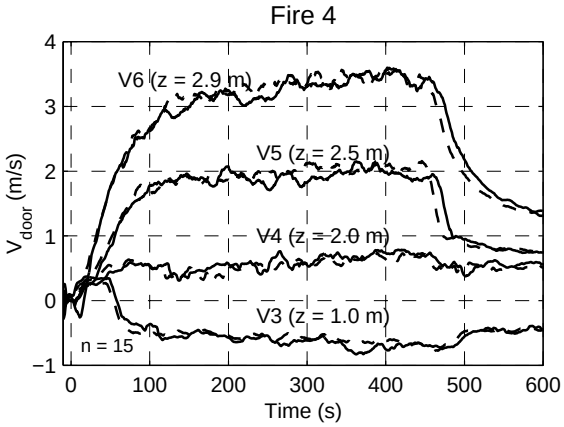


*Figure 33j. Door flow velocities 3–6.*

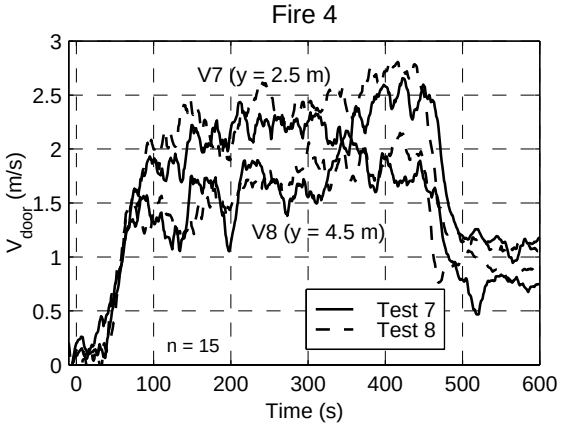


*Figure 33k. Door flow velocities 7–8.*

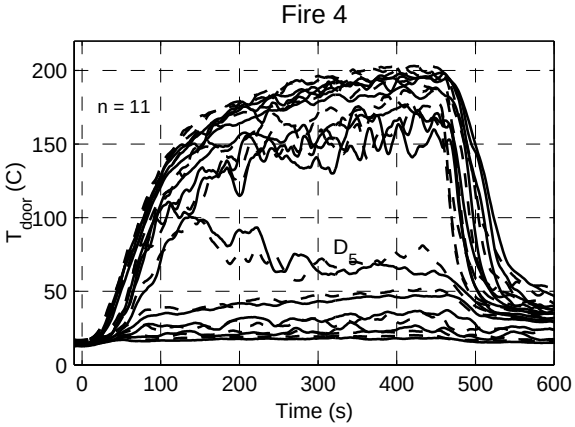


*Figure 33l. Door flow temperatures.*

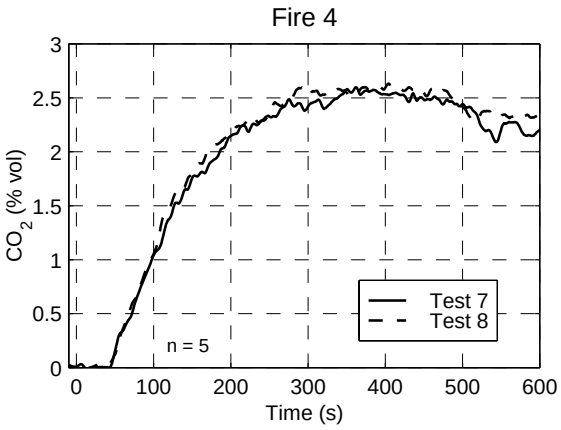


*Figure 33m. $CO_2$ concentration.*

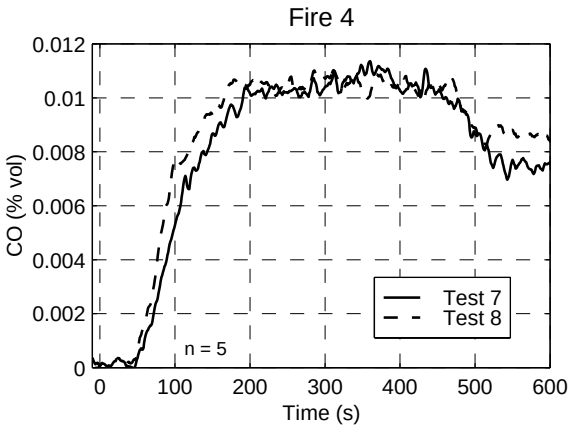


*Figure 33n. CO concentration.*

# Appendix G: Results of the room fire type 5

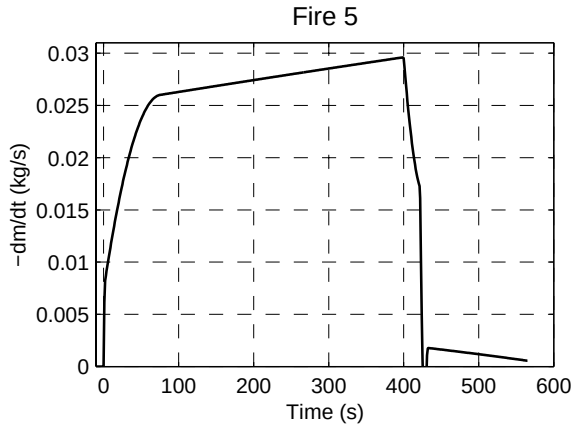


*Figure 34a. Mass loss rate.*

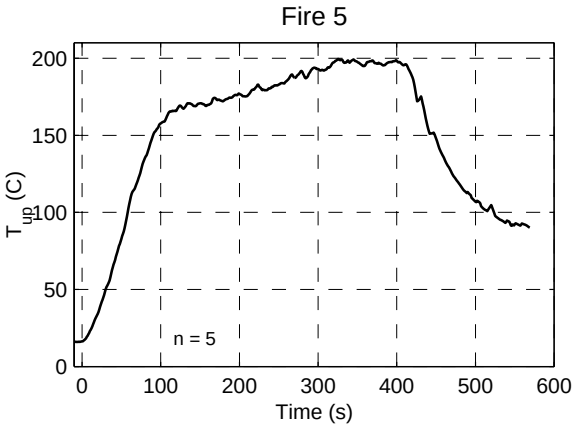


*Figure 34b. Upper layer temperature.*

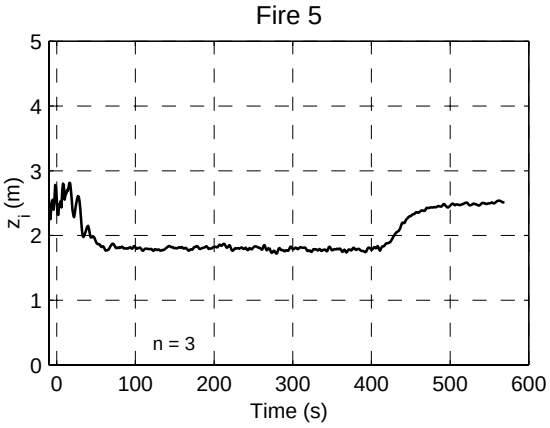


*Figure 34c. Interface height.*


*Figure 34d. Lower layer temperature.*

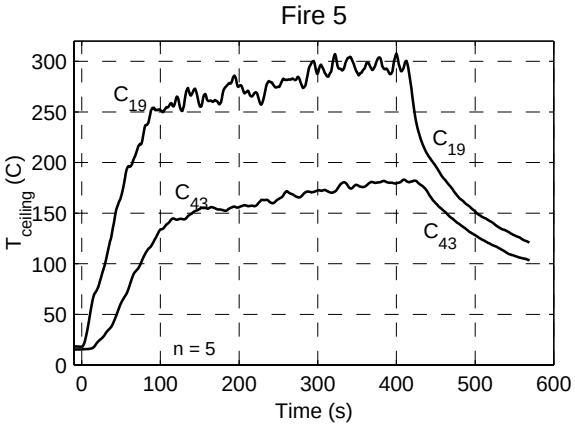


*Figure 34e. Ceiling jet temperatures.*

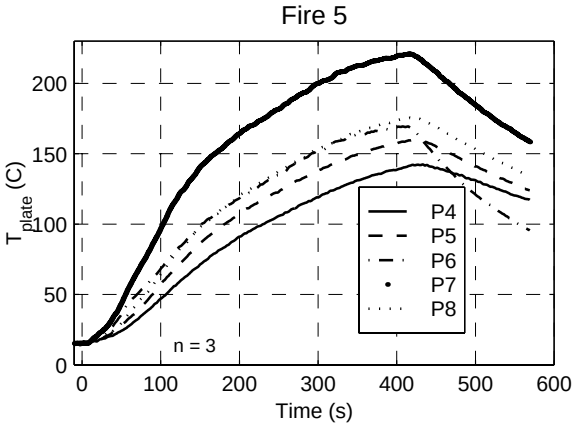


*Figure 34f. Plate temperatures.*

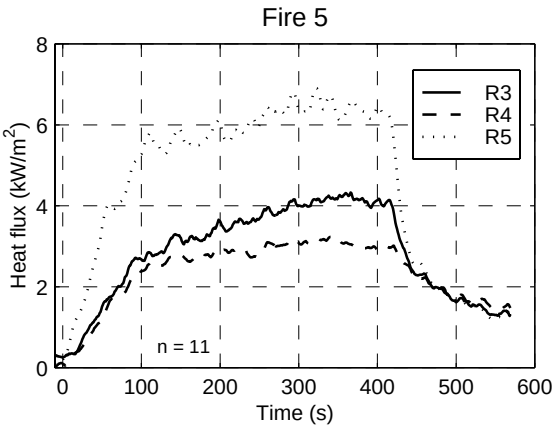


*Figure 34g. Heat fluxes.*

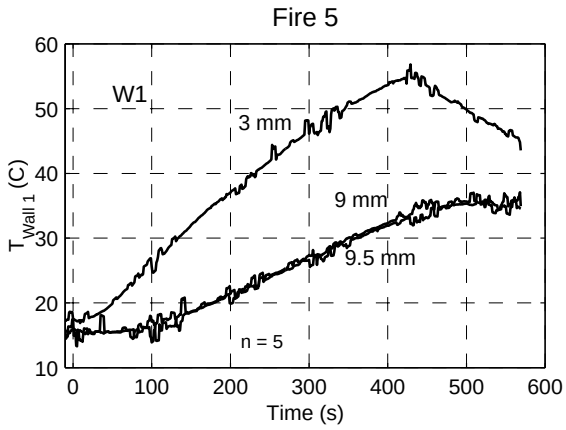


*Figure 34h. Wall temperatures W1. Distances (mm) are from the wall surface.*

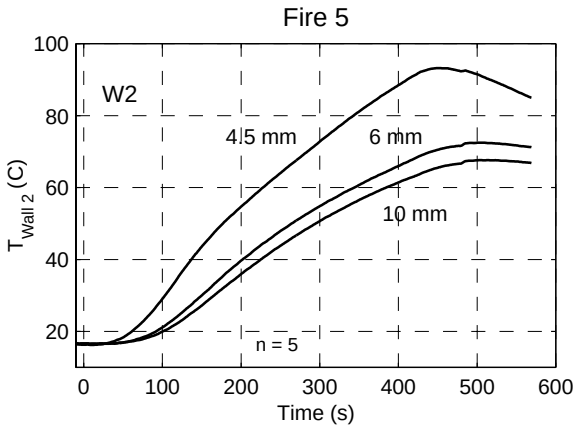


*Figure 34i. Wall temperatures W2. Distances (mm) are from the wall surface.*

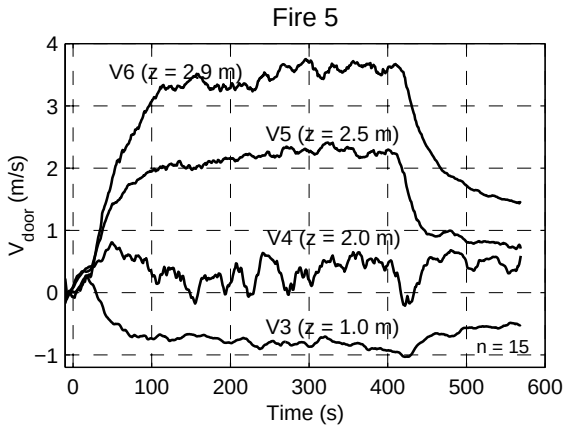


*Figure 34j. Door flow velocities 3–6.*

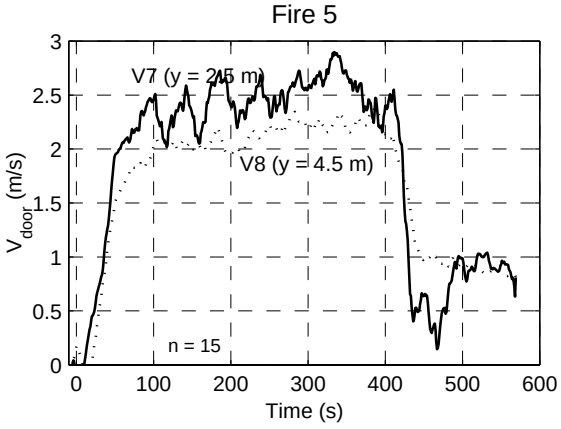


*Figure 34k. Door flow velocities 7–8.*

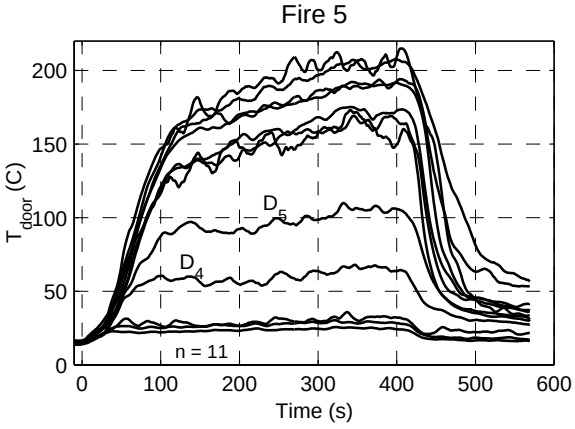


*Figure 34l. Door flow temperatures.*

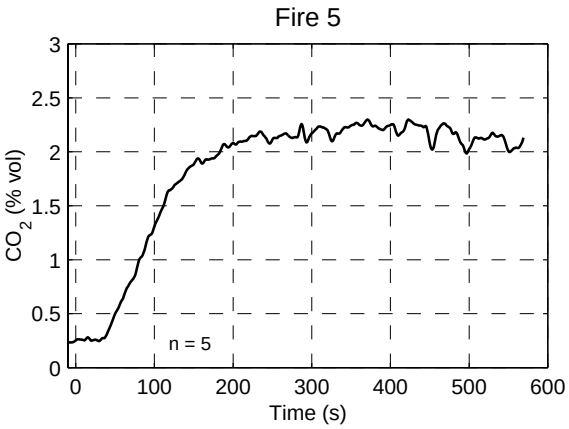


*Figure 34m. $CO_2$ concentration.*

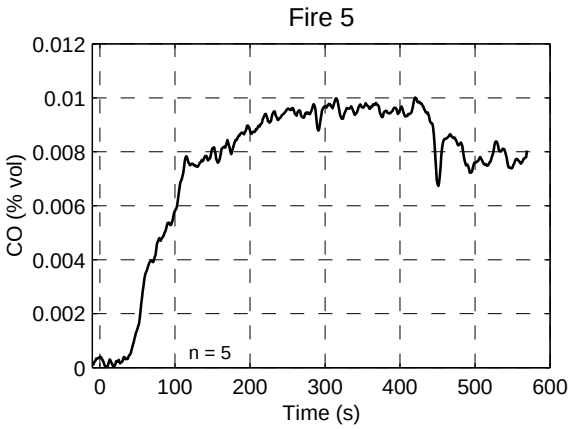


*Figure 34n. CO concentration.*

# Appendix H: Results of the room fire type 6

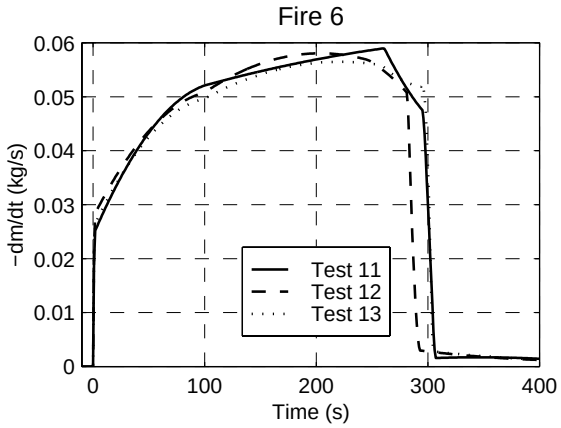


*Figure 35a. Mass loss rate.*

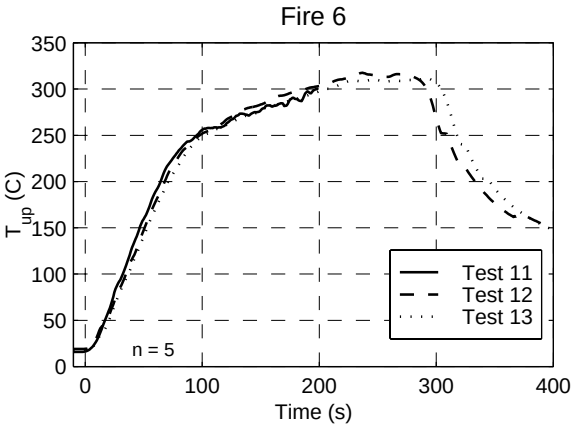


*Figure 35b. Upper layer temperature.*

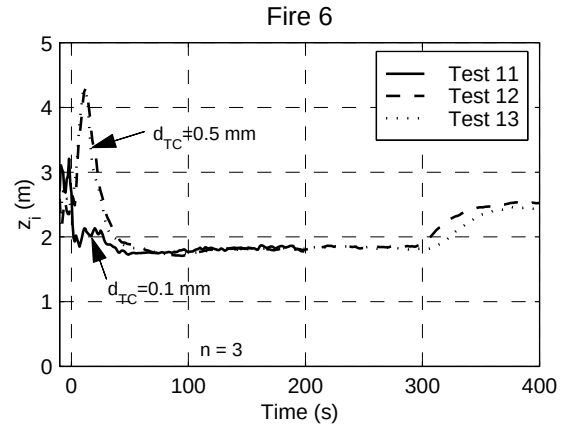


*Figure 35c. Interface height.*

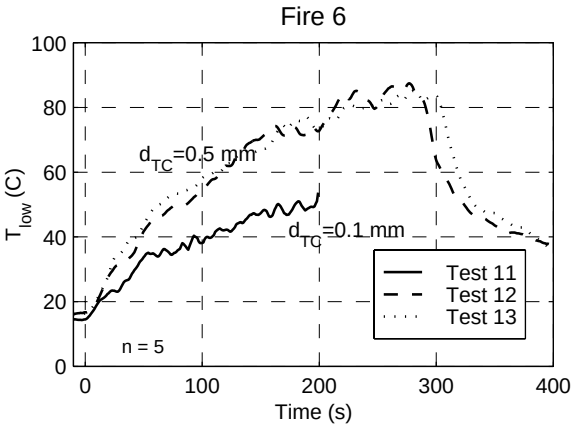


*Figure 35d. Lower layer temperature.*

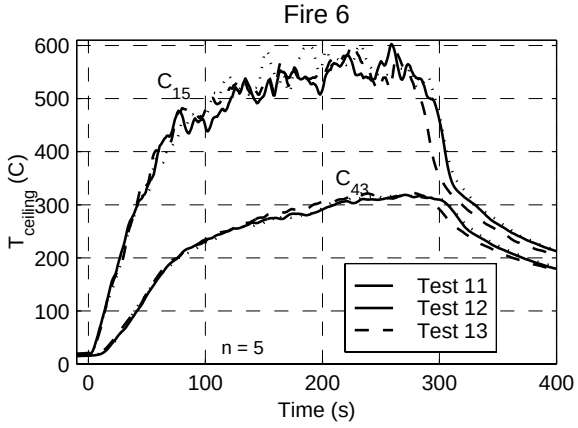


*Figure 35e. Ceiling jet temperatures.*

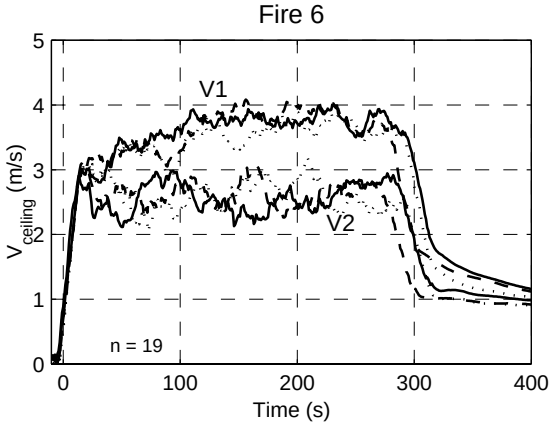


*Figure 35f. Ceiling jet velocities.*

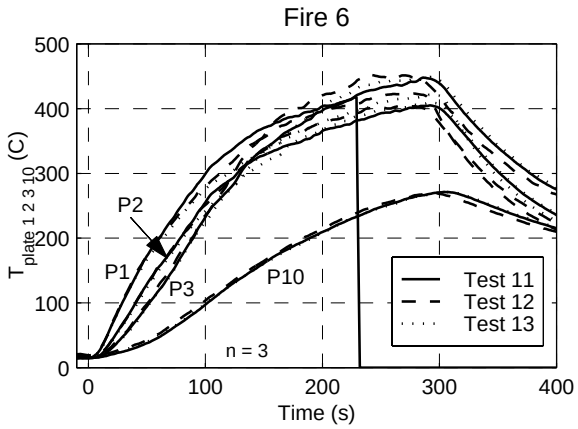


*Figure 35g. Plate temperatures (wall).*

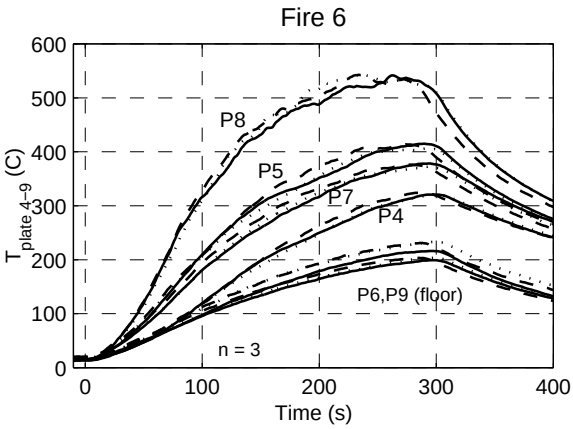


*Figure 35h. Plate temperatures (ceiling & floor).*

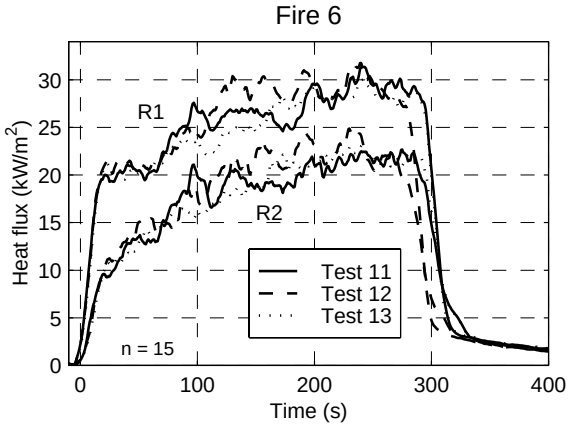


*Figure 35i. Heat fluxes (wall).*

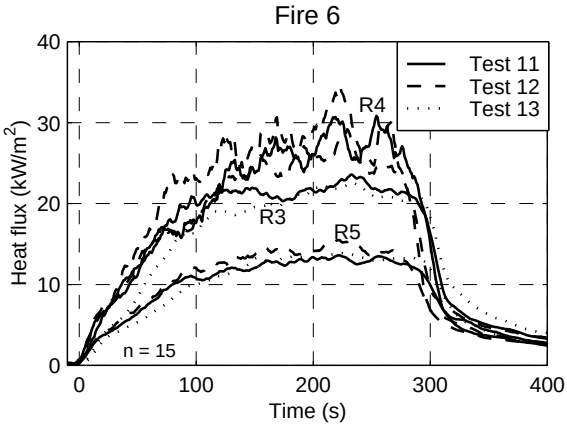


*Figure 35j. Heat fluxes (ceiling).*

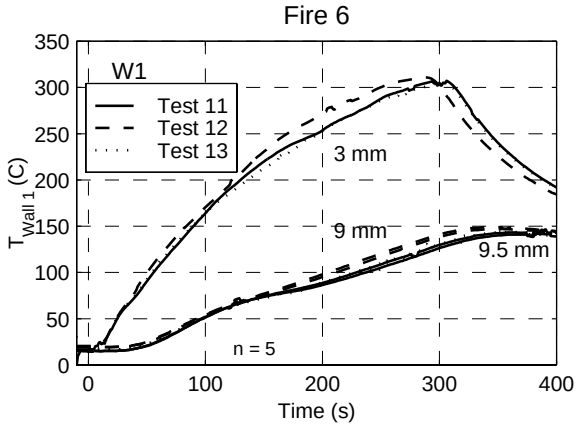


*Figure 35k. Wall temperatures W1.*

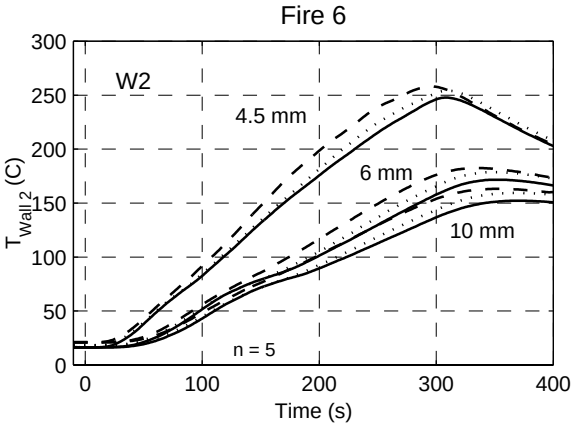


*Figure 35l. Wall temperature W2.*

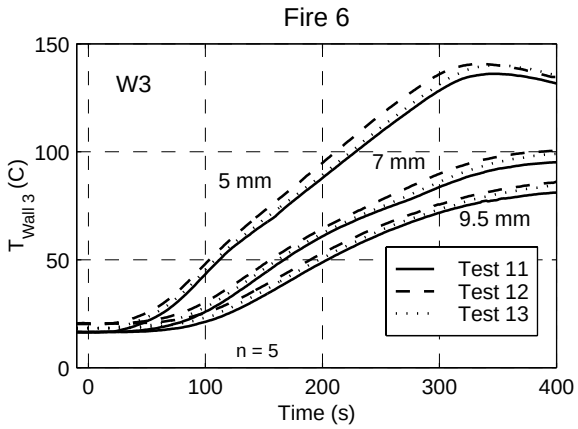


*Figure 35m. Wall temperature W3.*

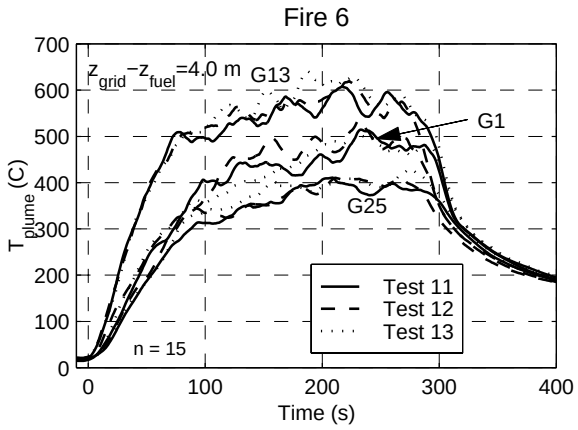


*Figure 35n. Grid temperatures. G13 is the at the center of the grid. G1 and G25 at corners.*

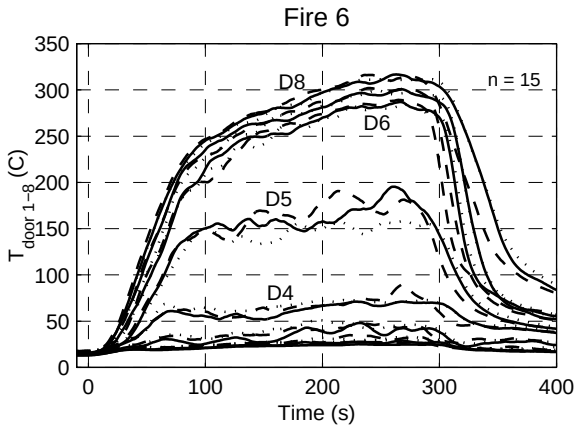


*Figure 35o. Door flow temperatures 1–8.*

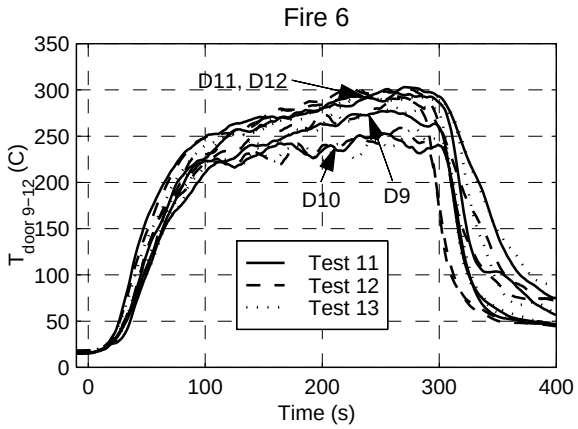


*Figure 35p. Door flow temperatures 9–12.*

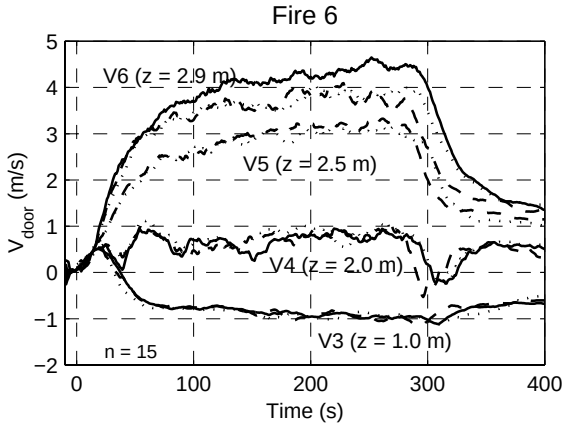


*Figure 35q. Door flow velocities 3–6.*

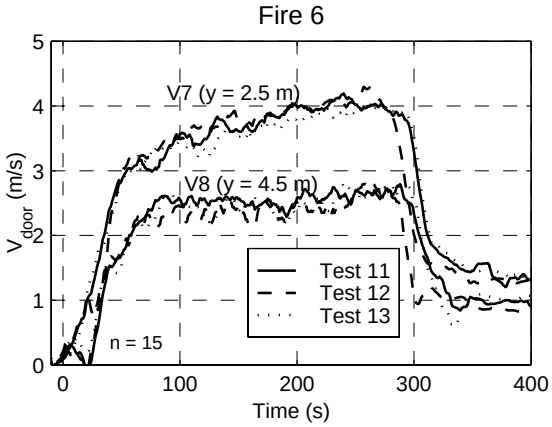


*Figure 35r. Door flow velocities 7–8.*

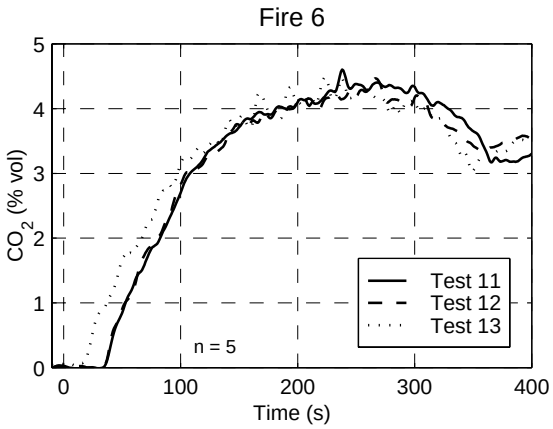


*Figure 35s. $CO_2$ concentration.*

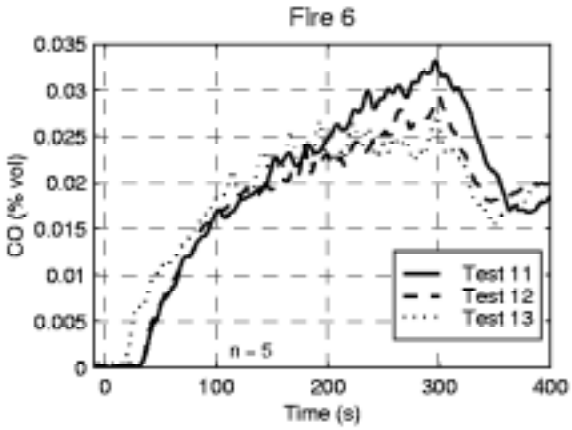


*Figure 35t. CO concentration.*

# Appendix I: Results of the room fire type 7

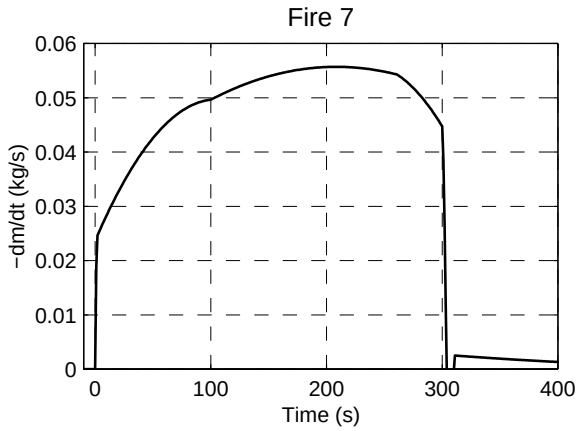


*Figure 36a. Mass loss rate.*

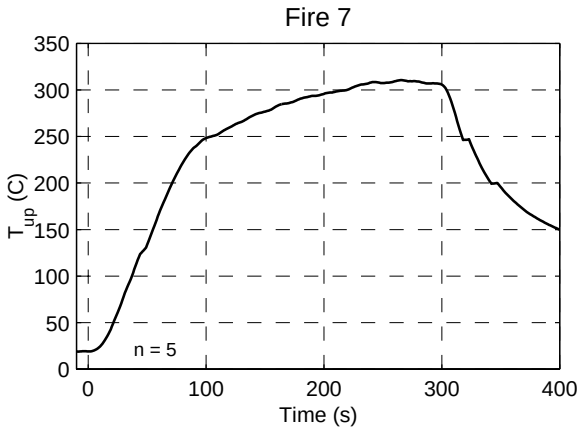


*Figure 36b. Upper layer temperature.*

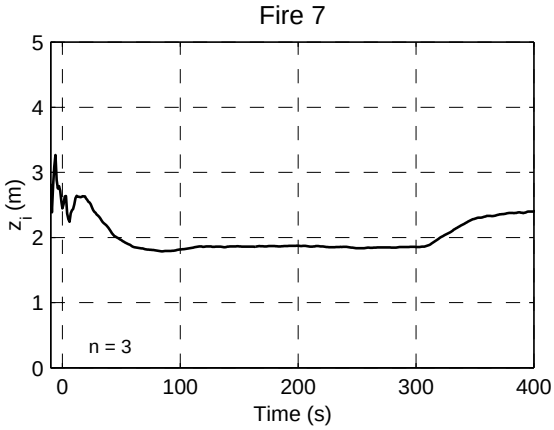


*Figure 36c. Interface height.*

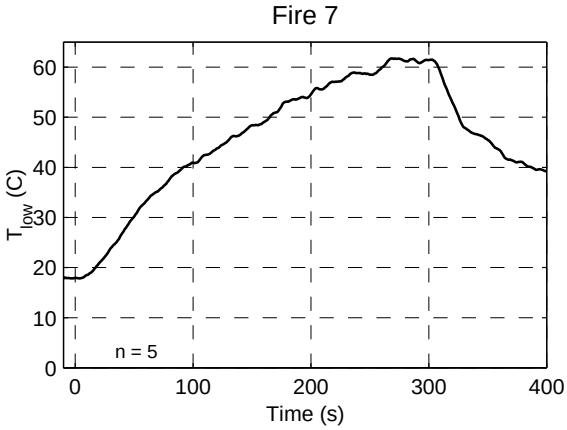


*Figure 36d. Lower layer temperature.*

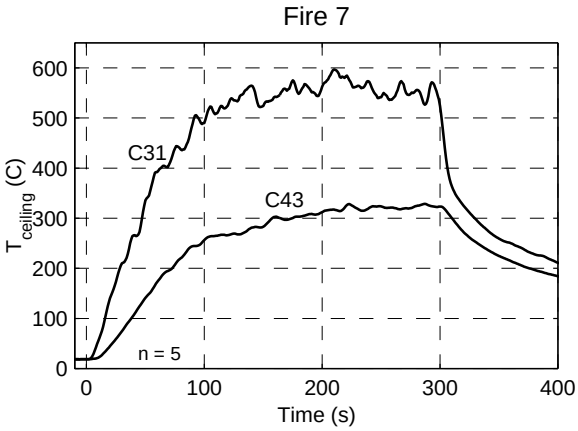


*Figure 36e. Ceiling jet temperatures.*

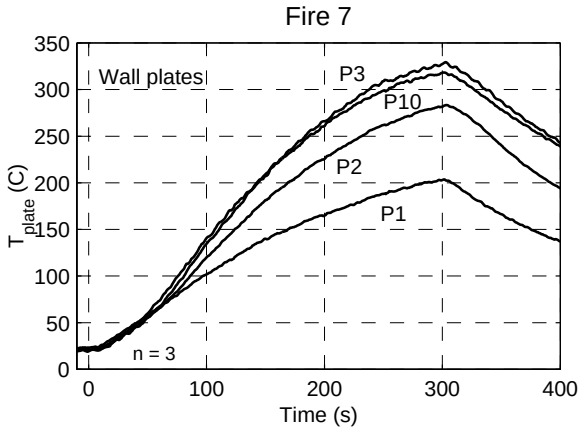


*Figure 36f. Plate temperatures (wall).*

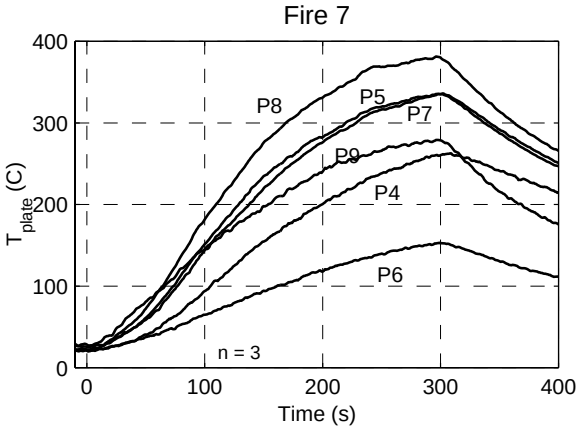


*Figure 36g. Plate temperatures (ceiling & floor).*

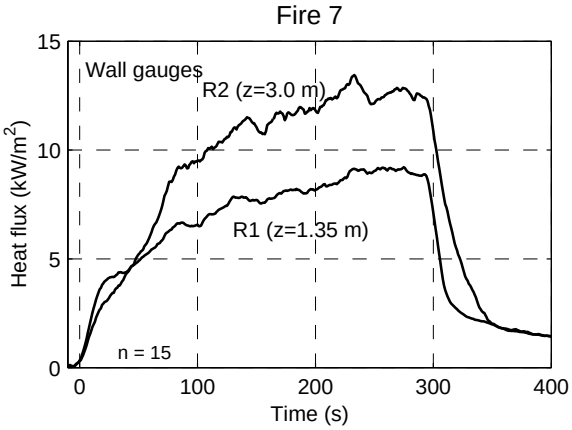


*Figure 36h. Heat fluxes (wall).*

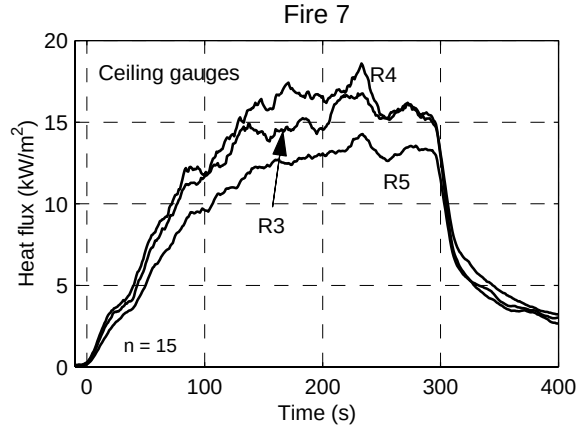


*Figure 36i. Heat fluxes (ceiling).*

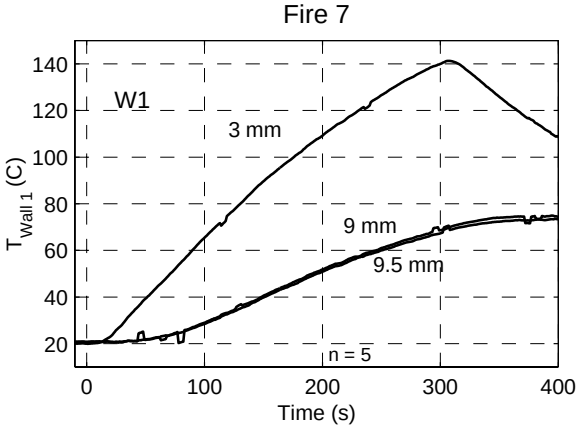


*Figure 36j. Wall temperatures W1.*

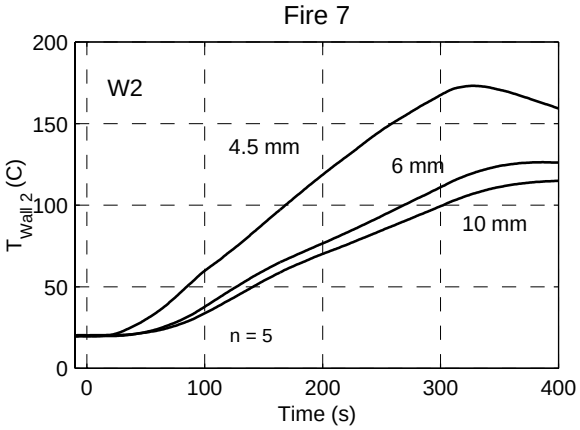


*Figure 36k. Wall temperatures W2.*

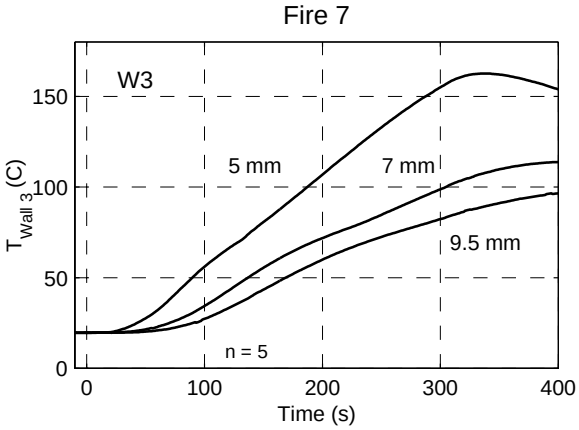


*Figure 36l. Wall temperature W3.*

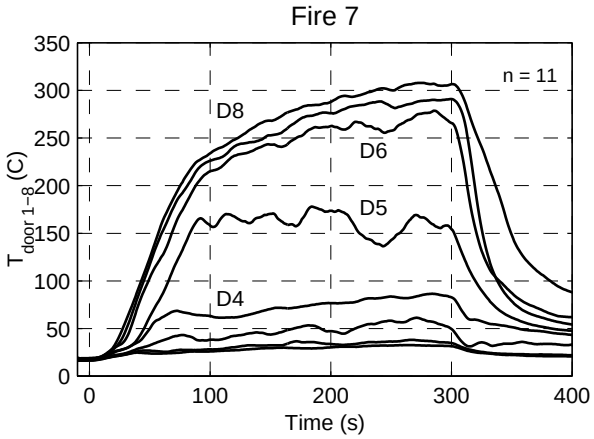


*Figure 36m. Door flow temperatures 1–8.*

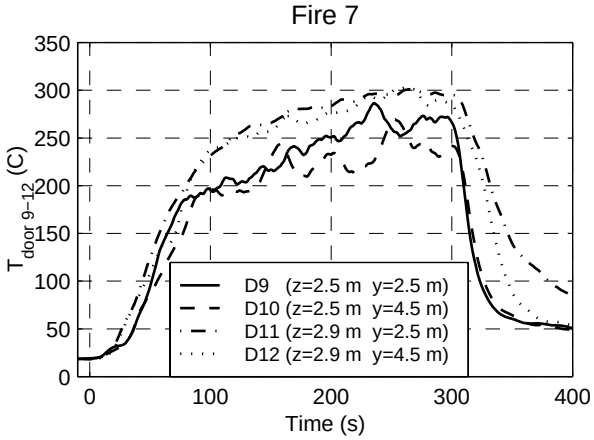


*Figure 36n. Door flow temperatures 9–12.*

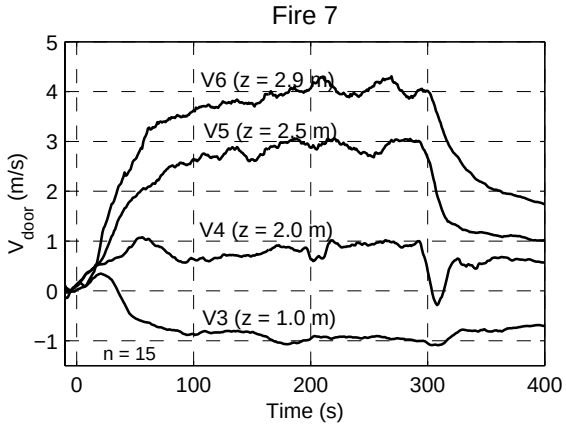


*Figure 36o. Door flow velocities 3–6.*

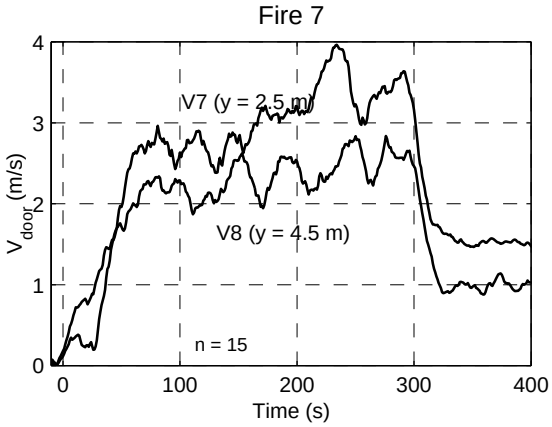


*Figure 36p. Door flow velocities 7–8.*

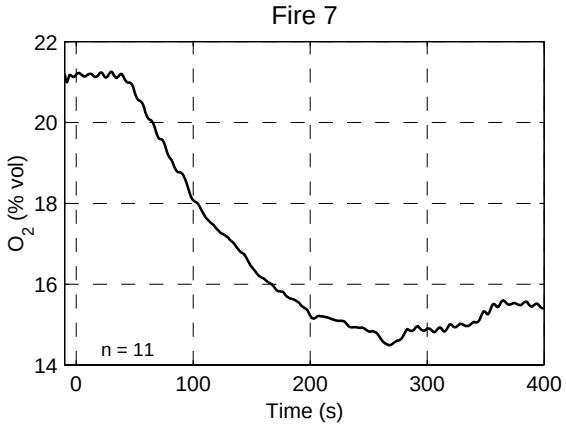


*Figure 36q. $O_2$ concentration.*


*Figure 36r. $CO_2$ concentration.*

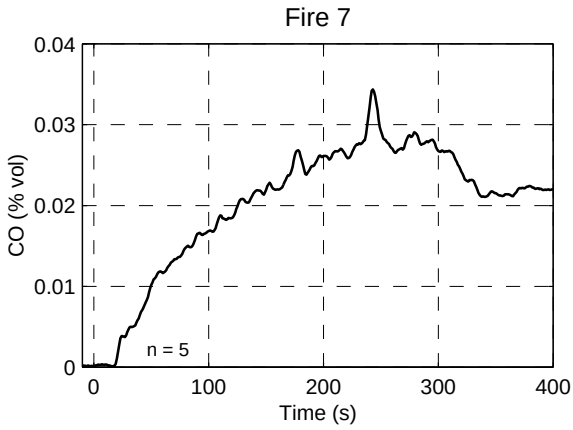


*Figure 36s. CO concentration.*

# Appendix J: Results of the room fire type 7B

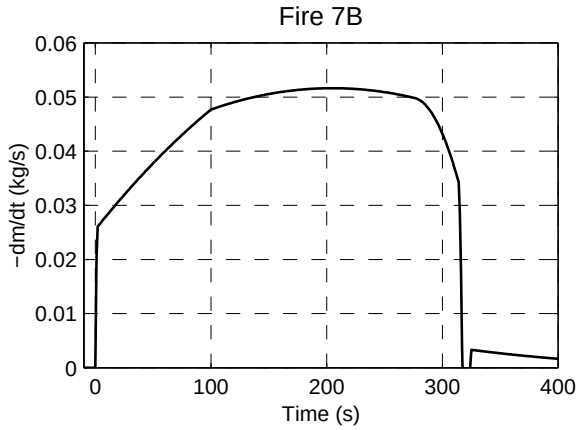


*Figure 37a. Mass loss rate.*

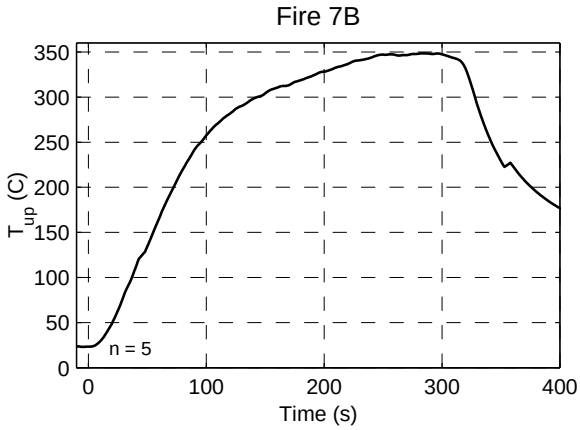


*Figure 37b. Upper layer temperature.*

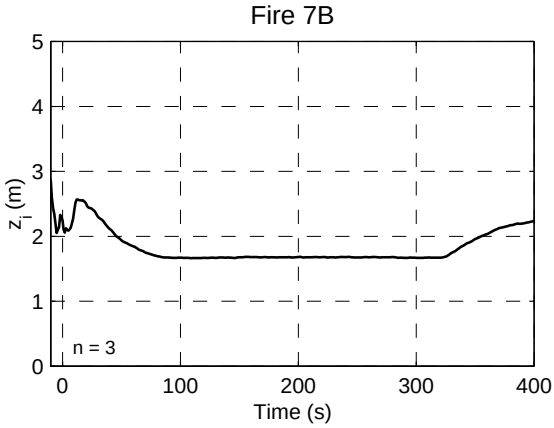


*Figure 37c. Interface height.*

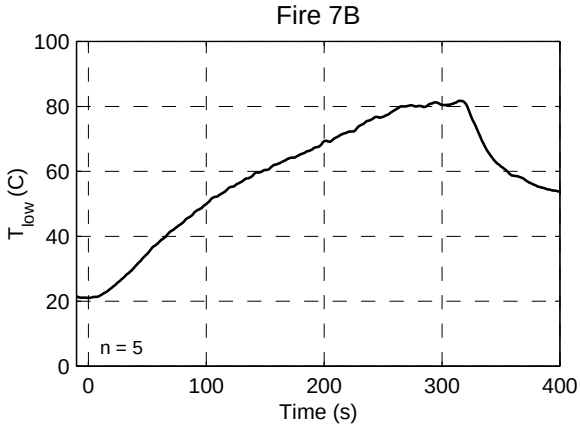


*Figure 37d. Lower layer temperature.*

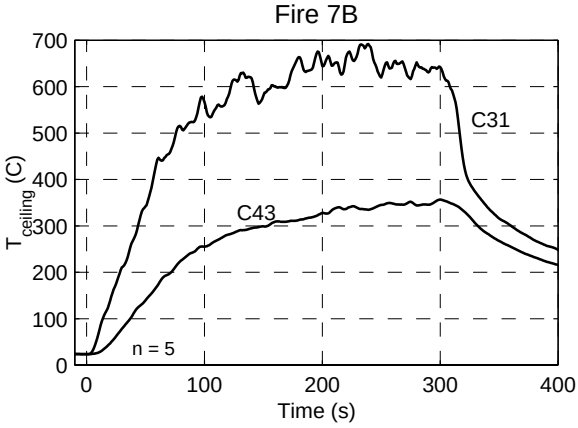


*Figure 37e. Ceiling jet temperatures.*

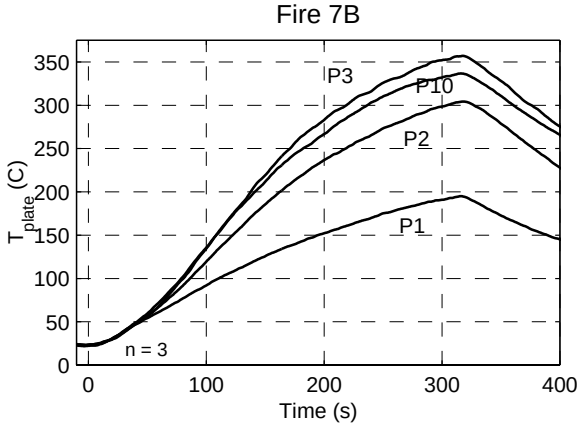


*Figure 37f. Plate temperatures (wall).*

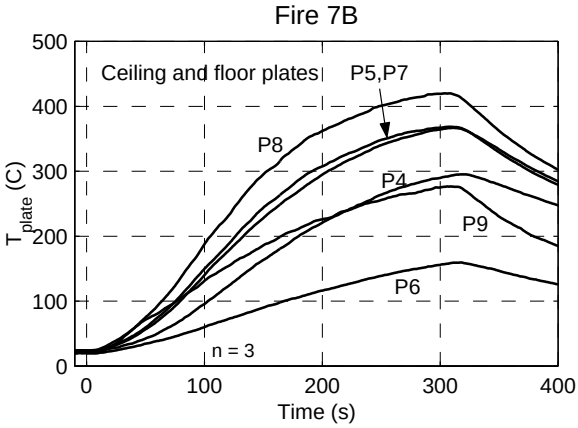


*Figure 37g. Plate temperatures (ceiling & floor).*

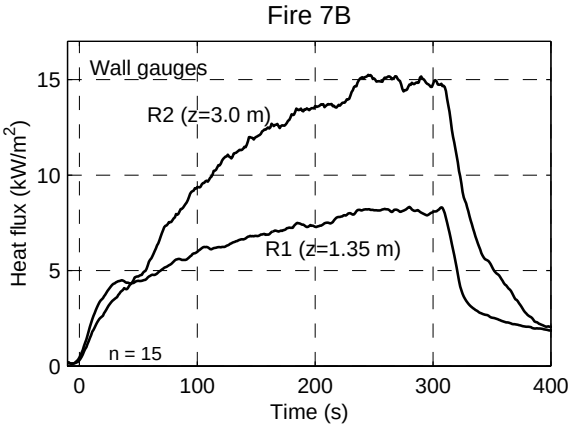


*Figure 37h. Heat fluxes (wall).*

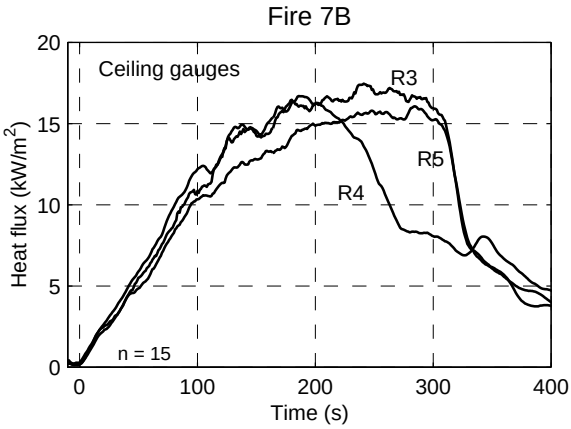


*Figure 37i. Heat fluxes (ceiling).*

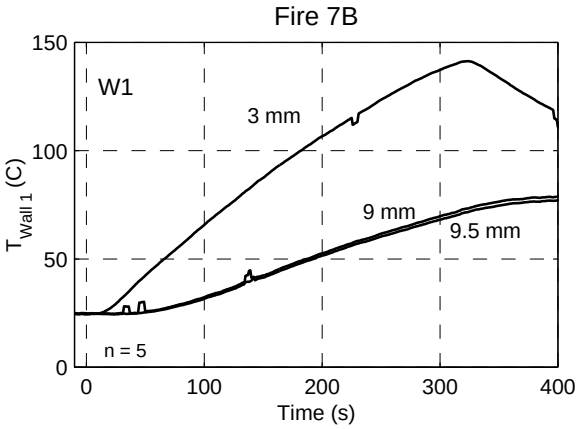


*Figure 37j. Wall temperatures W1.*

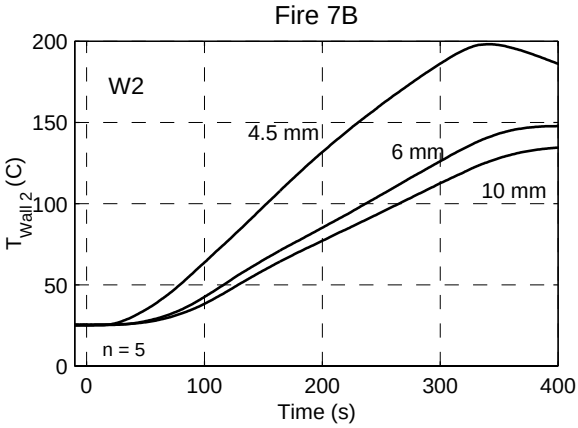


*Figure 37k. Wall temperatures W2.*

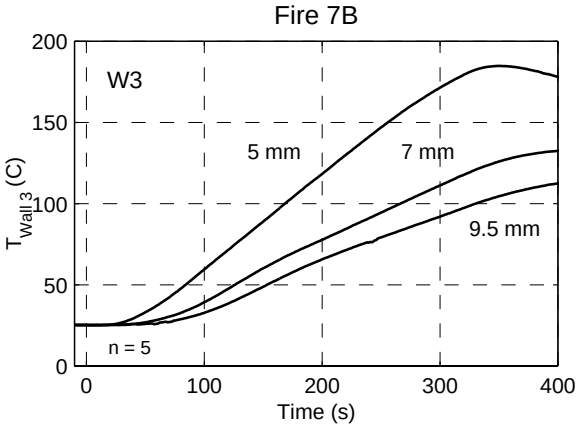


*Figure 37l. Wall temperature W3.*

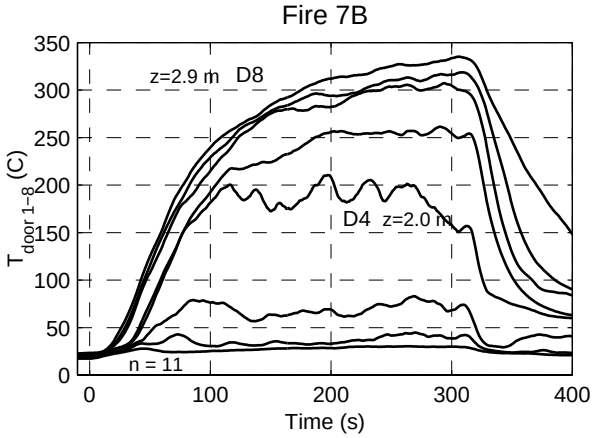


*Figure 37m. Door flow temperatures 1-8.*

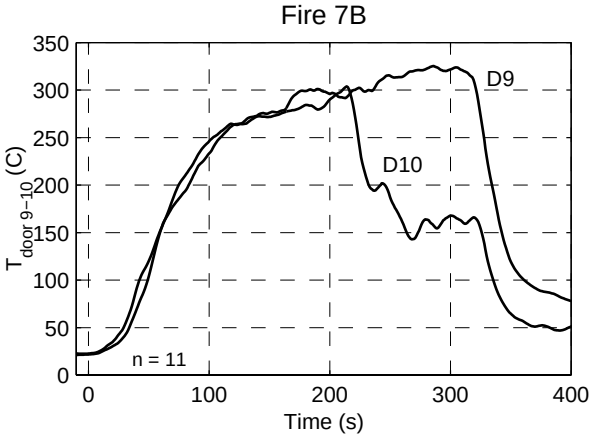


*Figure 37n. Door flow temperatures 9-12.*

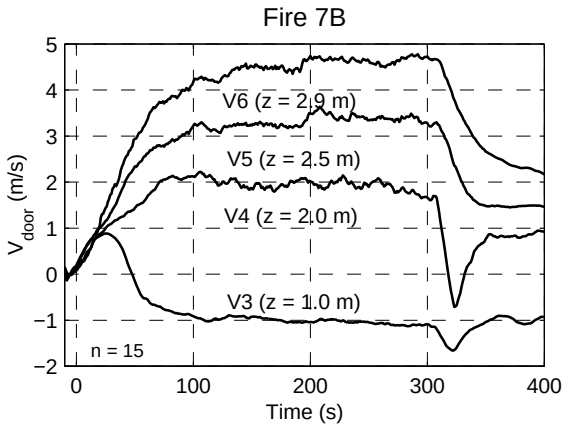


*Figure 37o. Door flow velocities 3–6.*

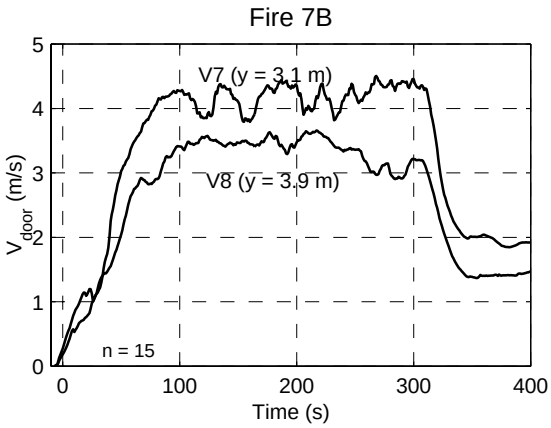


*Figure 37p. Door flow velocities 7-8.*

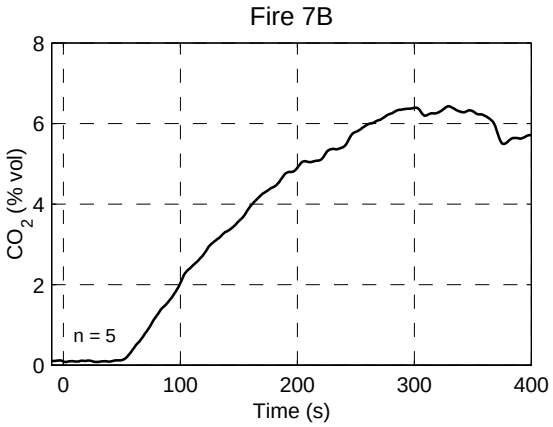


*Figure 37q. $CO_2$ concentration.*


*Figure 37r. CO concentration.*

# Appendix K: Results of the room fire type 8

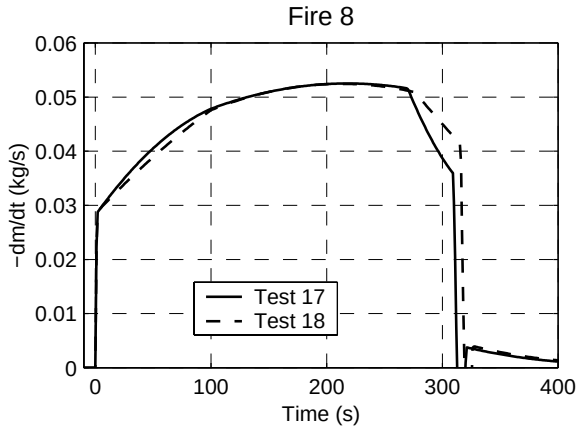


*Figure 38a. Mass loss rate.*

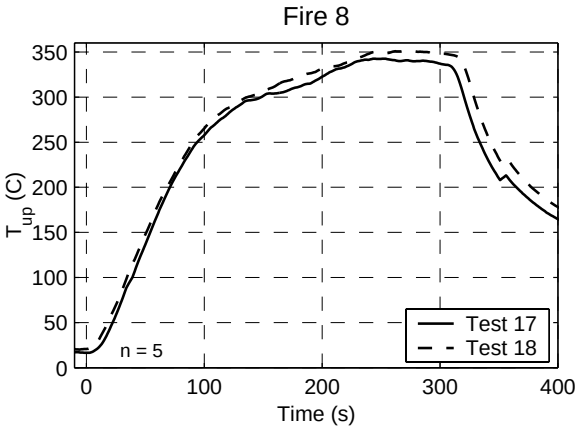


*Figure 38b. Upper layer temperature.*

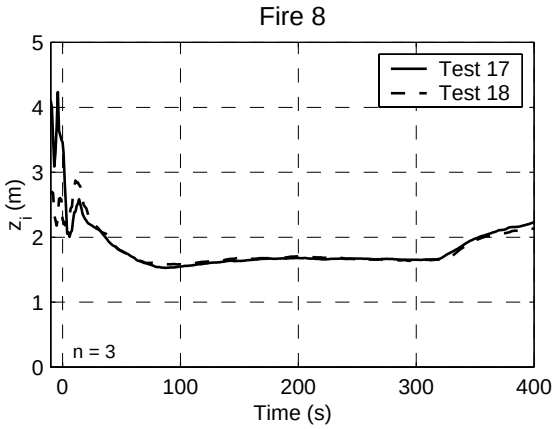


*Figure 38c. Interface height.*

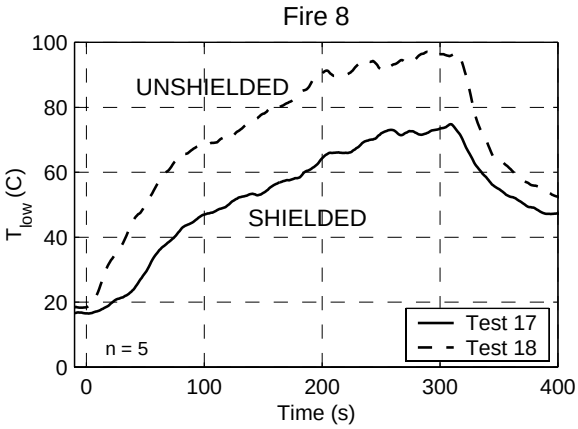


*Figure 38d. Lower layer temperature.*

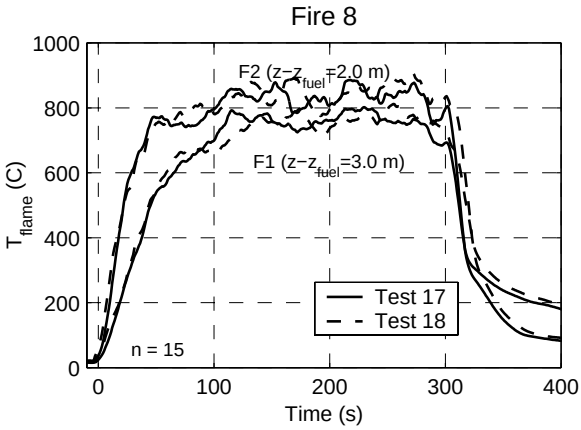


*Figure 38e. Flame temperatures.*

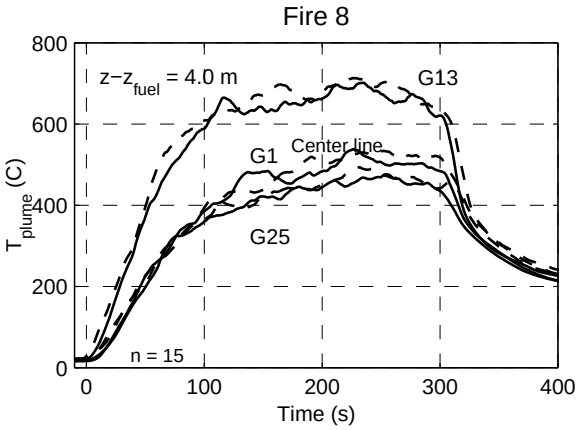


*Figure 38f. Plume temperatures.*

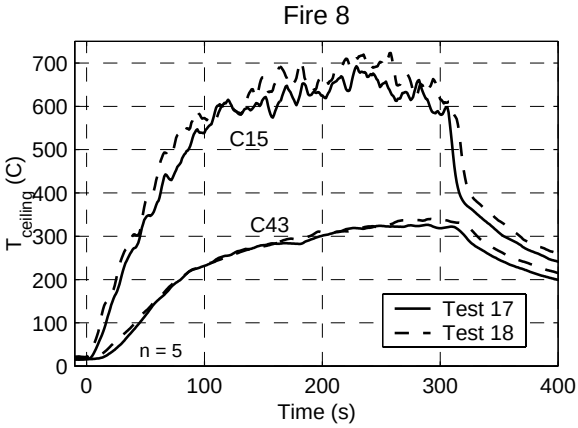


*Figure 38g. Ceiling jet temperatures.*

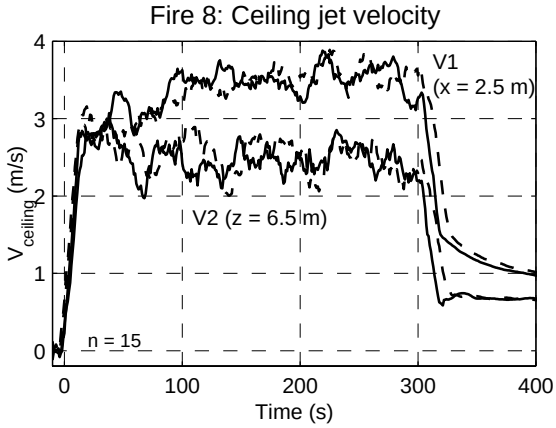


*Figure 38h. Ceiling jet velocities..*

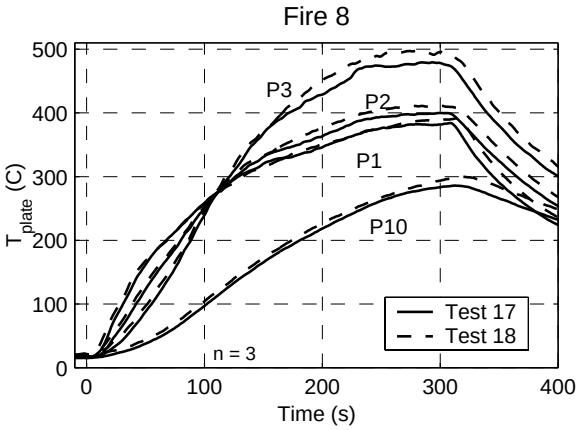


*Figure 38i. Plate temperatures (wall).*

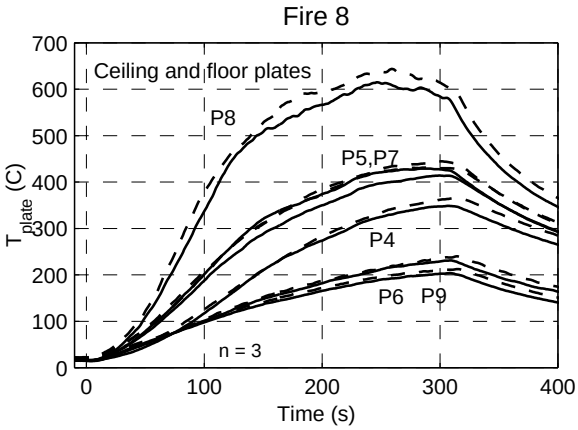


*Figure 38j. Plate temperatures (ceiling & floor).*

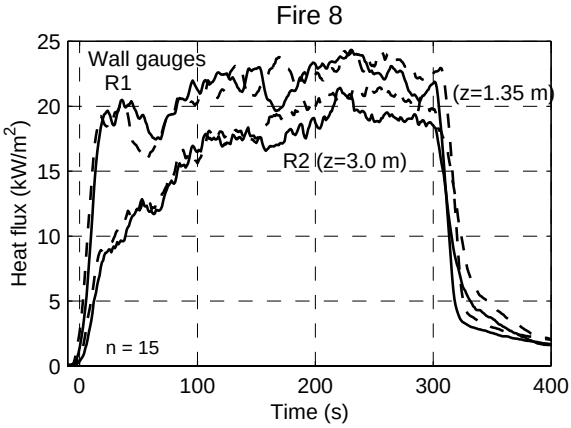


*Figure 38k. Heat fluxes (wall).*

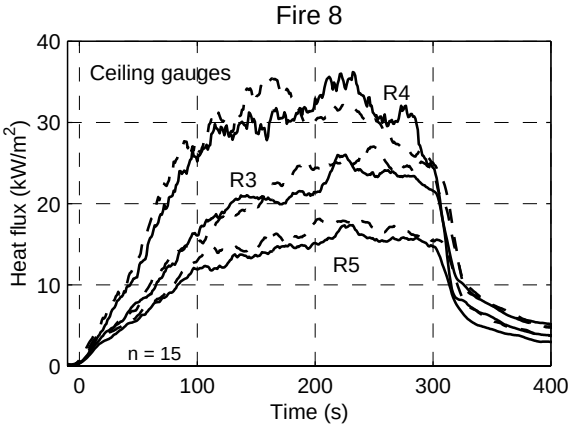


*Figure 38l. Heat fluxes (ceiling).*

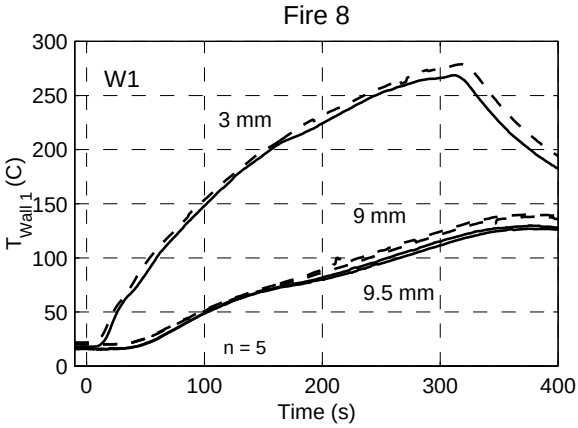


*Figure 38m. Wall temperatures W1.*

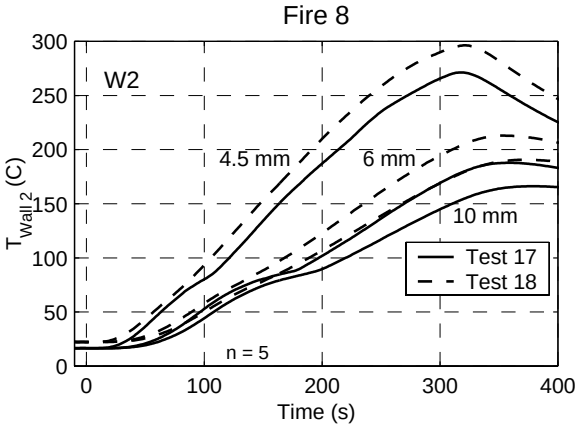


*Figure 38n. Wall temperature W2.*

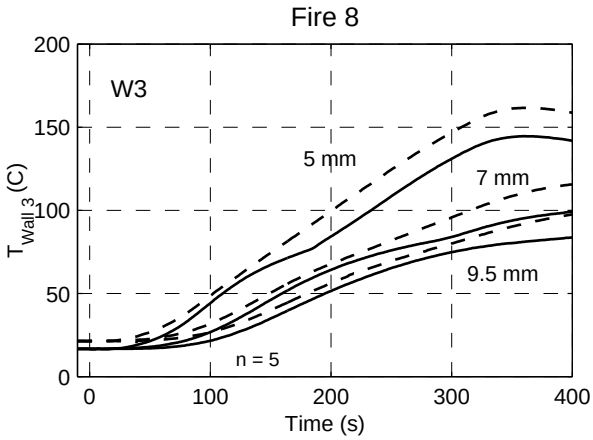


*Figure 38o. Wall temperatures W3.*

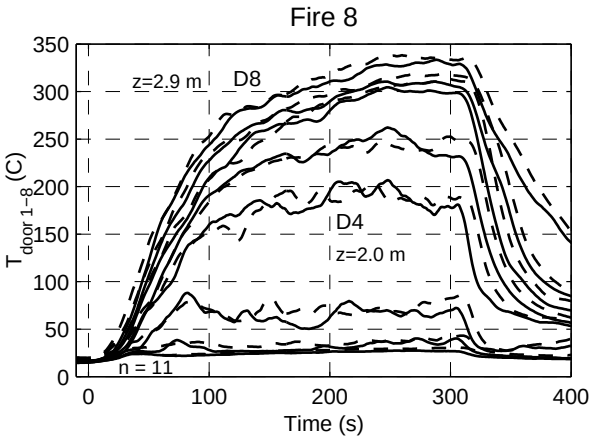


*Figure 38p. Door flow temperatures 1–8.*

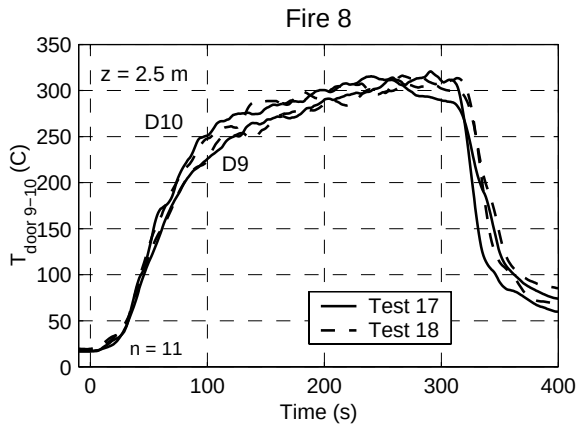


*Figure 38q. Door flow temperatures 9–10.*

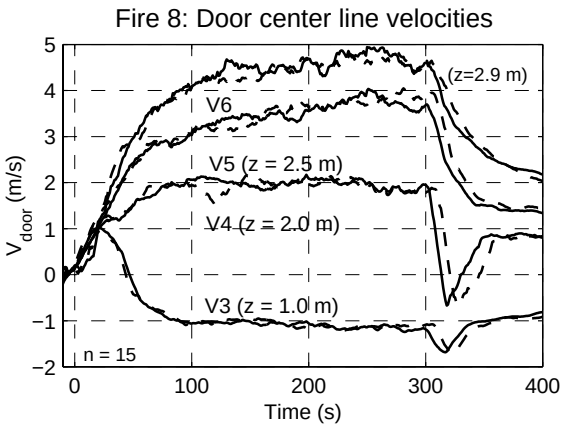


*Figure 38r. Door flow velocities 3–6.*

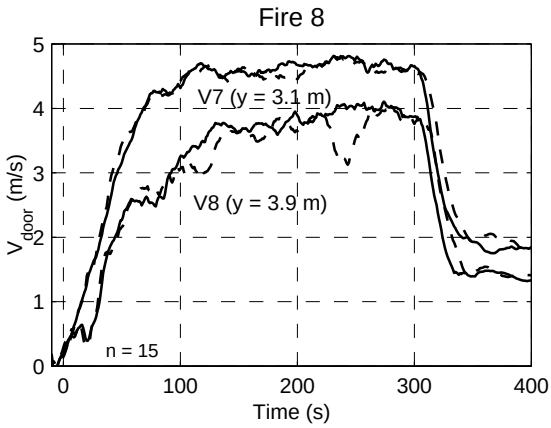


*Figure 38s. Door flow velocities 7–8.*

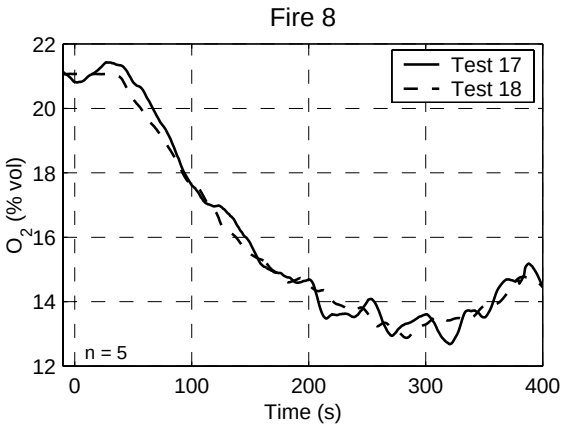


*Figure 38t. $O_2$ concentration.*

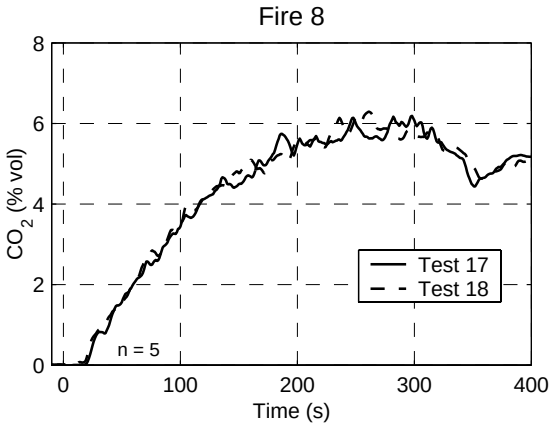


*Figure 38u. $CO_2$ concentration.*

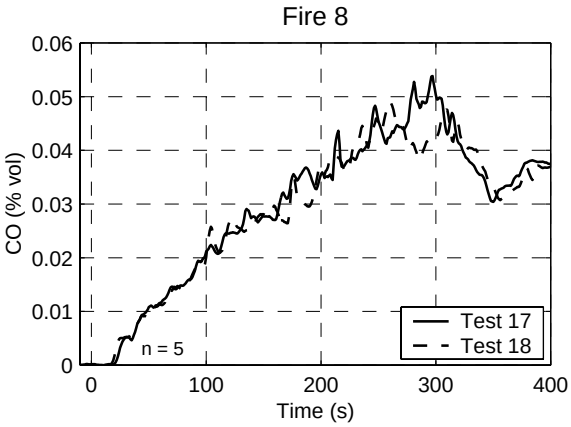


*Figure 38v. CO concentration.*

# Appendix L: Results of the room fire type 9

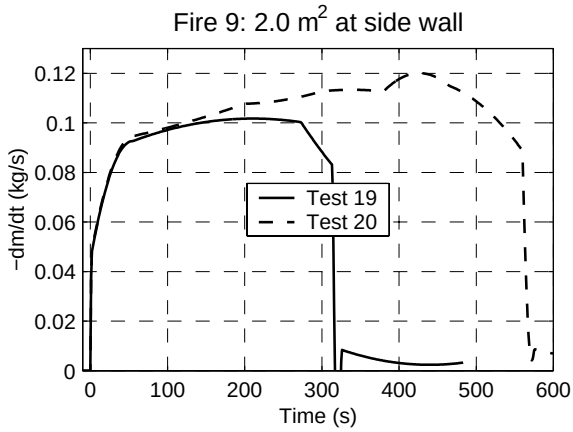


*Figure 39a. Mass loss rates in Fire 9.*

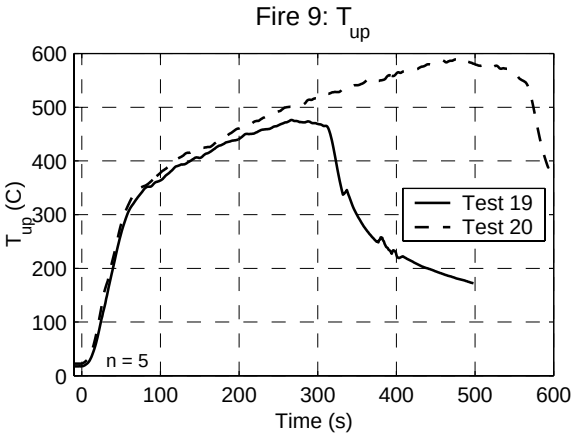


*Figure 39b. Upper layer temperatures.*

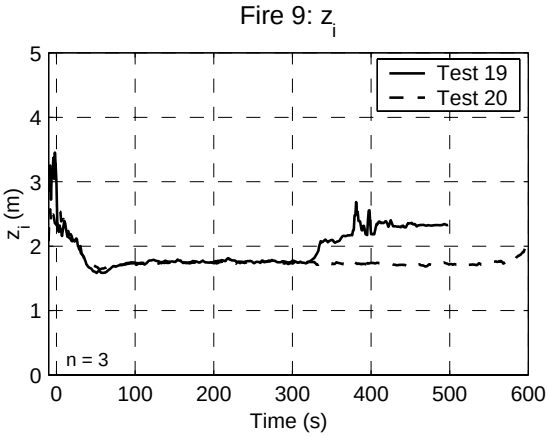


*Figure 39c. Layer interfaces.*

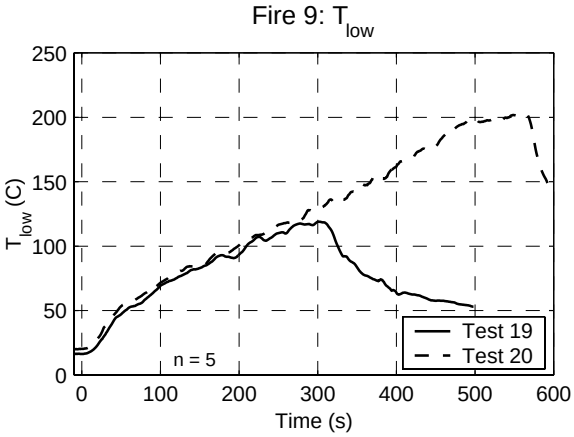


*Figure 39d. Lower layer temperatures.*

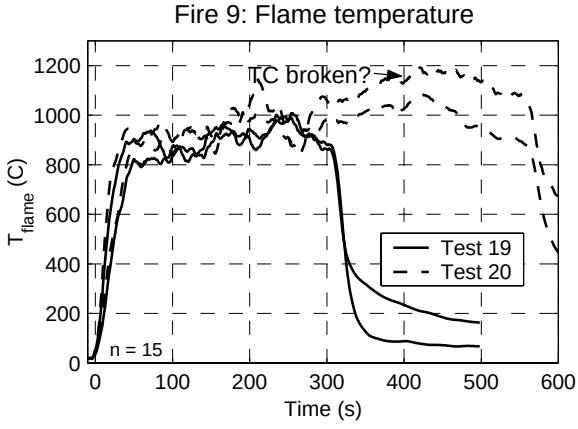


*Figure 39e. Flame temperatures.*

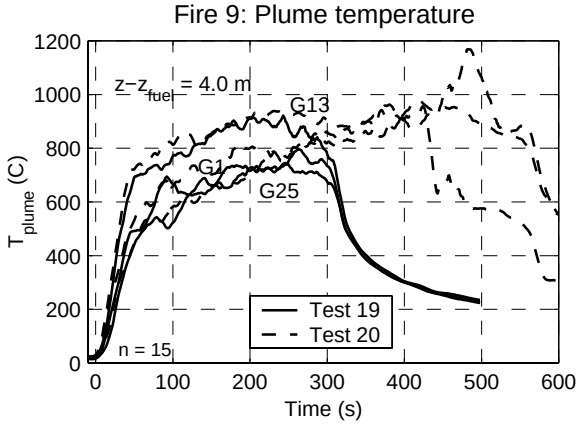


*Figure 39f. Plume temperatures.*

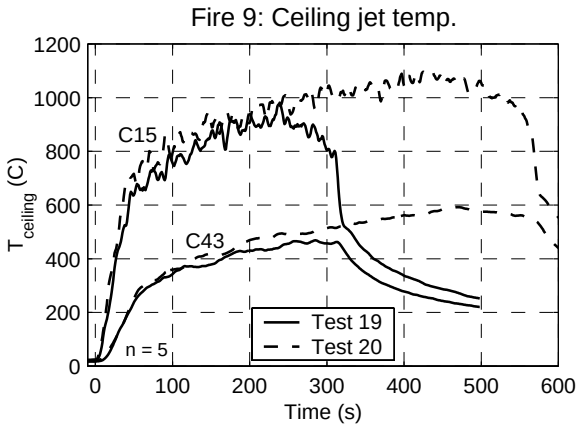


*Figure 39g. Ceiling jet temperatures.*

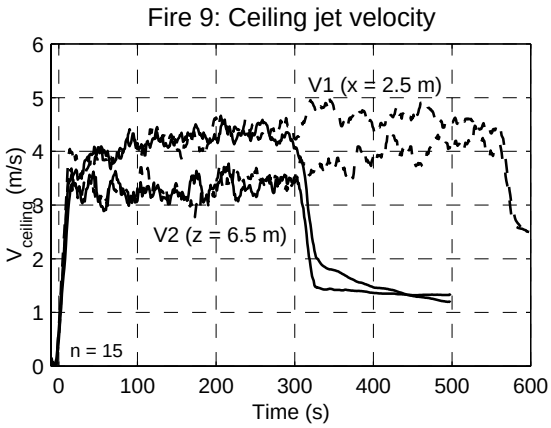


*Figure 39h. Ceiling jet velocities.*

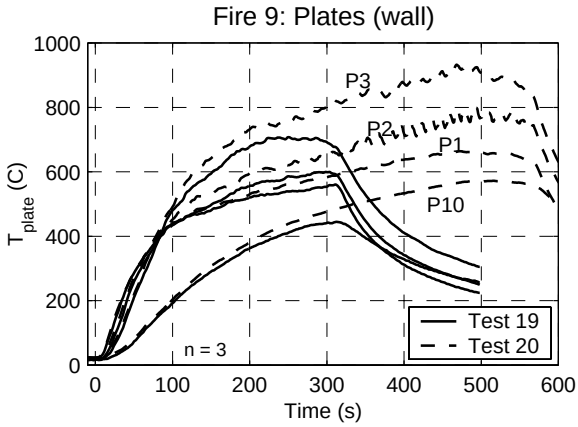


*Figure 39i. Plate temperatures (wall).*

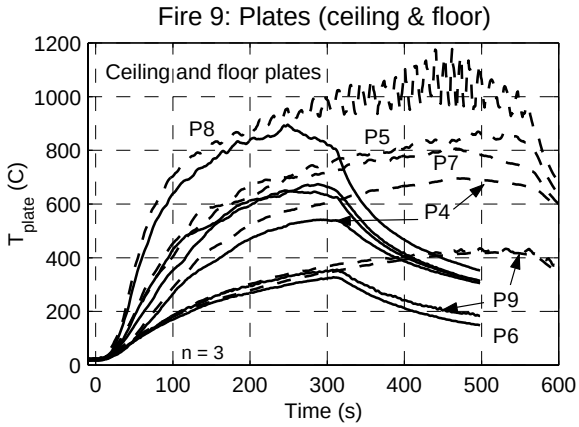


*Figure 39j. Plate temp. (ceiling & floor)*

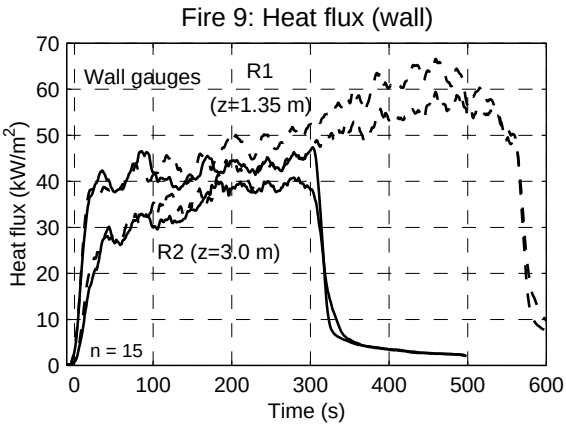


*Figure 39k. Heat fluxes (wall).*

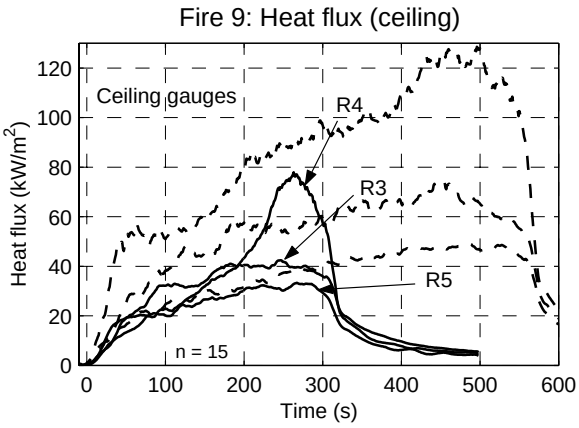


*Figure 39l. Heat fluxes (ceiling).*

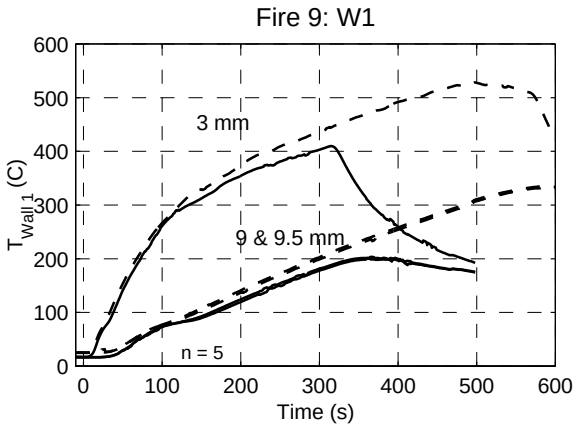


*Figure 39m. Wall temperatures W1.*

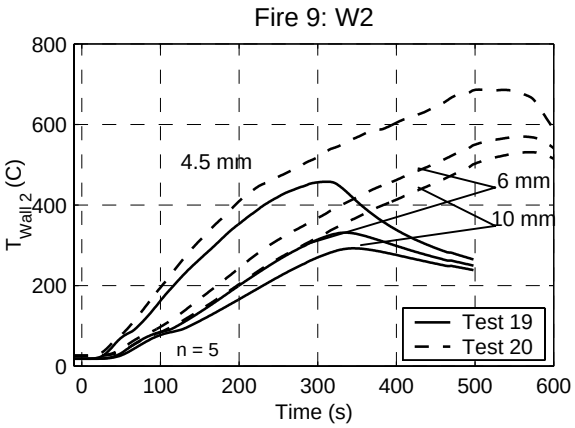


*Figure 39n. Wall temperatures W2.*

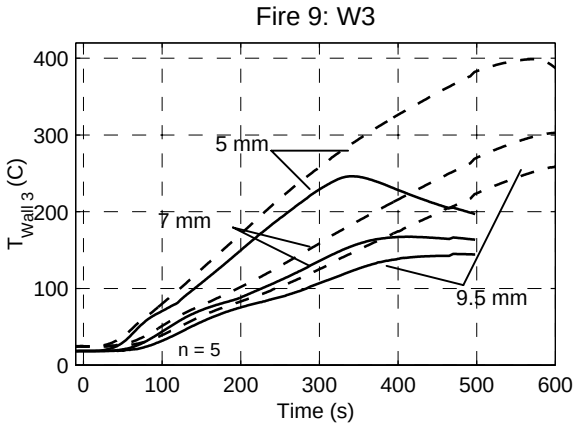


*Figure 39o. Wall temperatures W3.*

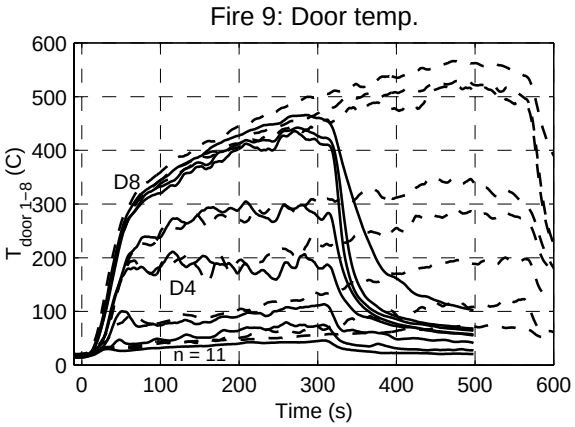


*Figure 39p. Door flow temperatures 1–8.*

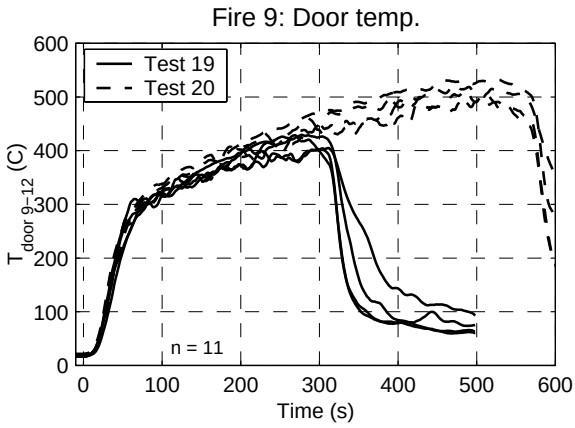


*Figure 39q. Door flow temp. 9–2.*

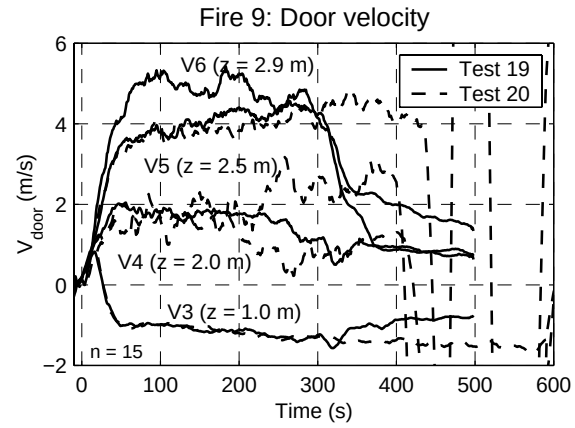


*Figure 39r. Door flow velocities 3–6.*

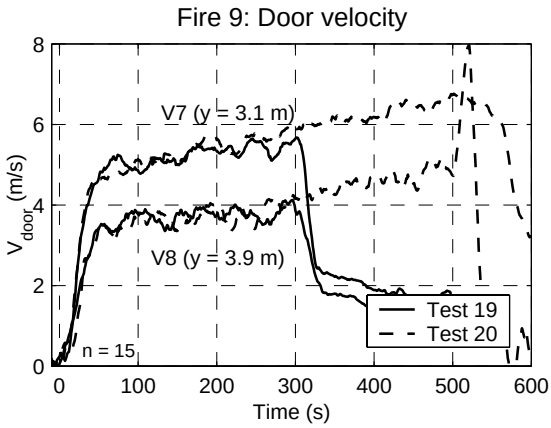


*Figure 39s. Door flow velocities 7–8.*

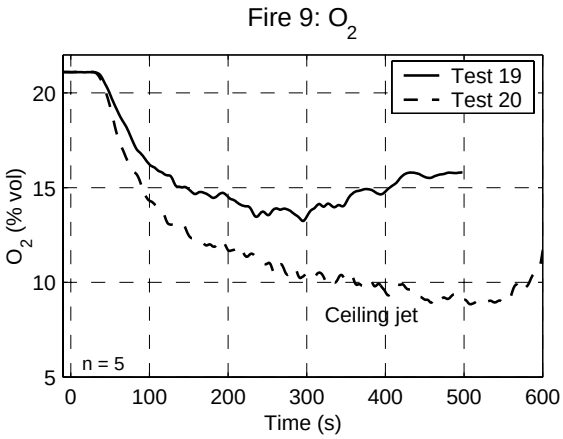


*Figure 39t. $O_2$ concentrations (Test 20 gas samples taken from the ceiling jet).*

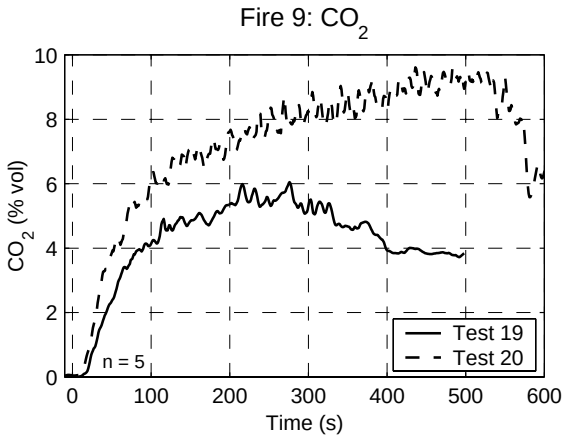


*Figure 39u. $CO_2$ concentrations (Test 20 gas samples taken from the ceiling jet)*

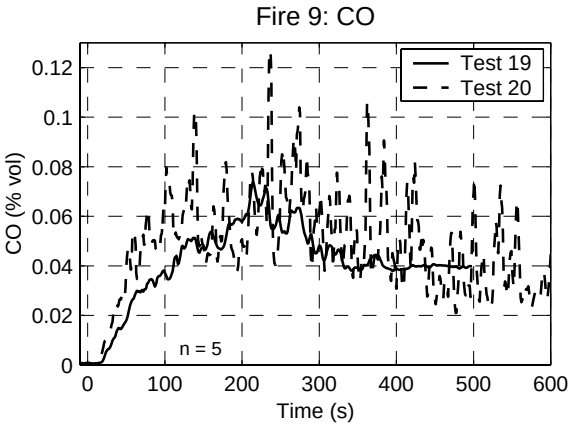


*Figure 39v. CO concentrations (Test 20 gas samples taken from the ceiling jet)*

# Appendix M: Results of the room fire type 10

The following figures show the results of the interlaboratory calibration test (Test 14).

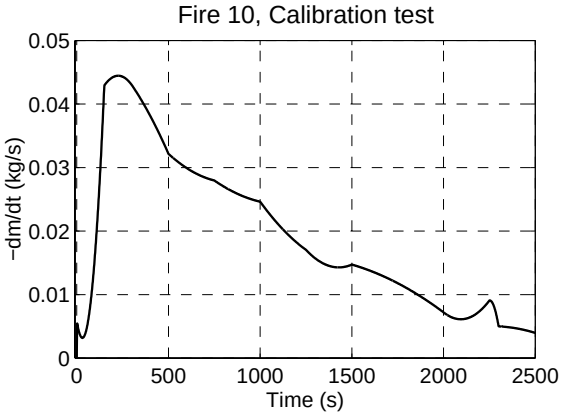


*Figure 40a. Mass loss rate in Fire 10.*

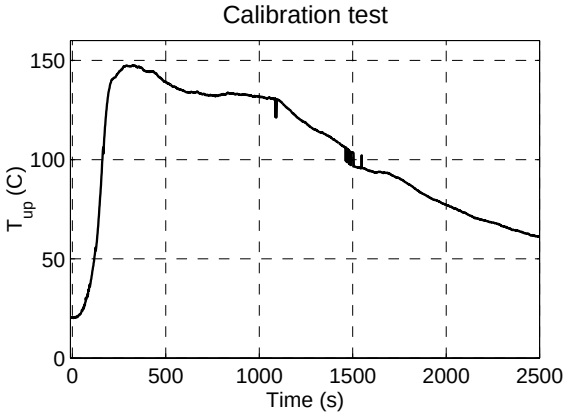


*Figure 40b. Upper layer temperature.*

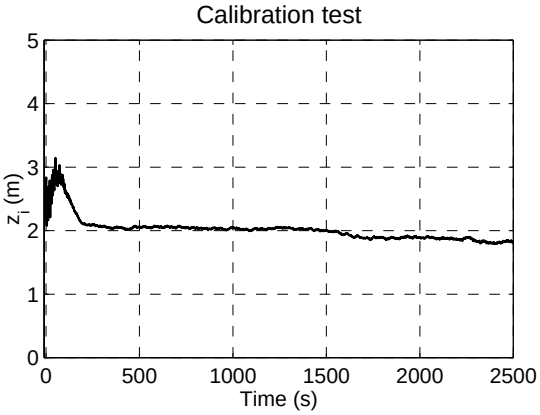


*Figure 40c. Layer interfaces.*

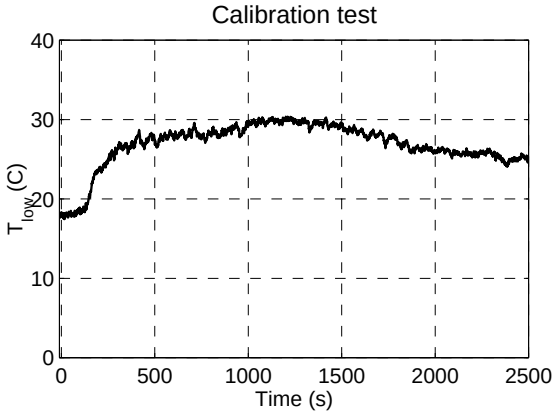


*Figure 40d. Lower layer temperatures.*

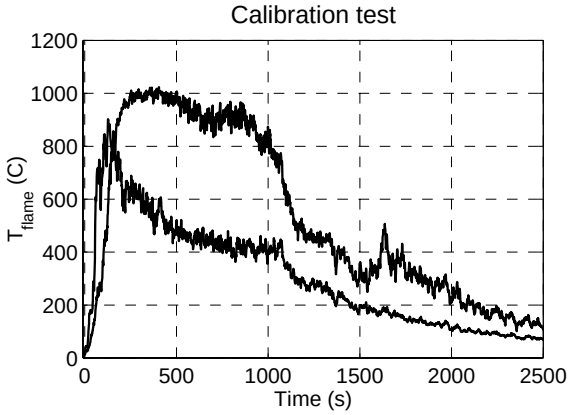


*Figure 40e. Flame temperatures.*

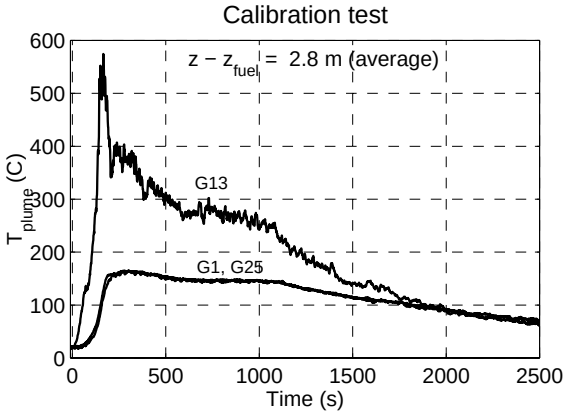


*Figure 40f. Plume temperatures.*

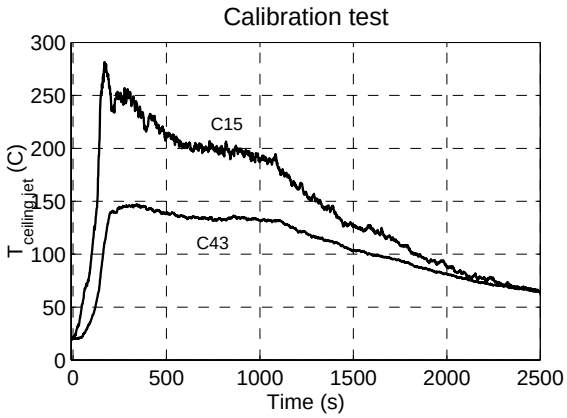


*Figure 40g. Ceiling jet temperatures.*

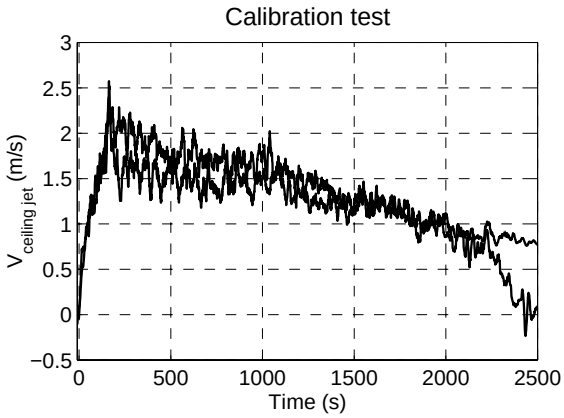


*Figure 40h. Ceiling jet velocities.*

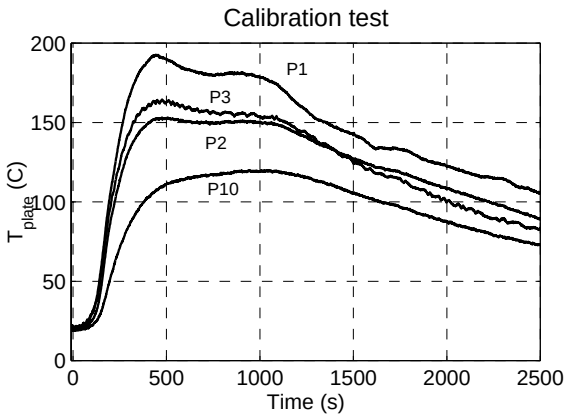


*Figure 40i. Plate temperatures (wall).*

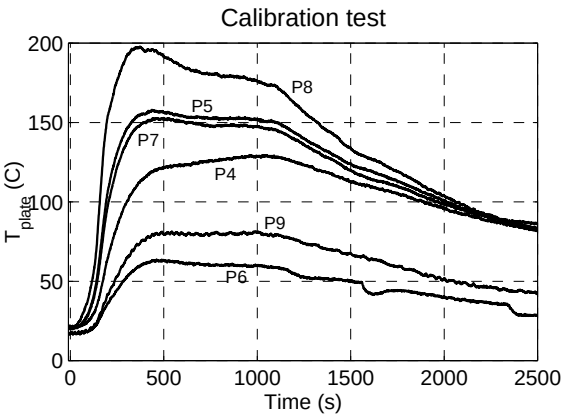


*Figure 40j. Plate temp. (ceiling & floor)*

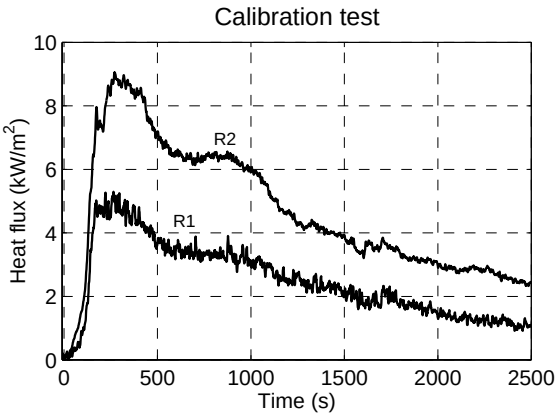


*Figure 40k. Heat fluxes (wall).*

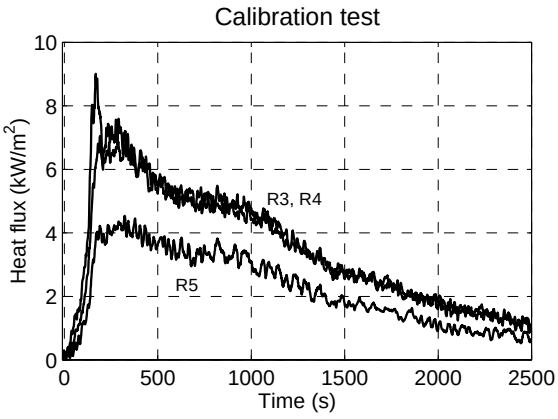


*Figure 40l. Heat fluxes (ceiling).*

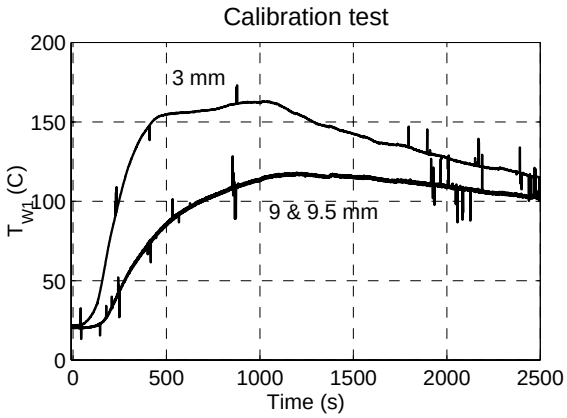


*Figure 40m. Wall temperatures W1.*

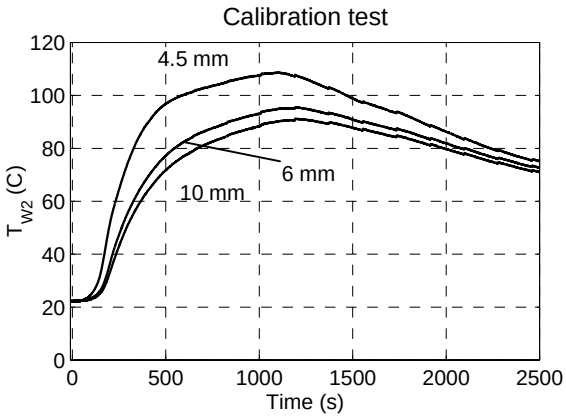


*Figure 40n. Wall temperatures W2.*

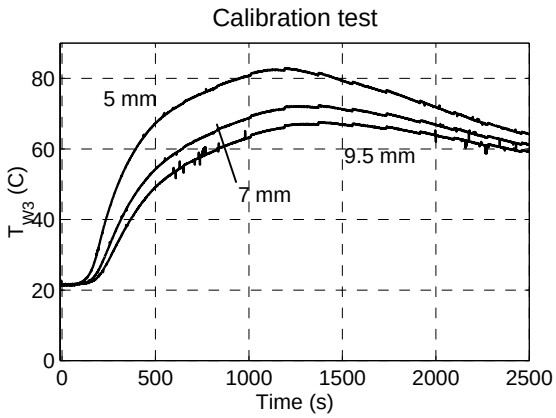


*Figure 40o. Wall temperatures W3.*

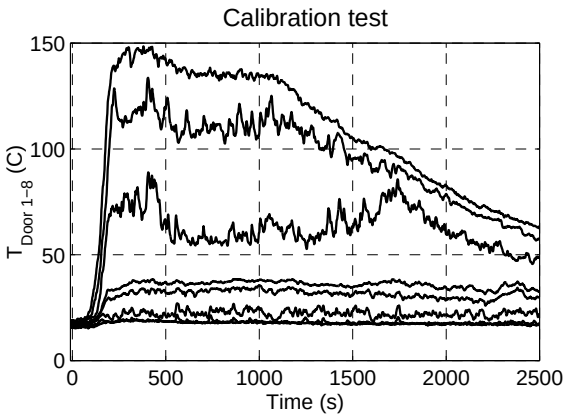


*Figure 40p. Door flow temperatures 1–8.*

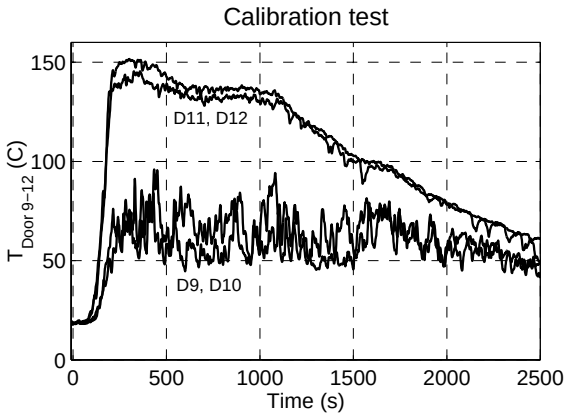


*Figure 40q. Door flow temp. 9–2.*

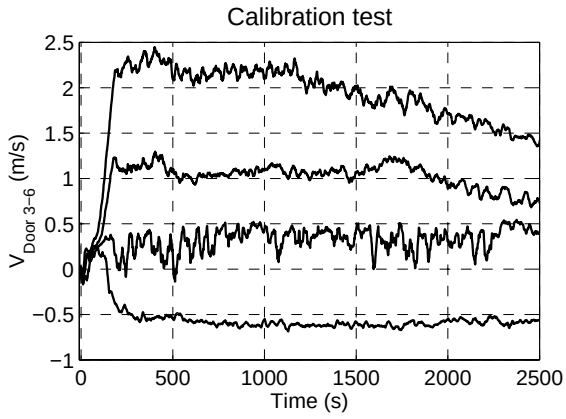


*Figure 40r. Door flow velocities 3–6.*

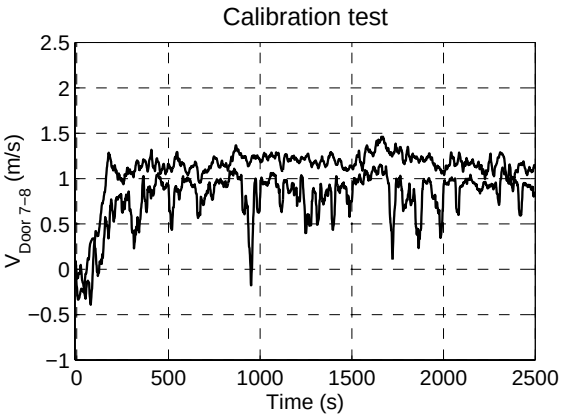


*Figure 40s. Door flow velocities 7–8.*

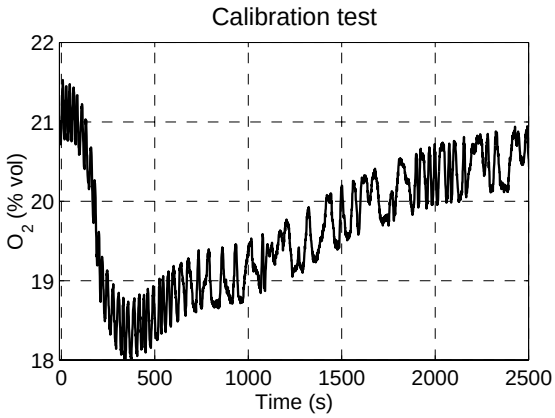


*Figure 40t. $O_2$ concentration. The source of the fluctuations is unknown.*

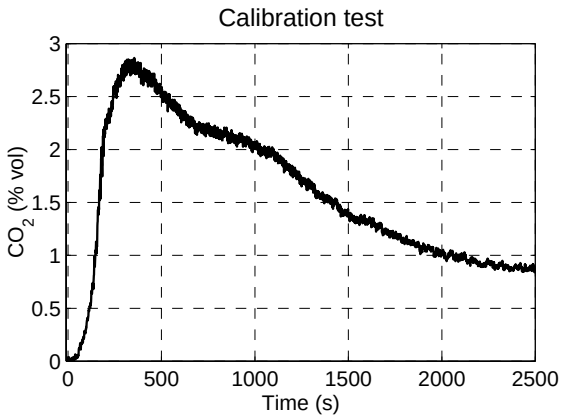


*Figure 40u. $CO_2$ concentration.*

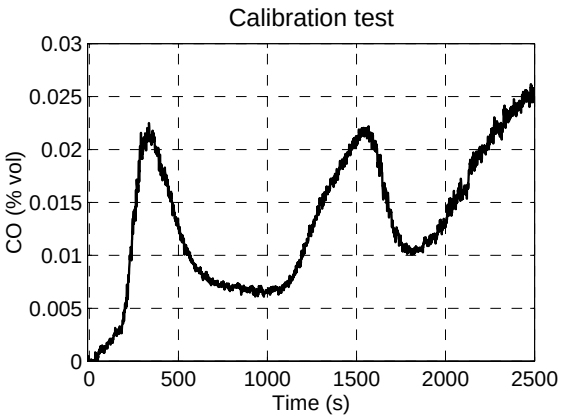


*Figure 40v. CO concentration.*

# Appendix N: Results of the hall fire type 1

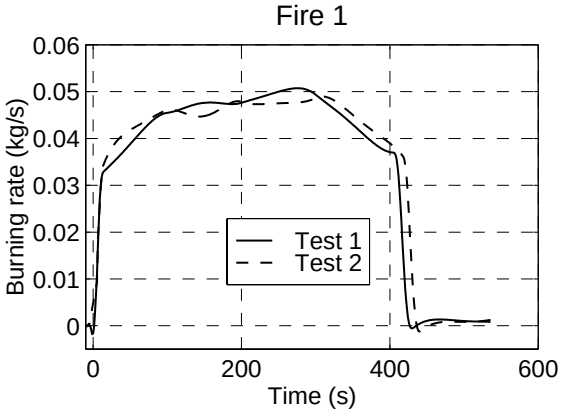


*Figure 41a. Mass loss rates in Fire 1.*

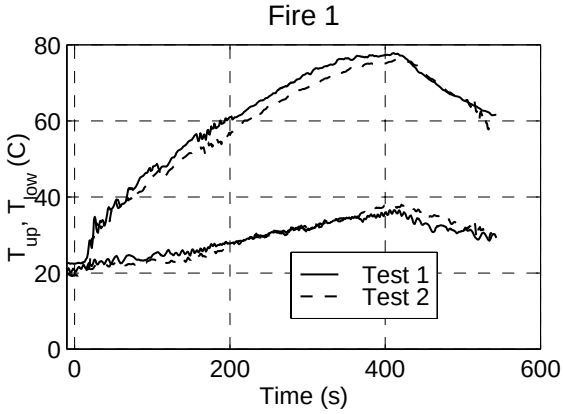


*Figure 41b. Upper and lower layer temperatures.*

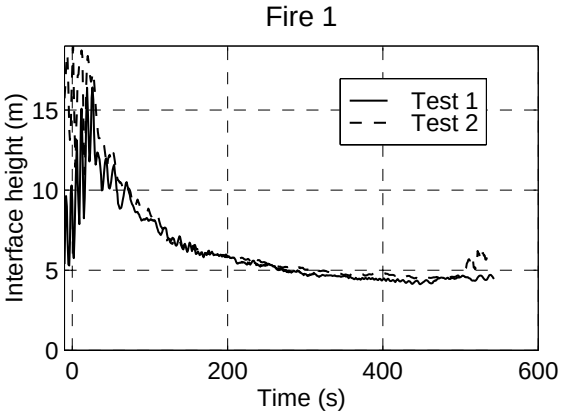


*Figure 41c. Interface heights.*

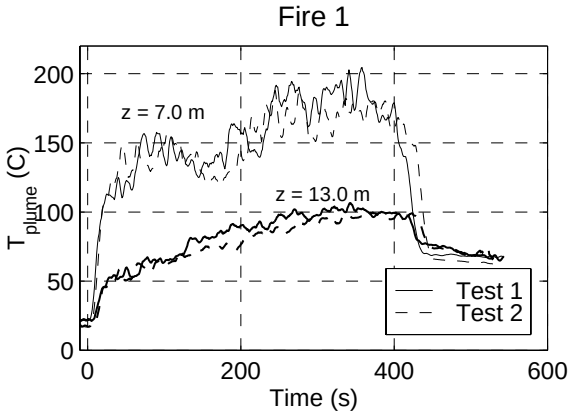


*Figure 41d. Plume temperatures.*

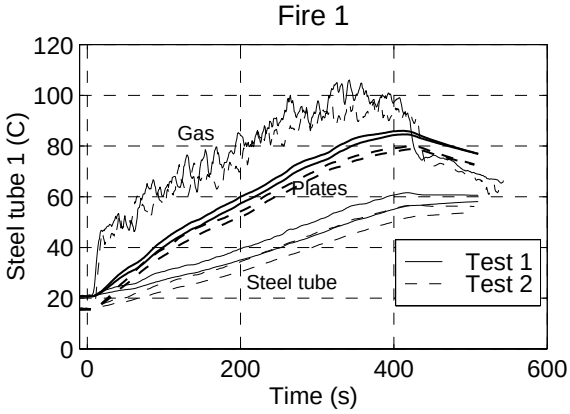


*Figure 41e. Steel tube 1 temperatures.*

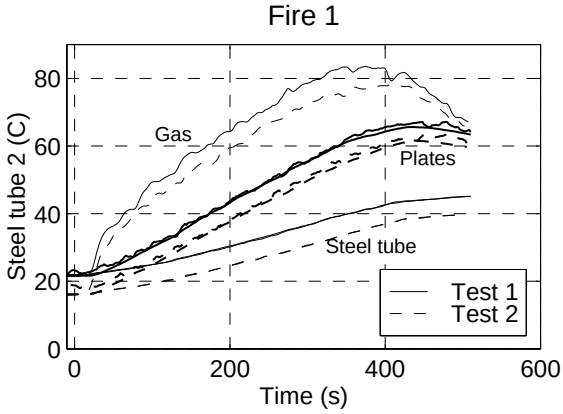


*Figure 41f. Steel tube 2 temperatures.*

# Appendix O: Results of the hall fire type 2

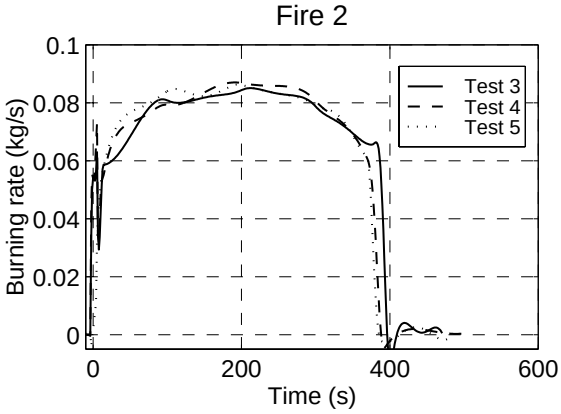


*Figure 42a. Mass loss rates in Fire 2.*

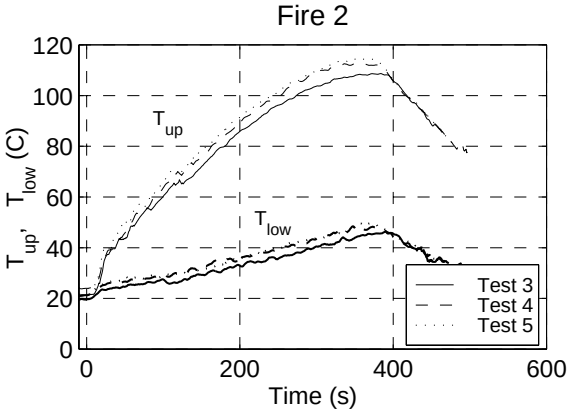


*Figure 42b. Upper and lower layer temperatures.*

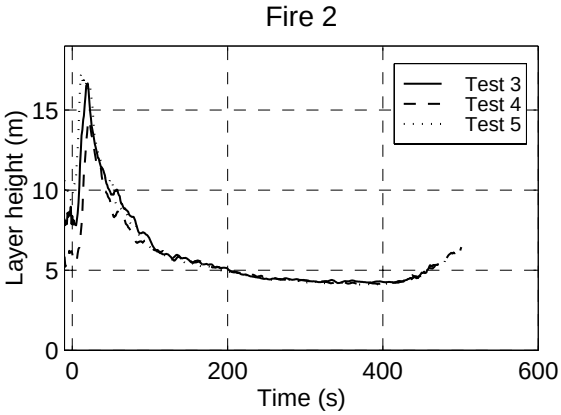


*Figure 42c. Layer interface heights.*

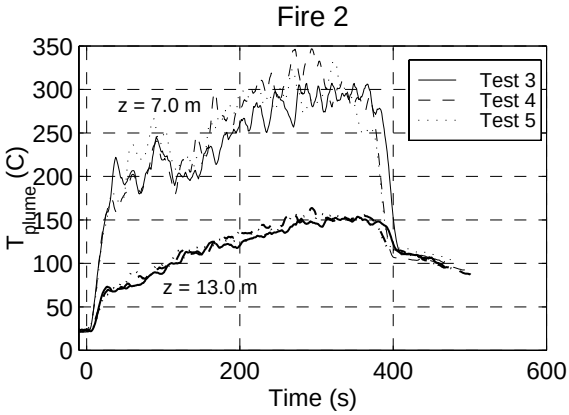


*Figure 42d. Plume temperatures.*

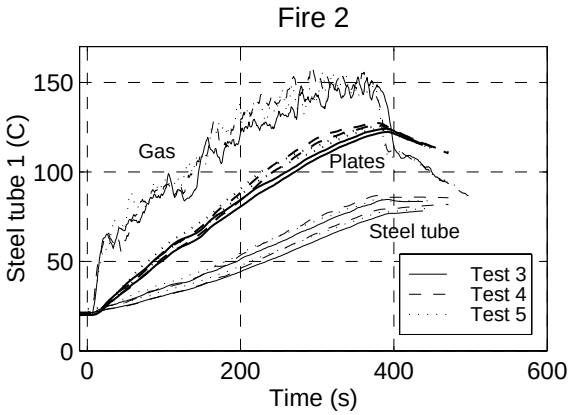


*Figure 42e. Steel tube 1 temperatures.*

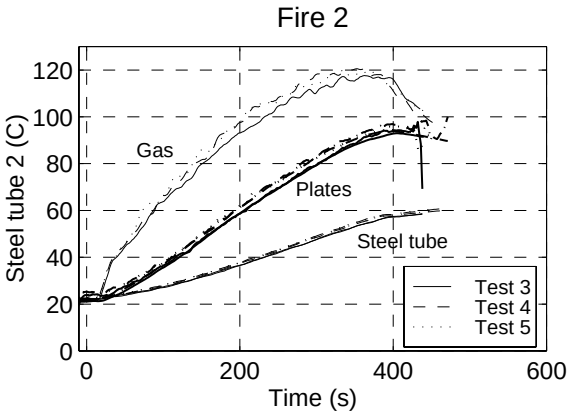


*Figure 42f. Steel tube 2 temperatures.*

# Appendix P: Results of the hall fire type 3

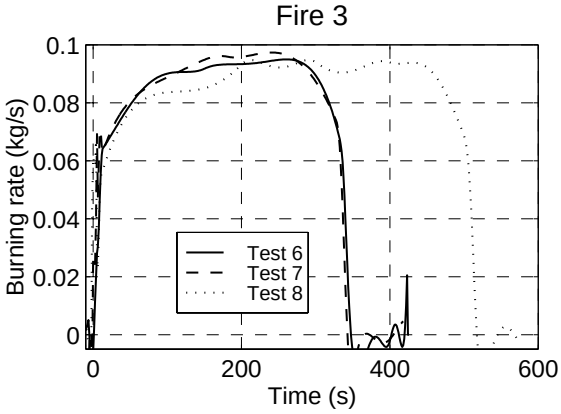


*Figure 43a. Mass loss rates in Fire 3.*

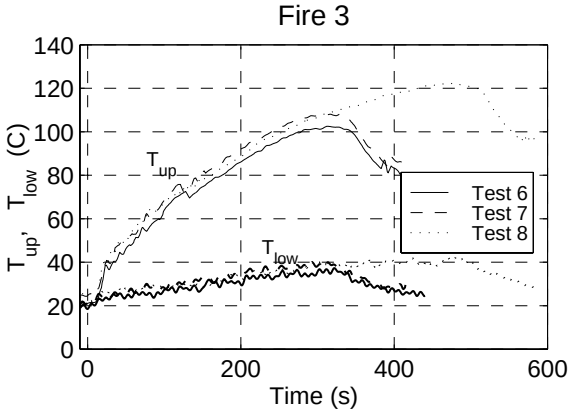


*Figure 43b. Upper and lower layer temperatures.*

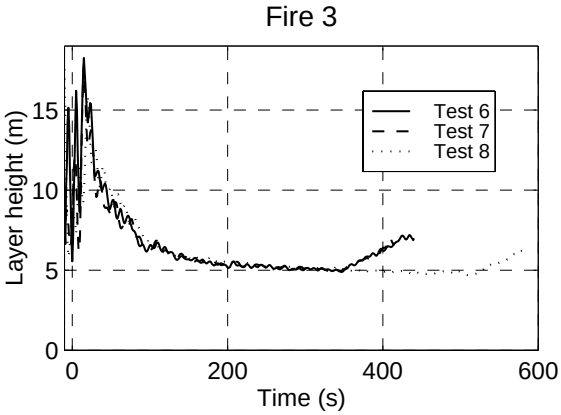


*Figure 43c. Layer interface heights.*

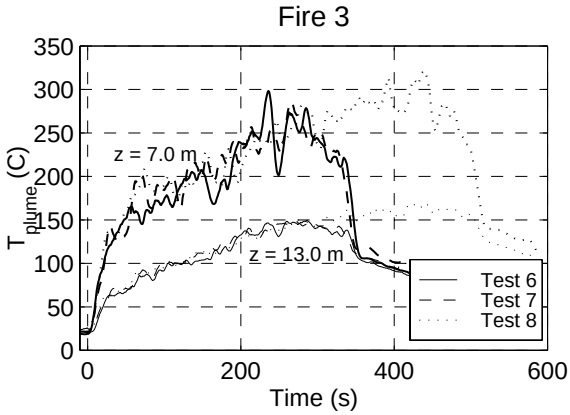


*Figure 43d. Plume temperatures.*

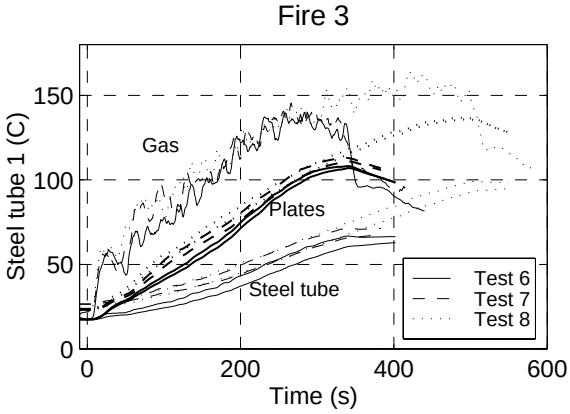


*Figure 43e. Steel tube 1 temperatures.*

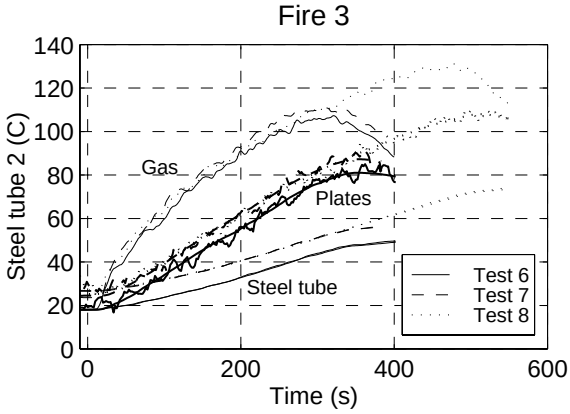


*Figure 43f. Steel tube 2 temperatures.*

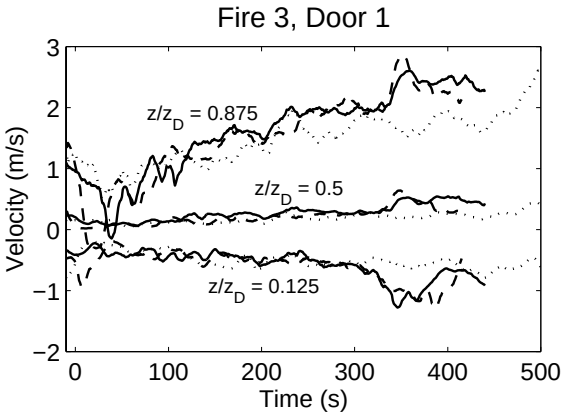


*Figure 43g. Flow velocities in Door 1 at x = 0 m. Door height $z_D$ = 4.0 m.*

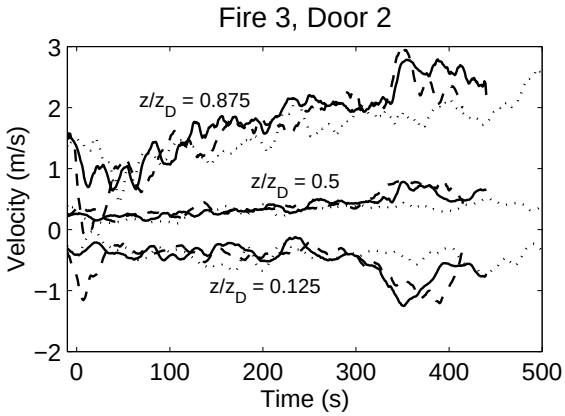


*Figure 43h. Flow velocities in Door 2 at x = 27.0 m. Door height $z_D$= 4.0 m.*

Published by

VTT

Vuorimiehentie 5, P.O.Box 2000, FIN-02044 VTT, Finland
Phone internat. +358 9 4561
Fax +358 9 456 4374

Series title, number and report code of publication

VTT Research Notes 2104
VTT–TIED–2104

Author(s)
Hostikka, Simo, Kokkala, Matti & Vaari, Jukka

Title

# Experimental Study of the Localized Room Fires
## NFSC2 Test Series

Abstract

Two series of full scale fire tests have been carried out with an objective to produce well-documented data for the zone model and CFD code verification. The first test series consisted of 21 tests in $10 \times 7 \times 5$ m$^3$ test enclosure with $2.4 \times 3.0$ m$^2$ to ambient. The walls and ceiling were made of light weight concrete. Systematic variations of the fire size and locations were made to determine their effect on the fire environment. Burning rates, gas temperatures, wall temperatures, heat fluxes, flow velocities and species concentrations were measured during the tests. The second series consisted of eight tests in a $27 \times 13 \times 19$ m$^3$ test hall. Burning rates, gas temperatures and steel tube temperatures were measured to provide information about the smoke filling rate and heating of the steel structures. The boundary conditions were varied by changing the fire size and using mechanical exhaust of the smoke gas and open doors to ambient.

Keywords
fire tests, room fires, experimentation, fire safety, fire prevention, concrete structures, walls, ceilings, burning rate, gas temperature, heat flow

Activity unit
VTT Building and Transport, Building Physics, Building Services and Fire Technology,
Kivimiehentie 4, P.O.Box 1803, FIN–02044 VTT, Finland

| ISBN | Project number |
|---|---|
| 951–38–5837–5 (soft back ed.)<br>951–38–5838–3 (URL: http://www.inf.vtt.fi/pdf/) | R7SU00803 |

| Date | Language | Pages | Price |
|---|---|---|---|
| August 2001 | English | 49 p. + app. 46 p. | B |

| Name of project | Commissioned by |
|---|---|
| Natural fire safety concept:Full scale tests, implementation in the Eurocodes and development of a userfriendly design tool | ECSC (the European Steel and Coal Community), Rautaruukki Oyj, VTT |

| Series title and ISSN | Sold by |
|---|---|
| VTT Tiedotteita – Meddelanden – Research Notes<br>1235–0605 (soft back edition)<br>1455–0865 (URL: http://www.inf.vtt.fi/pdf/) | VTT Information Service<br>P.O.Box 2000, FIN-02044 VTT, Finland<br>Phone internat. +358 9 456 4404<br>Fax +358 9 456 4374 |

VTT TIEDOTTEITA – MEDDELANDEN – RESEARCH NOTES

VTT RAKENNUS- JA YHDYSKUNTATEKNIIKKA – VTT BYGG OCH TRANSPORT – VTT BUILDING AND TRANSPORT

2048 Kuosa, Hannele. Älykkäät betonit ja betonirakenteet. 2000. 35 s. + liitt. 9 s.

2049 Lehtinen, Jari. Rakennushankkeen turvallisuusjohtaminen. Korkea rakennuskohde. 2000. 77 s. + liitt. 16 s.

2051 Karhu, Vesa & Loikkanen, Kaisu. Japanese and Chinese construction and facilities management software markets. Preliminary study. 2000. 58 p. + app. 4 p.

2053 Luoma, Marianna & Pasanen, Pertti. Ilmanvaihtojärjestelmien puhdistus 15 toimisto-rakennuksessa. Puhdistuksen ja säädön vaikutus toimistotilojen kanavien puhtauteen, ilmanvaihtuvuuteen, tuloilman laatuun ja työntekijöiden työoloihin. 2000. 43 s. + liitt. 6 s.

2054 Riihimäki, Markku & Lehtinen, Erkki. Luonnonkiviteollisuuden markkinat. 2000. 57 s. + liitt. 19 s.

2056 Kuosa, Hannele & Vesikari, Erkki. Betonin pakkasenkestävyyden varmistaminen. Osa 1. Perusteet ja käyttöikämitoitus. 2000. 141 s.

2069 Simonson, Carey J. Moisture, thermal and ventilation performance of Tapanila ecological house. 2000. 141 p. + app. 5 p.

2070 Nieminen, Jyri & Salonvaara, Mikael. Hygrothermal performance of light steel-framed walls. 2000. 26 p.

2072 Paiho, Satu, Leskinen, Mia & Mustakallio, Panu. Automaatiojärjestelmän hyödyntäminen energiatietoisen käytön apuvälineenä. 2000. 63 s.

2075 Häkkänen, Helinä, Britschgi, Virpi & Kanner, Heikki. Nuorten aikomus hankkia ajokortti. 2000. 71 s. + liitt. 4 s.

2076 Leivo, Markku & Holt, Erika. Betonin kutistuma. 2001. 57 s.

2078 Ratvio, Juha. Ultralujan betonin käyttösovellukset. Esitutkimus. 2001. 45 s. + liitt. 13 s.

2079 Laukkanen, Kyösti & Unhola, Timo. Ajoharjoitteluratojen liukasaluetutkimus. Laboratorio- ja kenttäkokeet 2000. 2000. 58 s. + liitt. 8 s.

2082 Tiuri, Ulpu, Sarja, Asko & Laine, Juhani. Korjauskonsepti. Korjausrakentamisella asunto kaikkiin elämänvaiheisiin 2001. 45 s. + liitt. 130 s.

2083 Tarvainen, Veikko, Pietilä, Jukka & Serenius, Matti. Puun öljykuivaus, öljykyllästys ja värjäys. 2001. 65 s. + liitt. 9 s.

2084 Hietaniemi, Jukka, Mangs, Johan & Hakkarainen, Tuula. Burning of Electrical Household Appliances: An Experimental Study. 2001. 60 p. + app. 23 p.

2085 Valkiainen, Matti, Klobut, Krzysztof, Leppäniemi, Sami, Vanhanen, Juha & Varila, Reijo. PEM-polttokennoon perustuvat mikro-CHP-järjestelmät. Tilannekatsaus. 2001. 60 s.

2090 Koukkari, Heli, Petäkoski-Hult, Tuula, Rönkä, Kimmo, Regårdh, Elina, Lappalainen, Veijo, Eerikäinen Miia, Norvasuo, Markku & Koota, Jaana. Esteetön asuinkortteli. 2001. 112 s. + liitt. 68 s.

2091 Toratti, Tomi. Puurakenteiden seisminen suunnittelu. 2001. 57 s. + liitt. 16 s.

2093 Andstén, Tauno. Käsisammuttimien käyttö ruokaöljypalojen sammutuksessa. Kirjallisuustutkimus. 2001. 28 s.

2100 Pakanen, Jouko, Möttönen, Veli, Hyytinen, Mikko, Ruonansuu, Heikki & Törmäkangas, Kaija. Dynaamisten HTML-sivujen ja multimedian hyödyntäminen taloteknisten järjestelmien käytön, huollon ja vikadiagnostiikan opastamiseen. 2001. 20 s. + liitt. 10 s.

2101 Toratti, Tomi. Seismic design of timber structures. 2001. 53 p. + app. 16 p.

2102 Kolari, Sirpa & Luoma, Marianna. Ilmanvaihtojärjestelmän puhtaan asennusmenetelmän kehittäminen. 2001. 47 s.

2103 Koivu, Tapio, Mäntylä, Kaj, Loikkanen, Kaisu, Appel, Mikael & Pulakka, Sakari. Innovaatiotoiminnan kehittäminen kiinteistö- ja rakennusklusterissa. Lähtökohtia ja kokeiluja. 2001. 81 s. + 19 s.

2104 Hostikka, Simo, Kokkala, Matti & Vaari, Jukka. Experimental Study of the Localized Room Fires. NFSC2 Test Series. 2001. 49 p. + app. 46 p.